

PDF hosted at the Radboud Repository of the Radboud University Nijmegen

The following full text is a publisher's version.

For additional information about this publication click this link.

<http://hdl.handle.net/2066/26978>

Please be advised that this information was generated on 2017-12-05 and may be subject to change.

Extended defects in GaN:
Selective etching and optical properties

Lukasz Macht

Cover

Front:

Large volume defect in N-polar GaN after PEC etching

Back:

A preparation sequence of a TEM sample by Focused Ion Beam

Extended defects in GaN: Selective etching and optical properties

Lukasz Macht

Thesis – Radboud Universiteit Nijmegen / Katholieke Universiteit Nijmegen

Illustrated – With references – With summary in Dutch

Printed by PrintPartners Ipskamp, Enschede

Cover design by Lukasz Macht

Extended defects in GaN: Selective etching and optical properties

een wetenschappelijke proeve op het gebied van
de Natuurwetenschappen, Wiskunde en Informatica

Proefschrift

ter verkrijging van de graad van doctor
aan de Radboud Universiteit Nijmegen
op gezag van de Rector Magnificus Prof. Dr. C.W.P.M. Blom,
volgens besluit van het college van decanen
in het openbaar te verdedigen op maandag 26 september 2005
des namiddags om 13.30 uur precies

door

Łukasz Macht

geboren op 7 juni 1975
te Warschau, Polen

Promotor Prof. Dr. P.K. Larsen

Co-promotor Dr. J.L. Weyher

Manuscriptcommissie Prof. Dr. J.J. Kelly
(Debye Institute, Utrecht University)
Prof. Dr. T. Suski
(Institute of High Pressure Physics, Warsaw)
Dr. P.C.M. Christianen

for fun...

Preface

Preface in general, is a place for the author's own, uninhibited recollections and also, in case his message is not really clear, it is a way to point readers in the right direction. Well, I'm going to leave that second part out and let you find your own way.

It is now exactly one day until I send this book to printers and I have to admit I have extremely mixed feelings. On one hand, I'm very happy that this huge effort is finally ending and I'll have it over within two months and on the other hand, I'm quite sad that it is all over so soon. I've spent the last 4.5 years having a whole load of fun - while working; and at the same time being surrounded by some of the finest people I've ever met. These lines are meant to show my appreciation for their help as well as their good humour and friendliness. There are four people I would like to thank in particular: Jan, Maarten, Martha, and Poul Larsen (in alphabetic order). I still remember the night I had arrived for my interview talk and dragged Martha up from bed to get the key to the room I was staying at. After that, all I ever had for Martha was administrative problems to solve; some I didn't even know I had, because she had already solved them. I am very grateful to Jan and Poul for taking chance on me and accepting me for this position. I did have an interview but those are known to be misleading and I'm happy that both Jan and Poul have accepted me despite the interview. I would also like to thank Jan for all the professional and not so professional conversations that have helped me focus on my tasks. Maarten was my mirror and I was his. All four and some years of my PhD we have been testing each other and both found each other acceptable, whether in doing our work or playing table soccer. In fact we have problems with stopping to mirror each other and we do it now at another company I'd like to thank Paul and John for always having the time for my questions - and more importantly for having the time to answer them. I'm very grateful to Victoria, a former PhD student,

for all the help with theory of photoluminescence in GaN, and methodology of optical measurements. I'm also grateful for the first descriptions of the Dutch society coming from eastern European viewpoint. I'd like to express my gratitude to Harry, Peter and Wil for all the support they have given me and for not shouting at me if I broke something. I would especially like to thank Wil for never, ever, kicking me out the door when I came with yet another gadget I wanted made for the day earlier. I'd like to thank my fellow PhD students from the GaN project: Andrzej, Corina and Mariusz. They have created for me a "little Poland" in Nijmegen, partly because Andrzej and Mariusz are Polish and partly because Corina never let us forget it and vehemently insisted on speaking English. I want to thank Corina and Andrzej for agreeing to be my paranimfen, despite the chance that I might need their help at the defence. There are two reasons I am indebted to Eric (Yes - I will write it with 'c'): for his never-ending good humour and for showing me that it is possible to keep coming back to a place you like to work at. Who knows - I might try to follow his footsteps one day. I want to thank all of the Solid State Physics III group for creating the best working conditions I could have wished for.

There are also several people outside the Solid State Physics III, one of them is Prof. John Kelly who made chapter 5 the best chapter in this thesis. I'd like to thank Daniel Kaminski for his insistence on looking at every problem from the chemical perspective. I want to thank all my friends who listened to me drone on and on about gallium nitride and never complained. Finally I'd like to thank my parents, who kept encouraging me to go on and my wife Edyta for all the support that she gave me during these years.

Veldhoven, July 2005.

Lukasz Macht

Contents

Preface	vii
1 Introduction	1
1.1 What is GaN and what can we use it for	1
1.2 Applications	5
1.3 Growth Methods	11
1.4 Substrates	18
2 Types of defects in GaN	25
2.1 Point defects	25
2.1.1 Vacancies	25
2.1.2 Interstitial and substitutional atoms	29
2.2 Line defects	33
2.3 Planar defects	37
3 Defects: etching and calibration	45
3.1 Introduction to defect selective etching	45
3.2 Etching of GaN.	46
3.2.1 Orthodox etches.	46
3.2.2 Photo-etching (photoelectrochemical – PEC or electro- less method).	49
3.3 Etching of Silicon Carbide.	51
4 Surface termination of dislocations	57
4.1 Introduction to etch pits	57
4.2 Eutecting etching of GaN:Zn	58
4.3 The significance of etch pits	59
4.3.1 Etching results	59

4.3.2	Morphology	63
4.3.3	Activation energy calculations	67
4.4	Conclusions	69
5	PEC etching of GaN	73
5.1	Introduction to PEC etching	73
5.2	Growth parameters and PEC methods	75
5.3	Results and discussion	76
5.3.1	Kinetics	76
5.3.2	Open-circuit photoetching kinetics	80
5.3.3	Morphology	84
5.4	Conclusions	87
6	Statistical PL of dislocations	91
6.1	Dislocation related luminescence	91
6.2	Samples and measurements	92
6.3	The origins of YL and BL bands	93
6.4	Conclusions	98
7	Micro PL mapping of GaN/Si	101
7.1	Patterned Si as alternative substrate	101
7.2	Growth parameters and measurement configuration	102
7.3	Results and Discussion	104
7.4	Conclusions	107
8	Polarity of GaN	109
8.1	Introduction	109
8.2	Experimental details	110
8.3	Influence of polarity on GaN properties	111
8.4	Conclusions	115
	Summary	119
	Samenvatting	123
	Publications list	127
	Curriculum Vitae	129

Chapter 1

Introduction

1.1 What is GaN and what can we use it for

GaN is a semiconductor compound belonging to the so called III-V group. The main interest in GaN is due to its wide, direct bandgap (E_g) of 3.42 eV, which allows for efficient light generation at wavelengths of about 365 nm. The light spectrum visible by humans covers the wavelength range 400 – 700 nm, which means that GaN can be used for generation of light in the ultra violet (UV) part of the spectrum. The possibility to grow ternary or quaternary alloys with gallium, indium and aluminium, such as InGaN, AlGaIn, InAlGaIn and other III-N compounds, allows bandgap engineering and it extends the emission spectrum from deep UV to yellow. The wide bandgap of GaN and AlGaIn is very valuable for high temperature electronics because the ratio of bandgap to the thermal energy kT is much higher than for other common semiconductors such as Si ($E_g= 1.1$ eV). The high drift velocity and break down voltage of these nitride compounds are furthermore very valuable for high frequency – high power electronic devices.

These valuable electrical and optical properties are further augmented by high thermal stability, physical hardness and high chemical stability. While the thermal stability of GaN allows freedom for high temperature applications and processing, its chemical stability presents a technological challenge. Conventional wet etching techniques used in semiconductor processing are not very successful for III-N device fabrication and so far dry-etching methods have to be used. A breakthrough in the field of wet chemical etching processes would be very beneficial for device technology development.

The high thermal stability makes the growth of GaN impossible by

common methods such as Czochralski or Bridgeman, which results in lack of free standing GaN wafers. That shortage of lattice matched substrates is the single, most important issue hampering a rapid development of III-N technology. Growth on foreign substrates leads to formation of various structural defects, most notably dislocations, due to lattice constant mismatch and differences in thermal expansion coefficients between GaN and the substrate. The properties of various substrates and their influence on GaN layers will be discussed later in this chapter.

Among the three crystal structures available to GaN, the wurtzite, zincblende, and rocksalt, the thermodynamically stable phase at ambient conditions is wurtzite structure. This structure has a hexagonal unit cell and thus two lattice constants, c (5.18\AA) and a (3.18\AA). It contains 6 atoms of both Ga and N, which are arranged in two interpenetrating hexagonal close packed (HCP) sublattices, each with one type of atoms, offset along the c axis by $5/8$ of the cell height ($5/8 c$). Figure 1 shows a schematic drawing of a GaN unit cell.

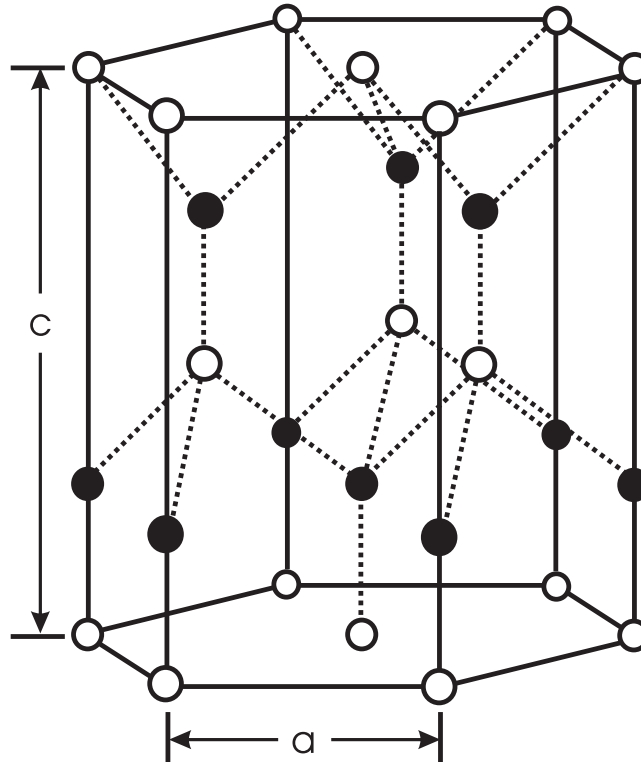


Figure 1: Wurtzite unit cell

All these properties relate only to wurtzite GaN. Cubic GaN is much less studied and even though scientific interest in it grows in popularity it is still not used for industrial applications.

Table 1.1 presents some basic physical parameters of wurtzite GaN in comparison with other frequently used semiconductors. As can be seen, GaN has the highest direct bandgap making it particularly suitable for applications involving light emission. At the same time its physical hardness is comparable to SiC which makes it difficult to process but also mechanically robust. The thermal properties, while not as good as for SiC or diamond, are still much better than other commonly used semiconductors and increase GaN's suitability for high power electronics.

Property	Si	Ge	GaAs	InP	SiC	GaN	Diamond
Energy bandgap (eV)	1.11	0.66	1.43	1.34	3.2	3.42	5.46-5.6
Bandgap type	Indirect	Indirect	Direct	Direct	Indirect	Direct	Indirect
Dielectric constant	11.7	16.2	12.9	12.5	9.7	8.9	5.7
Melting point (° C)	1412	937	1240	1060	3100	2500	4373
Thermal conductivity (W/cm·K)	1.3	0.58	0.46	0.68	3.6-4.9	1.8-2.4	6-20
Density (g/cm ³)	2.33	5.32	5.32	4.81	3.21	6.15	3.52
Bulk modulus (GPa)	98	75	75.3	71	220-250	205	442

Table 1.1: Basic properties for the most common semiconductors.

Historical brief

GaN has actually been known for many years. The first paper on GaN powder was published as early as 1932,¹ when it was prepared by reaction of NH₃ with Ga. The crystalline structure of GaN was described in 1937,² but it took additional 22 years before two reports about growth of GaN were published at the end of 1969 and beginning of 1970. The reactive evaporation method by Kosicki et al.³ was capable of growing mostly polycrystalline layers on various substrates (as claimed by Kosicki, but GaN was grown on GaAs in the report). The pioneering work of Maruska & Tietjen⁴ described hydride vapour phase epitaxy (HVPE) method used to produce epitaxial single-crystalline layers and this has become one of the milestones in the GaN history. The early 70s have been an era of characterization of basic GaN

parameters but it also gave birth to the first GaN based metal-insulator-*n-type* (m-i-n) light emitting diodes (LEDs).⁵

All was not well, however, the layers were still of a poor quality and no reliable p-type doping method was available. In 1986 Amano et al.⁶ used a low temperature AlN nucleation layer on sapphire substrates in order to improve the quality of the subsequently grown GaN. His technique drastically improved the wetting and strain relaxation of GaN improving the quality of layers. In the same year Amano demonstrated the use of silane (SiH₄) for suitable n-type doping, but it took him another three years to achieve p-type doping with low-energy electron irradiated Mg-doped layers. Although still not perfect it was sufficient to obtain a p-n junction based LED.⁷

In 1992 Shuji Nakamura from Nichia Chemical Industries shows p-type doping with thermally activated Mg and later he uses InGaN quantum wells as active material for LEDs which helps them achieve unprecedented brightness. The first commercial blue LEDs based on GaN see the light of day in the early 1994⁸ and Shuji Nakamura becomes the most influential person on the GaN research scene.

Another huge milestone is achieved at the end of 1995 when the first electrically operated GaN-based laser diode (LD) starts working in Nichia Laboratories,⁹ quickly transforming this small company into an internationally known high-tech enterprise. This first LD operated at 417 nm and it was the shortest lasing wavelength by any semiconductor device at that time. Further development concentrates on expanding available wavelengths' range, higher efficiencies and better beam quality. The current state-of-the-art emission wavelength for heteroepitaxial nitride-based LDs is 350.9 nm.¹⁰ The only homoepitaxial, i.e. grown on a GaN substrate, laser has been obtained at the High Pressure Research Center in Warsaw.

In the meantime the quest for high power electronics has started with the first GaN-based transistor in 1993¹¹ which was then, a so called, GaN MESFET. The potential in the field was so great that radio frequency (RF) devices are currently the most dynamically developed area of III-N research.

The following pages of the introduction chapter describe briefly the possible applications for GaN in current and future devices, as well as, growth methods and currently used substrates for growth of III-N materials.

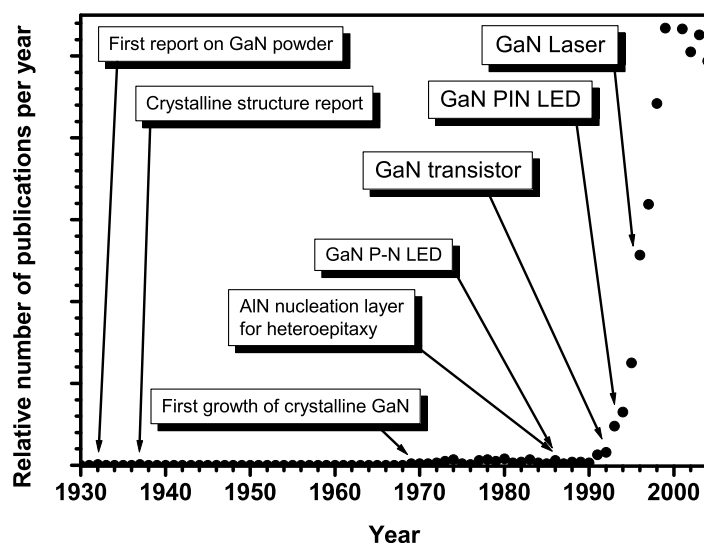


Figure 2: Amount of publications about GaN through the years and selected milestones.

1.2 Applications

High power electronics

By far the largest interest in electronic applications involving GaN nowadays lies in high frequency and high power devices. Along purely physical properties such as high chemical resistance and high thermal conductivity (especially prominent for devices grown on SiC substrates), additional electrical properties position GaN as prime candidate for high power microwave applications. The large bandgap enables devices to support internal electric fields about five times higher than Silicon or Gallium Arsenide. Higher electric fields result in higher breakdown voltages, combined with inherent high current handling capabilities of GaN high electron mobility transistors (HEMTs), lead to order-of-magnitude increases in power density.

As can be seen in tables 1.1 and 1.2, GaN excels in most transistor relevant categories and it is important to note that while already being introduced into production, the fundamental technologies are still being vigorously researched, which will certainly result in material improvements,

Attribute	Si	GaAs	SiC	GaN
Breakdown electric field (10^5 V/cm)	3.0	4.0	35	50
Saturation velocity (cm/s)	1.0×10^7	1.0×10^7	2.0×10^7	3.0×10^7
Electron mobility (cm^2/Vs)	1400	8500	800	1000
Johnson's Figure of Merit	1	11	110-410	790
Beliga's Figure of Merit	1	16	12-34	100
Keyes' Figure of Merit	1	0.46	6.1-16.6	8.6

Table 1.2: Material properties of common semiconductors relevant to RF applications at room temperature. Figures of merit are presented with respect to Si.

e.g. higher electron mobility value.

Over the years, various figures of merit for evaluating semiconductors for high frequency, high power applications have been proposed. These figures of merit attempt to account for the most relevant material properties and combine them into one number that represents a measure of the relative strengths of the alternative materials. The Johnson's figure of merit (JFM) is based on the frequency and power product of a semiconductor transistor.¹² It accounts for the fact that in an intrinsic device (one without parasitic effects) there is a trade-off between the time a carrier spends gaining energy in an electric field as it drifts through the device and the response time of the device. The value of JFM for GaN is 790 times that of silicon, about 70 times that of GaAs and about twice that of silicon carbide (SiC), another wide-bandgap semiconductor. This benchmark does not take into account the thermal effect occurring within the material. Thermal effects are gauged by the Keyes' figure of merit (KFM), which for GaN is not as high as for SiC. KFM is based on the thermal conductivity and the dielectric constant of the material. Even though dielectric constants of both SiC and GaN are similar, KFM for SiC is double that of GaN due to its superior thermal conductivity. However, the Baliga figure of merit, based on the dielectric constant, electron mobility and critical electric field, yields a figure for GaN that is approximately 100 times that of silicon, six times that of GaAs, and three times that of SiC. In other words, for high frequency, high power devices, GaN offers higher performance possibilities than competing materials.

The applications of such high frequency, high power transistors are quite

diverse, from compact radars to broadband wireless communication. Radar and satellite-communications links, which operate at frequencies ranging from hundreds of megahertz to tens of gigahertz, often have high power-amplification requirements, and would therefore benefit tremendously from gallium nitride. Many of the amplifiers in the transmitters of these radar systems and satellite-communications links still use traveling-wave tubes, a World War II-era technology.

Current broadband communication amplifiers are already being pushed to their limits. They use silicon technology that is only about 10 percent efficient, meaning that 90 percent of the power that goes into the transistors is wasted as heat. Powerful fans must continually blast this heat away from the amplifiers, which must also be outfitted with complex circuitry that corrects for the effects of harmonic and other distortions.

GaN transistors could double or triple the efficiency of base-station amplifiers, so that a given area could be covered by fewer base stations or, more likely, be flooded with more data at much higher rates. Freed from the fans and correction circuitry, due to their higher linearity and heat dissipation, it might even be possible to shrink an entire base station to the size of a small refrigerator, something that would fit on an antenna mast, rather than taking up space in a telephone company office.

To put numbers on all this information it can be mentioned that Fujitsu Laboratories has developed a GaN HEMT amplifier that emits 174 W at 63 V in a single device. Cree – manufacturer of high quality SiC and GaN-on-SiC substrates – has announced the development of GaN HEMTs with a CW power density of 32 W/mm at 4 GHz operation. And all that time GaN stays a relatively new material with plenty of potential for further scientific and technological improvement.

Light Emitting Diodes (LEDs)

Since 1960's when other semiconductor LEDs have come into existence, their lighting capabilities enforced their use solely as indicators. That was due to two reasons: the emission wavelength (λ), related to the bandgap of the material was in the red and infra-red part of the spectrum, $\lambda > 655$ nm, and the predicted high efficiency was realized only for low currents – higher currents decreased it substantially. Large effort in the field of material science and processing technologies allowed creation of LEDs able to emit other

colours of the visible spectrum, i.e. red through green and also increase their light generation efficiency, one thing was still missing: blue light.

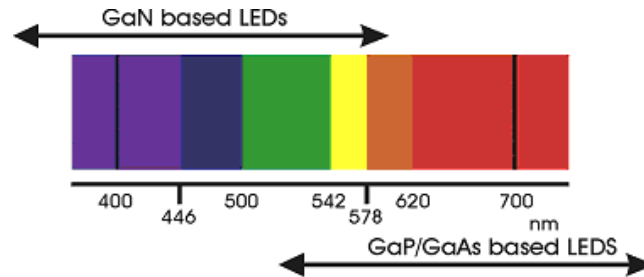


Figure 3: GaN LED spectral range vs. conventional LEDs

The one and single most important factor for GaN based light emitting diodes (LEDs) is its wide bandgap enabling not only operation at higher voltages but also generation of blue light (figure 3). The most important development in the field of LEDs since then have been the introduction of white LEDs in 1996. These can be made by a UV GaN LED emitting in the 450–470 nm spectral range, which excites proper phosphors emitting white light (e.g. Yttrium Aluminum Garnet – YAG). This approach gives a kind of bi-color white light which lacks certain colors to create true white. Also the directional pattern leaves a lot to be desired – the center spot seem bluish to the human eye while the off-axis light has a yellow tint to it.



Figure 4: GaN-based white LEDs by Toyoda-Gosei Co., Ltd.

Another approach is to combine monochromatic LEDs mounted close to each other to create a ‘digital’ white colour. The digital solution offers many advanced technical features and performance parameters when compared with the analogue technology described above, including wide dynamic

colour control with white-point tuning and full dimming capability without colour variation. A similar development of elegant broadband or Red Green Blue (RGB) sensors, LED drivers and address and control devices support "colour management" in these versions of the technology. Another method of obtaining various colours is the possibility of tuning the bandgap by making alloys such as InGaN, AlGaIn or InAlGaIn.

Further technology steps ensure continuing progress in control and power characteristics of the future white and blue LEDs. The applications for those devices are much too numerous to list as a whole but the most important include: various kinds of RGB indicators, full colour public displays, spectrally tuneable light sources as well as myriad of medical purposes requiring UV light. In fact first UV water purifiers based on 280 nm AlGaIn LEDs have been presented in 2004. They are "instant-on", potentially much cheaper, easily portable, and have a higher theoretical efficiency than mercury lamps used so far. The first biosensors which use UV LEDs have also been demonstrated recently. They're measuring absorption peaks at 280 nm and 340 nm wavelengths.

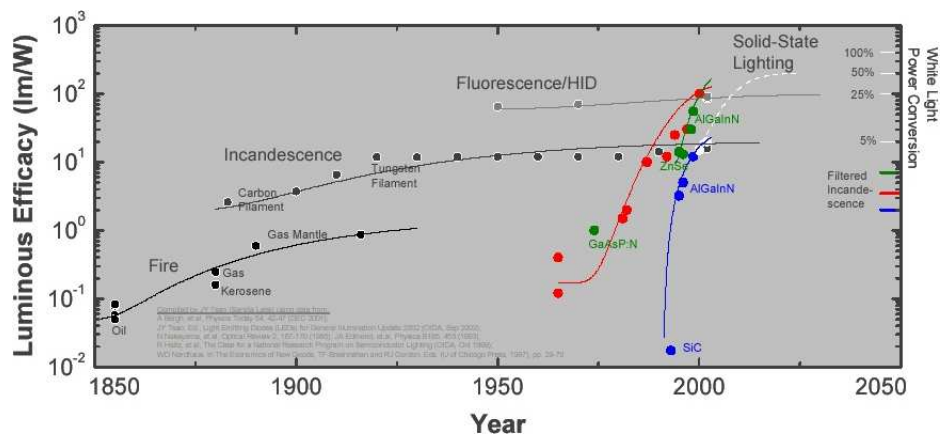


Figure 5: Projected efficiency of solid state lighting vs. past and current light sources

Solid state lighting (SSL) is an area where particularly white LEDs will flourish. With the possible 50% power conversion efficiency LEDs might be much better light sources than commonly used incandescent lamps. While running costs of LED lighting are already below those of incandescent one the initial purchase is still an issue with the estimated total ownership costs still in favour of light bulbs by 3:1 ratio. However, according to SSL roadmap by

Sandia National Laboratories these costs will turn in favour of LEDs already by 2007.¹³

Figure 5 shows the projected efficiency of solid state light sources over the next years and compares it to the efficiency of past and present light sources of different origin.¹³

Nowadays however, the main reasons driving markets in the direction of GaN based LEDs are still their indicator properties mostly used for mobile phone keyboard backlights or, as in the case of new VW cars, blue dashboard illumination.

Laser Diodes (LDs)

Quite a logical extension of LED technology leads to the creation of laser diodes. However, in the case of GaN it turned out not to be simple. Due to the growth on foreign substrates the density of dislocations in GaN layers is extremely high (10^9 – 10^{10} cm²). While it only decreases the efficiency in LEDs, it reduces lasers lifetime to a point where they're not practical. The breakthrough came at the end of 1995 in laboratory of Shuji Nakamura. Thanks to the unique geometry of his two-flow MOCVD reactor he managed to obtain lasing despite high density of dislocations. This result created an enormous interest from a large number of electronic companies.

The short emission wavelength of GaN-based LDs has one enormous benefit. The size of the laser spot achievable by focusing of the beam is limited by diffraction and it is directly proportional to the wavelength. Smaller laser spot allows a better resolution for reading of the optically stored information and allows a data density proportional to the inverse square of that resolution. Current Digital Versatile Discs (DVDs) store 4.7 GB of data on one side of a single layer disc using 650 nm wavelength. By switching to 405 nm available to GaN diodes, the focused laser spot size becomes almost two times smaller and the density grows fourfold. Along with other developments in the field, the size of new DVDs – called Blu-Ray – will become 26 GB. The first commercial devices have already been launched in 2003 and 2004 with more to follow in the next years. Other companies researching holographic methods of data storage utilizing GaN LDs, promise data storage of 1.6 TB on a CD-size disks by the year 2010. In order to judge the dynamics of GaN LD development it is enough to mention that today's \$9 million per year market is expected to grow to over \$270 million by 2008,

with 95% of that value dedicated to DVD applications.

UV photodetectors

The same high bandgap which provides for blue light emission is equally responsible for blue light absorption. GaN/AlGa_N-based UV detectors are superior to other UV detectors in their sensitivity, reliability and the conversion efficiency precisely because they are solar blind and have excellent thermal and chemical stability. Because the ozone layer absorbs solar radiation at wavelength range lower than 290 nm, the optical detectors operating at those wavelengths would have not be blinded by the Sun and therefore highly sensitive, virtually eliminating radiation noise. Commercial applications for UV detectors include flame sensors in industrial equipment, sensors in jet engine applications, and consumer sensors for UV dosing. The last one can already be purchased from APA Enterprises if you plan to spend holiday in a sunny place. Solid state UV detectors for biological applications are as important as UV LEDs or LDs; they allow to transform bulky, purely laboratory-housed equipment into mobile medical or research stations greatly aiding medical services in remote locations.

1.3 Growth Methods

All the numerous applications described above need mass-produced devices, which performance is equally linked to processing technologies and growth methods. Due to lack of commercially available GaN wafers, GaN layer growth must commence on foreign substrates by a variety of methods.

The three most popular growth methods currently used by researchers and manufacturers alike are Metal Organic Chemical Vapour Deposition (MOCVD), Molecular Beam Epitaxy (MBE) and Hydride Vapour Phase Epitaxy (HVPE). Each of these methods has its own benefits and disadvantages shortly described in this section. A unique method of growing free standing single crystal GaN is also discussed despite the fact it is not yet industrially applicable.

MOCVD

By far the most common technique for growing of GaN and other nitrides' layers is MOCVD. The principle of MOCVD is quite simple. Atoms are

deposited by decomposing organic molecules (precursors) while they are passing over the hot substrate. The undesired remnants are removed or deposited on the walls of the reactor. For growth of III-N layers the source materials generally used are trimethylgallium (TMGa) for Ga, trimethylaluminium (TMAI) for Al, and trimethylindium (TMIn) for In. Ammonia is used as source for nitrogen and the carrier gases can be nitrogen and/or hydrogen.

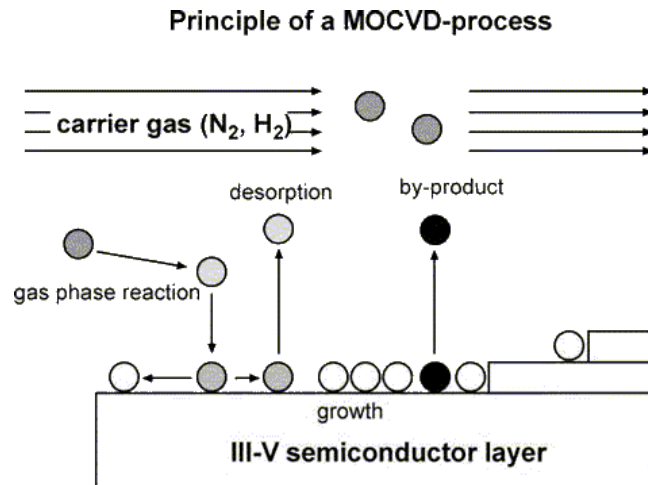


Figure 6: The principle of MOCVD

The carrier gas carries precursor molecules over the substrate placed on a graphite susceptor inside the reactor. RF heater warms up the susceptor which in turn provides the substrate and its vicinity with the energy for decomposition of the precursor molecules. Subsequently GaN is deposited on the substrate and remnants of the decomposition evaporate into the chamber and are carried away by the overall gas flow. Due to the large lattice mismatch between the foreign substrates and the III-N layers a very thin, so-called, nucleation layer is deposited to release the strain and enable single-crystalline growth. Typical pressure in the reactor is 50 mbar with the typical substrate temperature during growth of the main GaN layer set at 1100 - 1200 °C to ensure proper ratio between deposition and desorption. The growth rate achievable in those conditions varies in the range of 1 $\mu\text{m}/\text{h}$ which makes MOCVD suitable for growth of most electrical applications but definitely not bulk growth.

Doping is realized by means of Si for n-type and Mg for p-type with methyl silane (MeSiH₃) and biscyclopentadienyl (Cp₂Mg) as their respective



Figure 7: Aixtron reactors, (a) single 2 inch wafer R'n'D reactor and (b) multi-purpose industrial reactor capable of 5x10 inch or 95x2 inch wafer runs (5x10 inch Si wafers shown).

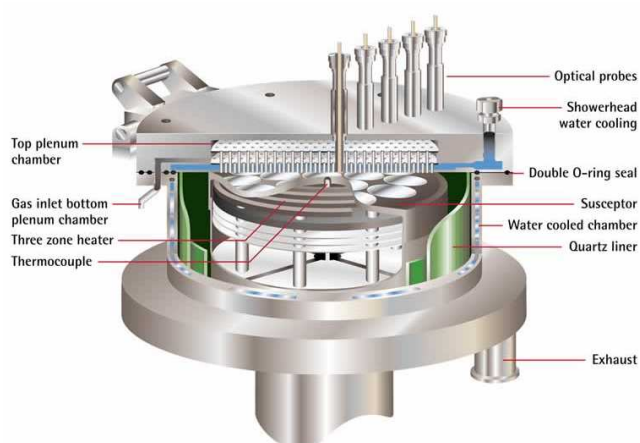


Figure 8: Example of wafer placement within a multi wafer reactor chamber (Thomas Swan Scientific CCS-MOCVD 19x2 inch configuration)

sources. The substrates used for this growth method are very varied with the most common being sapphire and SiC for their good compromise between costs and performance. However, a strong effort is made to improve quality of GaN grown on Si or GaAs wafers due to the fact that those materials are already well established and large size, high quality wafers are commercially available at a relatively low price. No matter the substrate used for growth, there is also a multitude of techniques used to improve quality of layers, many of which are patented. The most widespread method is growth of a

low temperature buffer layer made of either AlN or GaN prior to growth of the main GaN layer. Other tricks include silane treatment to obtain 3D-island nucleation which is later followed by lateral overgrowth.

MOCVD is also the favoured method for industrial production. Almost all GaN layers for common products have been manufactured by this technique. MOCVD reactor construction is not an easy matter therefore designs are developed by specialized companies such as Aixtron AG and Thomas Swan Scientific Equipment Ltd. The range of products encompasses single 2-inch size wafer R&D reactors to industrial ones able to grow on 95 2-inch size wafers in a single run. Figure 7 shows photographs of 2 such systems from Aixtron AG and fig. 8 shows a schematic diagram of placement of 19 2-inch wafers inside a single chamber of a similar reactor by Thomas Swan Scientific. The use of MOCVD system is complicated, in fact, it is necessary to optimise growth in each and every reactor. Additionally, the layers are prone to contamination by impurity atoms from gas sources or the ones adsorbed on the reactor walls in previous runs (memory effects). Nevertheless, MOCVD is a versatile technique compromising between quality and yield. While not having the best possible control over grown layers in terms of interfaces or doping levels, it allows to produce high performance devices in large quantities.

MBE

MBE is an Ultra-High-Vacuum (UHV)-based technique for producing high quality epitaxial structures with very good thickness control. A variant of this method is called atomic layer epitaxy and it allows thickness control with monolayer (ML) accuracy. Since its introduction in the 1970s as a tool for growing high-purity semiconductor films, MBE has evolved into one of the most widely used techniques for producing epitaxial layers of metals, insulators and superconductors as well, both at the research and the industrial production level. The principle underlying MBE growth is relatively simple: it consists essentially of atoms or clusters of atoms, which are produced by heating up an elemental or molecular source. They then migrate in an UHV environment and impinge on a hot substrate surface, where they can diffuse and eventually incorporate into the growing film. The rate of growth depends on the flux of material in the molecular beams which can be controlled by the temperature and switched on and off with

shutters. Typical growth rates are 1 ML per second, or 1 micron per hour, which is equivalent to a partial pressure of 10^{-6} mbar in the flux arriving at the substrate in the molecular beams. Great trouble is taken to ensure that only negligible quantities of impurity atoms are introduced into the material: substrates are carefully prepared and cleaned; ultra pure sources are used; the base pressure of the reaction chamber is kept in the low 10^{-10} mbar range and the walls of the chamber are cooled with liquid nitrogen.

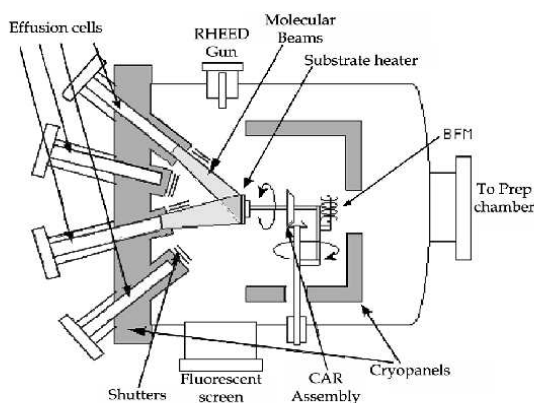


Figure 9: Schematics of an MBE system

Despite the conceptual simplicity, a great technological effort is required to produce systems that yield the desired quality in terms of material purity, uniformity and interface control. The choice of MBE and other growth techniques depends on the desired structure and needs. For example, for devices such as quantum wells (QWs) or distributed Bragg reflectors (DBRs), or even novel designs of transistors, where quality of interface and tight thickness control is required, MBE is the growth tool of choice. However, in the case of mass production, MBE suffers from a lower yield, compared to MOCVD systems. Not only is the growth rate smaller but also reactor and sample preparation is much more time consuming. In addition, the size range of MBE systems starting at 1x1 inch wafer reactors ends at 4x8 inch reactor by Riber or 7x6 inch one from Veeco.

HVPE

HVPE is used to grow various types of semiconductors such as InP, GaAs, GaN, and related compounds. In each case, the reactants are delivered to the

substrate in the gas phase, reacting HCl with the group three component, and delivering the group five component as a hydride. Growth of GaN is done by bubbling HCl gas with a nitrogen carrier gas through a gallium boat in the source zone at 800 ° C forming GaCl₃; ammonia, with nitrogen carrier gas, is transported to the substrate through a separate quartz tube. All of this takes place in a heated quartz chamber and the substrate, mostly sapphire, is placed on a SiC coated graphite susceptor which is heated to ~1100 ° C.

HVPE is characterized by very high growth rates of >100 μm/h, compared to ~1-2 μm/hour for the other methods, which allows a reduction in the density of threading dislocations resulting from a mismatch in lattice constants, from 10¹⁰ down to 10⁶ cm⁻². It doesn't allow growth of heterostructures as well as the other methods due to largely inaccurate thickness control; and the impurity concentration is not as low as in high vacuum deposition system such as MBE. However, thanks to its high growth rate and therefore sheer thickness potential for GaN layers, it might be a method of creation of free standing GaN substrates. In fact, such substrates have been available from Samsung for a some time already, but the available volume is nowhere near the industrial demand. Some manufacturers also use the HVPE technology to produce LEDs, since it estimated to reduce the use of ammonia by at least one order of magnitude compared to MOCVD. Also, HVPE uses pure metals as starting materials rather than metalorganic precursors, which are a factor of 10 more expensive per gram of metal. With further deposition control measures HVPE might become the best solution for growth of low complexity optoelectronic devices.

High Nitrogen Pressure Solution method

The three techniques mentioned above concentrate on growth of thin GaN layers upon various substrates due to lack of commercially available GaN single crystal substrates. The High Pressure Research Center in Warsaw has developed a method to grow free standing GaN platelets, namely so called “high nitrogen pressure solution” method. GaN is crystallized in gas pressure chambers with volume up to 1500 cm³ allowing crucibles with the working volume of 50-100 cm³. The high pressure—high temperature reactor consisting of the pressure chamber and the multizone furnace is equipped with additional systems necessary for in-situ annealing in vacuum,

electronic stabilization and programming of pressure and temperature and cooling of the pressure chamber. Bulk crystals are produced from gallium melts saturated with 1 at.% nitrogen at temperatures up to 1700 °C and nitrogen pressures of 20,000 atm. The structural properties of the bulk crystals are excellent with very narrow X-ray rocking curve widths for all crystals planes, low dislocation densities, and negligible strain. The optical and electrical properties of the bulk crystals are, however, poor compared to heteroepitaxial GaN layers on sapphire and other substrates, a consequence of high residual impurities (oxygen, carbon) and point defect concentrations (believed to be primarily Ga vacancies).

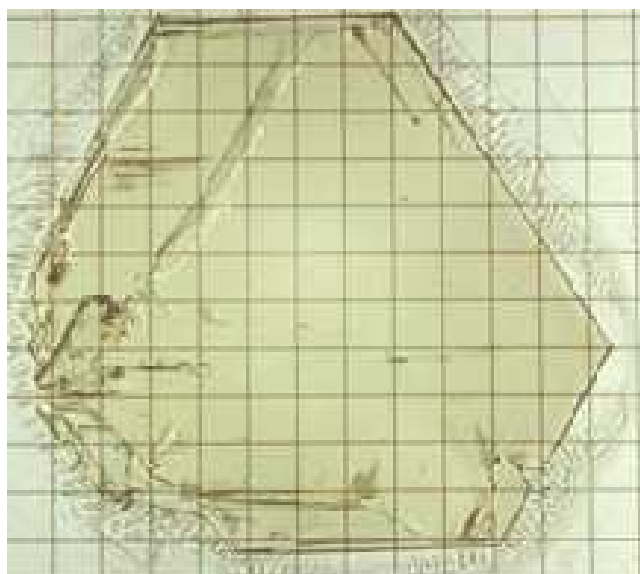


Figure 10: GaN platelet grown by HNPS method at Unipress, Warsaw

Such substrates could be used for production of real state-of-the-art devices due to their extremely low density of dislocations (~ 5 -8 orders of magnitude less than other GaN layers) and complete matching of thermal expansion coefficients. However, at present the volume of production as well as the size of such GaN single crystals disallow their use for other than research purposes. However, laboratory scale prototype series of lasers have been achieved.

In addition to these four methods there is a multitude of specific variants of those consisting mostly of technological innovations introduced into the heating, gas purification, delivery or characterisation systems. Each of them

has potential to significantly improve the quality of GaN layers, but does not constitute an entirely new growth method. Apart from these techniques also the choice of substrate used has significant impact on the quality and potential applications of GaN.

1.4 Substrates

The choice of substrates is highly dependent on the application, with regard to defect density and type of defects as well as their influence on optical, electrical and physical properties of GaN layers. Additionally it will have consequence on the processing steps needed in further product development. Nowadays there are two most common substrates used for GaN growth, namely sapphire and SiC. Additionally, a lot of effort is put into research of growth on alternative cheaper substrates such as GaAs or Si. Some specific growth modes require more exotic substrates such as Lithium Gallate (LiGaO_2), ELOG or SmartCutTM which will be discussed later.

Sapphire

Sapphire, (Al_2O_3), was the first substrate used in the study of GaN epitaxy by HVPE in 1969, and it is still the most commonly used substrate for GaN growth. The large lattice constant (30% larger than GaN) leads to a 15% mismatch of sapphire with GaN due to 30 misorientation of GaN lattice in respect to sapphire. Such large mismatch leads to a high dislocation density (10^{10} cm^{-2}) in the GaN epitaxial films which reduces the charge carrier mobility, the minority carrier lifetime, and decreases the thermal conductivity, all of which degrade device performance. Additionally, sapphire's thermal expansion coefficient is greater than GaN, thus, producing biaxial compressive stress in the layer as it is cooled from the deposition temperature. For thick films, such as can be grown by HVPE, the stress can cause both the film and the substrate to crack. The thermal conductivity of sapphire is low (about $0.25 \text{ W/cm}\cdot\text{K}$ at 100°C), thus, it is relatively poor at dissipating heat compared to other substrate materials. The cleavage planes of epitaxial GaN layer are not parallel to those of sapphire, making laser facet formation as well as cleaving very difficult. Sapphire is electrically insulating, thus, all electrical contacts must be made to the front side of the device, reducing the area available for devices and significantly complicating device

fabrication. In addition, there is evidence that oxygen from the sapphire causes unintentional doping in the GaN layer, raising its background electron concentration. However, with a proper nitridation and an optimized LT buffer layer of either AlN or GaN, very smooth GaN films can be obtained.

Currently, epi-ready sapphire substrates can be purchased from many manufacturers in sizes ranging from less than 1 cm², through the most popular 2 inch wafers (as low as 40\$/piece) up to 4 inch wafers (~\$350/piece). The availability of large size substrates plays an important role in the industrial growth of GaN/Sapphire based devices.

Silicon carbide

Silicon carbide (SiC) has several advantages over sapphire for GaN epitaxy, including a smaller lattice constant mismatch (3.1 %) for c-plane oriented films, and a much higher thermal conductivity (3.8 W/cm·K) which is important for high power applications. The crystal planes in epitaxial GaN are parallel to those of the SiC substrate, making facet formation by cleaving easier. Conductive substrates are available, making electrical contacts to the backside of the substrate possible, thereby simplifying the device structure compared to sapphire substrates. However, SiC does have its disadvantages. Gallium nitride epitaxy directly on SiC is problematic, due to poor wetting between these materials. Even though the lattice constant mismatch for SiC is smaller than that for sapphire, it is still sufficiently large to cause a large density of defects to form in the GaN layers. Preparing smooth silicon carbide surfaces is difficult, thus, its achievable surface roughness is an order of magnitude (1 nm RMS) higher than that for sapphire (0.1 nm RMS). This roughness and also subsurface polishing damage are sources of defects in the GaN epitaxial layer. SiC's thermal expansion coefficient is less than that of AlN or GaN, thus, the films are typically under biaxial tension at room temperature. Lastly, the cost of silicon carbide substrates is high, and currently single crystal SiC is produced by relatively few manufacturers. Cree, Inc. is specializing in SiC substrates and delivers them in 2 inch and 3 inch sizes with prices starting from \$500/piece up to \$4000/piece depending on the size and quality standard.

Silicon

The favorable physical properties, high quality, and low cost of silicon (Si) make it a very attractive substrate for GaN-based devices. Silicon wafers are very low priced and are available in very large sizes due to its mature development and large-scale production. Silicon has good thermal stability under GaN epitaxial growth conditions. The crystal perfection of silicon is better than any other substrate material used for GaN epitaxy and its surfaces can be prepared with extremely smooth finishes. The possibility of integrating optoelectronic GaN devices with Si electronic devices is also very attractive. However, the quality of GaN epitaxial layers on Si is much poorer than that on sapphire or silicon carbide, due to large lattice constant and thermal expansion coefficient mismatch, and the tendency of silicon to form an amorphous silicon nitride layer when exposed to reactive nitrogen sources. GaN grown on Si (111) is highly defective and non-radiative recombination channels reduce the luminescence efficiency of many optoelectronic devices. Nevertheless, the incentives for using Si substrates remain high, and good progress in reducing the defect density by using epitaxial lateral overgrowth or pendeoepitaxy has been reported. Many GaN devices have been demonstrated on Si substrates including LEDs and HEMTs.

Gallium Arsenide

GaAs can be advantageous as a substrate for GaN epitaxy due to its similar structure, since both GaAs and GaN are III-V compounds, the shared element (Ga), and parallel cleavage planes between the film and substrate. Additionally GaAs has a well-established process technology, and there are several readily available substrate orientations of both polar and non-polar varieties, and the possibility to make low resistance ohmic contacts. However, a large lattice constant and thermal expansion coefficient mismatch, poor thermal conductivity and low thermal stability offset these benefits.

Maintaining a smooth surface during all stages of GaN film growth is particularly important for GaN on GaAs, as it is a major cause of crystal defects and polytype inclusions. GaAs (001) is one of the few semiconductor substrates on which zincblende GaN epitaxial films form easily. GaAs can be easily wet etched, as opposed to sapphire, making GaN films easier to separate from GaAs. It has a lower yield strength than sapphire so cracking

and plastic deformation are more likely to occur in GaAs rather than the GaN film. The last two features make GaAs (111) substrates potential templates for creating freestanding thick GaN films and thus single crystal GaN substrates for device fabrication. Since the decomposition rate of GaAs in NH_3 or in UHV rapidly increases at temperatures above 700°C , it limits the growth temperature of GaN, and hence, its growth rate. Even a small amount of GaAs decomposition is detrimental to zincblende GaN epitaxy, as surface roughening or faceting enhances the onset of wurtzite growth. Because MBE is capable of depositing epitaxial GaN films at a relatively low temperature, it has been more commonly employed than MOCVD or HVPE on GaAs substrates.

GaAs substrates can be purchased from all major electronic materials manufacturers in sizes up to 6 inch with price for the standard 2 inch wafer of \$100. With current development of growth technology already 8 inch wafers have been demonstrated, however they're not in mass production yet.

Free standing GaN

Gallium nitride itself is the best choice as a substrate for GaN epitaxy and device fabrication, as it eliminates all problems associated with heteroepitaxy. Homoepitaxy offers better control compared to heteroepitaxy over the crystal polarity, dopant concentration, and strained layer thickness. Gallium nitride homoepitaxy of smooth films in a two-dimensional growth mode does not require nitridation or buffer layers, as is required for sapphire and silicon carbide. Although there are several techniques under development for producing bulk GaN crystals including growth by vapour phase transport, growth from supercritical fluids, and growth from sodium fluxes, only high pressure growth from solutions and hydride vapour phase epitaxy have produced reasonably large area crystals. These methods have already been discussed in previous section.

Exotic substrates

There are also some additional more exotic substrates used for GaN growth. One of them is Lithium Gallate. LiGaO_2 is the most closely lattice matched foreign substrate currently being considered for GaN growth, with an average lattice constant mismatch of only 0.9 % in the basal plane. GaN epitaxial layers can possibly be grown on LiGaO_2 without using buffer layers. The

quality of very thin layers of GaN grown on LiGaO₂ is better than films of similar thickness on sapphire or 6H-SiC substrates. It is a polar crystal which may facilitate control of the GaN film polarity, it is also easily etched, and therefore easier to transfer the GaN film to another substrate for better heat dissipation, or for producing thick free-standing GaN epitaxial films for subsequent homoepitaxy. It is relatively inexpensive in comparison to SiC. The main disadvantages to LiGaO₂ are its low thermal stability under MOCVD growth conditions, low thermal conductivity, high thermal expansion coefficients, and that it is an electrical insulator (i.e. conductive LiGaO₂ substrates are not possible).

Lithium Gallate can be easily grown by standard semiconductor crystal growth methods such as e.g. Czochralski method and the price of these substrates is comparable to price of sapphire ones, with similar technical quality.

ELOG substrates

Epitaxial Lateral OverGrowth (ELOG) substrates are also used for GaN growth. To fabricate an ELOG, growth of thin GaN layer is performed on sapphire or SiC wafer, followed by a deposition of a ~ 100 nm thick SiO₂ mask to form stripes several μm wide. A thick layer of GaN is grown over the mask. As the thickness of the epilayer increases, it grows laterally on the SiO₂ stripes. At about $10 \mu\text{m}$ thickness the GaN epilayers which grow at the two edges of the SiO₂ stripes coalesce and a continuous flat GaN layer is formed on the patterned substrate. The dislocation density in the GaN surface layer grown on the SiO₂ stripes is small, usually $2 \times 10^7 \text{ cm}^{-2}$. The lifetime of the InGaN/GaN/AlGaIn-based laser diodes grown on such substrate increased from a few hours to more than 1000 h. In a such laterally epitaxially overgrown (LEO) GaN layer, alternate stripes have high and low dislocation density. Since the device is fabricated on the GaN stripes with low density of defects, the size of the device is limited by the width of these stripes. Also, the device fabrication requires careful alignment of the device structure with the underlying mask stripe. It is possible to make a multiple ELOG process by making the next SiO₂ mask over the high dislocation density GaN areas. Such process will result in overall reduction of dislocation density, however, the effort necessary to produce it drives up the cost of such layers.

Cree, Inc. has announced commencement of production of ELOG GaN substrates in June 2004. The size is 2 inches and GaN ELOG structure is grown on SiC, the pricing information is not freely available but such a wafer will cost in the vicinity of \$10,000.

SiCOI by Smartcut™

The final type of substrate worth mentioning is SiCOI (Silicon Carbide On Insulator) prepared by the so-called SmartCut™ technology. This technology involves using two substrates, one SiC and one other, such as Si. The SiC substrate is then implanted with ions which induces creation of a weakened layer at a certain depth. It is then bonded face-down onto a Si wafer, and cleaved at the weakened layer. With proper polishing, annealing and other processing steps a SiCOI substrates is created – a thin SiC layer bonded on top of cheap Si wafer. The remaining part of the original SiC substrate can be used to create more SiCOI wafers.

This method has the potential of supplying SiC performance with Si economy. However, it is quite new and there are still unresolved issues concerning heat dissipation and strain generation. Currently only Soitec, France, is offering SiCOI substrates for GaN epitaxy with the pricing information unavailable at this time.

Such a multitude of growth methods coupled with an equally astounding number of possible substrates does makes the lives of researchers and manufacturers very challenging. Each choice has to be calculated against possible gains in performance or cost-effectiveness as well as the requirements of the desired application. At the moment, however, research on structural, electrical and optical quality of GaN layers is still the key to future devices. All the defects generated either by substrate-layer mismatch or impurity incorporation will have impact on one or more aspects of device operation.

It is the researcher's responsibility to be able to find and identify these defects and their consequences; and make all the possible effort to prevent their existence in new and improved layers.

References

- [1] W.C. Johnson, J.P. Parsons, M.C. Crew, *J. Phys. Chem.* 36, 2651 (1932)
- [2] J.V. Lirmann, H.S. Schadanov, *Acta Physicochem. URSS* 6, 06 (1937)

- [3] B.B. Kosicki, D. Kahng, J. Vac. Sci. Technol. **6**, 593 (1969)
- [4] H.P. Maruska, J.J. Tietjen, Appl. Phys. Lett. **15**, 327 (1969)
- [5] J. I. Pankove, M. A. Lampert, Phys. Rev. Lett. **33**, 361 (1974)
- [6] H. Amano, N. Sawaki, I. Akasaki, Y. Toyoda, Appl. Phys. Lett. **48**, 353 (1986)
- [7] H. Amano, M. Kito, K. Hiramatsu, I. Akasaki, Jpn. J. Appl. Phys. **28**, L2112 (1989)
- [8] S. Nakamura, T. Mukai, M. Snegh, Appl. Phys. Lett. **64**, 1687, (1994)
- [9] S. Nakamura, M. Senoh, S. Nagahama, N. Iwasa, T. Yamada, T. Matsushita, H. Kiyoku, Y. Sugimoto, Jpn. J. Appl. Phys. **35**, L74, (1996)
- [10] K. Iida, T. Kawashima, A. Miyazaki, H. Kasugai, S. Mishima, A. Honshio, Y. Miyake, M. Iwaya, S. Kamiyama, H. Amano, I. Akasaki, Jpn. J. Appl. Phys. **43**, L499, (2004)
- [11] M.A. Khan, J.N. Kuznia, A.R. Bhatarai, D.T. Olsen. Appl. Phys. Lett. **62**, 1786 (1993)
- [12] "Materials for High Temperature Semiconductor Devices", National Materials Advisory Board, National Academy of Sciences, NMAB-474, Washington, D.C. (1995)
- [13] J.Y. Tsao, IEEE Circuits & Devices, **20**, 28 (2004)

Chapter 2

Types of defects in semiconductors and GaN

The fact that GaN has to be grown by a variety of methods on non-coherent substrates introduces a large number of various defects into the crystal structure. Line defects such as dislocations are caused by the differences in lattice constants and thermal expansion coefficients between GaN layer and the substrate. Some of them might be of a grown-in type, i.e. generated during growth due to the lattice mismatch, others might result from post-growth stresses due to difference in expansion coefficients between substrate material and GaN layer.

HVPE and MOCVD techniques also introduce foreign atoms either by desorption from reactor walls and substrates or due to the presence of impurities in gas sources. Hence, e.g. large quantities of oxygen can be found in unintentionally doped (UID) GaN. This chapter lists and describes various defects that can be found in semiconductor layers with particular emphasis on those found in GaN.

2.1 Point defects

2.1.1 Vacancies

Vacancies are the simplest to define of the point defects: they are missing atoms in the crystal structure. Obviously there are only two types of vacancies available to be found in GaN and they are labeled V_{Ga} and V_N for Ga- and N- vacancy, respectively. Due to the fact that vacancies

do not involve foreign atoms they are called intrinsic or native defects. Their concentrations cannot be determined by chemical analysis of mass spectrometry; however, positron annihilation is an effective tool for studying vacancy-type defects in semiconductors. Positrons get trapped at vacancies due to the missing ion core at the vacancy site.¹ The trapping is experimentally observed in two ways: as a narrowing of the momentum distribution of the annihilating electron-positron pair and as an increase in the positron lifetime.

According to theoretical calculations based on the density-functional theory, *ab initio* pseudopotentials and a supercell approach,² gallium vacancy is a deep acceptor. Additionally, for the most common n-type material, V_{Ga} constitutes the dominant native defect since all other native defects have much higher formation energies and, by implication, negligible concentrations. The outcome of those calculations shows that an isolated V_{Ga} has a charged state of 3- and the transition level to the 2- state is at energy of 1.1 eV above the top of the valence band. This result is confirmed by positron annihilation experiments where the increase of positron trapping at low temperatures is a direct evidence of a negative charge. It is also probable that impurities incorporated during growth, facilitate the formation of Ga vacancies by forming energetically stable vacancy-impurity complexes. The impurities most likely to form a complex with V_{Ga} are donors, since a negatively charged V_{Ga} acceptor and a positively charged donor attract each other and gain energy by forming a complex. Since silicon and oxygen are the most frequently introduced impurities in GaN they are also the most likely candidates for defect complexes: $V_{Ga}-O_N$ and $V_{Ga}-Si_{Ga}$.

Figure 1 shows atomic geometry of an isolated V_{Ga} and a $V_{Ga}-O_N$ complex. The electronic structures of either $V_{Ga}-O_N$ or $V_{Ga}-Si_{Ga}$ related defects are very similar; they both act as double acceptors. They also have comparable transition levels, which suggests that the V_{Ga} electronic structure dominates the electronic structure of the relevant defect. However, theoretical binding energies are much different and equal 0.23 eV and 1.8 eV for $V_{Ga}-Si_{Ga}$ and $V_{Ga}-O_N$, respectively. This difference can be most simply understood in terms of electrostatic attraction: in the $V_{Ga}-O_N$ complex V_{Ga} and O_N are the closest neighbours whereas in the $V_{Ga}-Si_{Ga}$ complex V_{Ga} and Si_{Ga} are only the second-closest. It is therefore clear that by far the most common is $V_{Ga}-O_N$ complex.

Positron annihilation studies of heteroepitaxial GaN layers³ show that

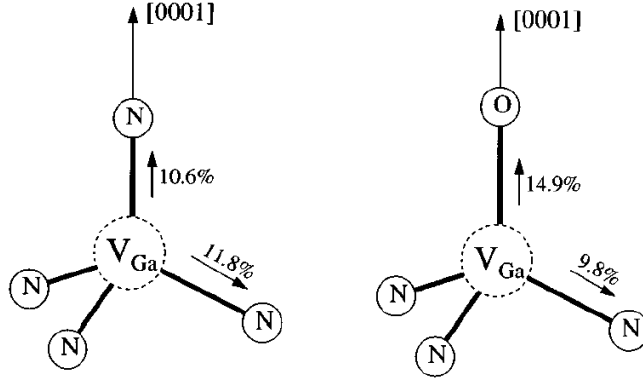


Figure 1: Atomic geometry of the Ga vacancy and the $V_{Ga}-O_N$ complex in the 3- and 2- charge state (where all defect levels are fully occupied). The numbers give the increase of the bond length in %. The bulk bond length is $d_0=1.94 \text{ \AA}$. [After Neugebauer *et al.*²]

the total acceptor concentrations are in very good agreement with the concentrations of Ga vacancies (isolated and/or in complexes), which indicates that they are the dominant acceptors in HVPE-grown GaN. However, using electron irradiation measurements it was shown that isolated V_{Ga} in GaN single crystals are already mobile at 600 K,⁴ which is much lower than temperatures employed during the growth process. The $V_{Ga}-O_N$ complex, however, is much more thermally stable and also SIMS results⁵ show that the O concentration depth profile is similar to the depth profile of V_{Ga} measured by positron annihilation. It is therefore quite likely that V_{Ga} exist as deep acceptors in GaN layers mostly in the form of $V_{Ga}-O_N$ complexes.⁶

Due to its energy position it is believed that $V_{Ga}-O_N$ among other sources is responsible for the “yellow luminescence” (YL). This conclusion is further supported by the fact that the formation energy of V_{Ga} increases with decreasing Fermi energy. This, in turn, means that with lowering the electron concentration of the sample the V_{Ga} concentration also decreases, while YL is only observed in n-type GaN. Also the fact that YL is suppressed in samples grown under Ga-rich conditions indicates that V_{Ga} is responsible for YL: Ga vacancies are simply much less likely to form under Ga-rich conditions.

Another theoretical work⁷ shows that also hydrogen atoms can be incorporated into complexes with Ga vacancies. Hydrogen can either compensate or passivate V_{Ga} in GaN; compensation occurs when unassociated hydrogen

donates an electron to a vacancy acceptor level, whereas passivation occurs when hydrogen forms a bound complex with the vacancy. Removal energies for hydrogen-vacancy complexes can be large and they strongly depend on the Fermi level. Complexes with 3 or 4 H atoms are predicted to be unstable and therefore make it impossible to completely passivate the V_{Ga} . There is no experimental proof of the existence of such complexes, but estimated vibration frequencies of hydrogenated V_{Ga} fall in the range of frequencies observed in infrared absorption spectra of hydrogen-implanted GaN.

In summary: V_{Ga} are the most common native defects in n-type GaN and they are mostly associated with oxygen atoms into $V_{Ga}-O_N$ complexes. Either isolated or bound in complexes V_{Ga} are deep acceptors with 3- or 2-charged states, respectively. They are also believed to be the primary source of the infamous yellow luminescence in n-type GaN layers.

The second available vacancy is the nitrogen vacancy (V_N), which, as a shallow donor, has been a major suspect for intrinsic conductivity of GaN since 1969.⁸ However, detailed numerical calculations showed that in n-type GaN the formation energy of V_N is about 4 eV⁹ and for a system in thermodynamic equilibrium such a high formation energy implies that it cannot occur in appreciable concentrations. The situation changes for p-type conditions when V_N has the lowest formation energy. The reason for that is the fact that the vacancies can become charged, thereby significantly lowering their formation energy. One of the ways of obtaining p-type conductivity is doping GaN layers with Mg atoms and thermally annealing them at 500 - 800 °C. The main reason for Mg-activation is the need for dissociation of a complex Mg-N-H formed during growth by methods containing hydrogen, such as MOCVD and ammonia MBE. Another reason for that annealing is that as-grown Mg-doped samples do not have a free Mg acceptor; instead V_N -Mg $_{Ga}$ complexes are created where the V_N compensates the Mg $_{Ga}$.¹⁰ Thermal annealing causes dissociation of these pairs and activates the p-type conductivity. Also beryllium atoms can form defect complexes with V_N in a similar way to that of Mg. In terms of energy, both the V_N -Mg $_{Ga}$ and the V_N -Be $_{Ga}$ complexes are bound with respect to their isolated components. Positron annihilation experiments show for p-type material the presence of both these complexes¹¹ and their charge is postulated to be neutral. The formation of these defect complexes is more probable under N-rich conditions than Ga-rich, as are the formation energies of interstitial defects. On the other hand isolated acceptors Be $_{Ga}$ and Mg $_{Ga}$ form easier in

Ga-rich conditions.

Another method for detecting V_N is electron irradiation. Electron energy of 0.42 MeV used for irradiating GaN samples is above the N-sublattice damage threshold while remaining below the damage threshold of Ga-sublattice, therefore V_N and nitrogen interstitials (N_I) can be readily created. Photoluminescence (PL) measurements performed subsequently show bound exciton lines arising from a hydrogenic donor with binding energy of 25 meV.¹² The hydrogenic donor is suspected to be an ionised V_N . The N_I created in the process of electron irradiation is much more mobile and is believed to form defect complexes with impurities. The most likely traps are oxygen or silicon substitutional donors and a mobile nitrogen interstitial is likely to deactivate those donors in N_I-O_N or N_I-Si_{Ga} complexes. Recent work,¹³ backed up by thermally dependent Hall measurement suggests that the binding energy of V_N is somewhat larger and amounts to 70 meV. In conclusion V_N is the most common intrinsic defect in p-type GaN and it is a shallow donor, which may be neutral or negatively charged. The binding energy of an isolated V_N is 70 meV but it can also form defect complexes with foreign atoms such as V_N-Mg_{Ga} or V_N-Be_{Ga} .

2.1.2 Interstitial and substitutional atoms

Interstitial atoms are the ones which are not situated in well defined lattice positions; instead they are placed in-between the atoms forming the periodic crystal structure. Substitutional atoms on the other hand are atoms which do not occupy their own position in the crystal. Both kinds of defects can be either intrinsic or extrinsic. The first kind involves only Ga or N atoms and so possible interstitials are N_I or Ga_I and substitutional (or antisite) Ga_N and N_{Ga} for gallium on an N site and nitrogen on a Ga site, respectively. Extrinsic substitutional involves all kinds of foreign atoms that might be incorporated into GaN layers and either occupy positions between normal crystal structure sites (interstitials) or substituting either N or Ga.

Intrinsic interstitials and substitutional atoms As already mentioned before, N_I is believed to be rather mobile at room temperature and does not form isolated defects; instead it deactivates such substitutional donors as O_N and Si_{Ga} to form N_I-O_N or N_I-Si_{Ga} complexes. On the other hand, theoretical calculations¹⁴ predict that N_I in the so called split configuration is

the most stable arrangement except for n-type GaN where a channel-centred configuration is the most stable one. The distinction is based on the position of the Fermi level. The diagram in fig. 2 shows the difference between the two configurations. In such case, hydrogen which is commonly incorporated during the growth or post growth processing, is easily incorporated into GaN layers because of the large electronegativity difference between gallium and nitrogen and the resultant electron transfer to the N atom. Hydrogen will therefore bind strongly to nitrogen interstitials or, as previously mentioned, gallium vacancies, thereby also becoming an interstitial defect.

Gallium interstitials can be generated by electron irradiation and subsequently detected by optically detected electron paramagnetic resonance (ODEPR) in the PL.¹⁵ The results are unambiguous on the form that this interstitial takes. It is, however, clear that its activation barrier for diffusion is sufficiently low to allow its long range migration and trapping by impurities or defects at room temperature.

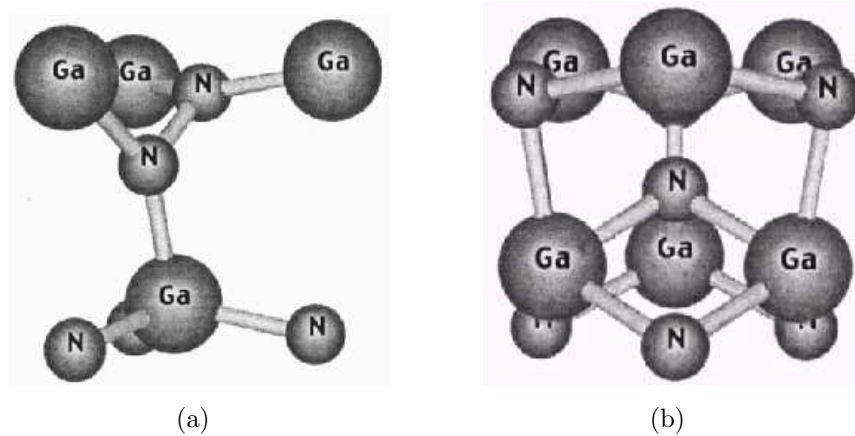


Figure 2: N Atomic structures for N_I : (a) Split-interstitial structure for N_I in the +3, +2, +1, neutral, and -1 charge states, (b) Channel-centered structure for N_I in the -3 charge state. [After A.F. Wright¹⁴]

The activation energy is estimated at 0.7 eV which is in good agreement with value of 0.9 eV predicted in the theoretical work of Limpijumnong et al.¹⁶ In n-type material the charge of Ga_I at thermal equilibrium is 1+ but for ODEPR measurements it needs to be excited to 2+ charge. Further work¹⁷ based on similar experimental results yields a tentative explanation in the form of two models for Ga_I-V_{Ga} Frenkel pairs. At this moment, however, it is not possible to elaborate more on the nature and distinct properties of these

defects because the technology involved is not perfected yet. It is also prudent to mention that the samples used in those measurements were specifically engineered to generate particular defects which are otherwise uncommon in standard growth GaN layers. In summary, there are two intrinsic interstitials: N_I which is quite mobile at room temperature and usually forms defect complexes with donors (N_I-O_N or N_I-Si_{Ga}) or interstitial hydrogen N_I-H_I and Ga_I which is also quite mobile and is tentatively proposed to form Ga_I-V_{Ga} Frenkel pair defects.

Extrinsic interstitials and substitutional atoms There are two reasons for foreign atoms to be found in GaN layers, those are: intentional doping which is meant to change the electrical properties of the sample making it either n- or p-type; or unintentional doping which is a result of impurity incorporation during the growth process.

At this time, commonly cited candidates for dominant unintentionally introduced donors at room temperature in GaN are Si, O and C. Si incorporates in place of Ga atom and O substitutes N. When electrically neutral, the Si activation energy is a few tens of meV below the conduction band.¹⁸ The exact Si activation energy is not well established; thermal, e.g. Hall effect, values can be as low as 12 meV¹⁹ but are more commonly found around 17 meV.¹⁸ On the other hand, infrared (IR) optical excitation spectra have given an activation energy for the shallowest observed donor of about 31 meV. Theoretical values previously derived for Si_{Ga} and O_N fall in the range 29.5 – 34.0 meV. The correlation between theoretical and experimental values shows that Si_{Ga} is a donor with binding energy of 30.2 meV and O_N is also a donor with a binding energy of 33.2 meV. Apart from being an unintentional dopant Silicon can be in fact also used for n-type doping of device layers. Oxygen is, however, a pure unintentional dopant which is currently believed to be responsible for n-type conductivity of unintentionally doped (UID) layers. It is also the origin of the most pronounced PL peak in the spectra of such samples – so called Donor Bound Exciton (DBE).

One of the methods of obtaining p-type conductivity is, as previously stated, Mg doping. In such case Mg is incorporated into Ga site and becomes an acceptor. However, it forms Mg-N-H complexes and/or traps V_N readily and therefore layers need to be annealed in order to dissociate these complexes and obtain p-type conductivity. Due to this and other problems with this material there have been attempts to use carbon as an

acceptor when it is built-in substitutionally into the N site. It should then act as a compensating centre for intrinsic donors to produce semi insulating (SI) or p-type material. Incidentally, in p-type material, carbon related deep levels are responsible for strong Y1,²⁰ otherwise attributed to V_{Ga} - O_N complexes. However, in p-type layers formation of gallium vacancies is negligible. Theoretical calculations²¹ show that for GaN layers grown under N-rich conditions (the most common way) the incorporation position for carbon is dependent on the Fermi level, i.e. on the background doping. For values higher than the middle of the bandgap C builds in on the N-site while for those below it creates C_{Ga} substitutional. This has been confirmed by experimental results²² on layers which have been intentionally doped by both Si and C. In samples where the carbon concentration is less than that of silicon, carbon substitutes for N, acting as an acceptor and partially compensating the material. However, when carbon densities exceed those for Si, GaN becomes semi insulating due to carbon occupation of both N and Ga sites. Because the formation energies of both substitutional sites are strong functions of the Fermi level, a self-compensation occurs. C_N formation lowers the Fermi level down to the range when C_{Ga} formation is more favourable, which effectively pins the Fermi level and causes semi-insulating behaviour. Growth in Ga-rich conditions causes the formation energy of C_N to be lowest for all values of Fermi level so in this case it would become a shallow acceptor in GaN:C.

There is also a third position that C may occupy in GaN layers according to theoretical calculations and that is as a channel interstitial. Recent experimental work²³ with the use of deep level optical spectroscopy and deep level transient spectroscopy have shown two deep band-gap states at -3.28 eV and -1.35 eV relative to the conduction band minimum in n-type compensated GaN:C:Si which are due to C_N acceptor and C_I which is in direct correlation with the theory.

In summary, foreign atoms most commonly present in the GaN layers can be either intentional or unintentional dopants. Oxygen and silicon, being the most common, are shallow donors in the O_N and Si_{Ga} configuration. Magnesium is used as a p-type dopant and incorporates as Mg_{Ga} acceptor. Carbon, on the other hand, can build in as a shallow acceptor C_N , or shallow donor C_{Ga} depending on the Fermi level position and growth stoichiometry. It can also build in as channel C_I interstitial in which case it becomes a deep acceptor.

2.2 Line defects

In the many years since GaN has become an important topic of semiconductor research, there has been no reliable way to make large size substrates for industrial purposes. Therefore the substrates of choice remain sapphire and silicon carbide (SiC). However, both these materials possess not only different crystallographic structure and lattice dimensions from those of GaN, but also different thermal expansion coefficients and therefore sample layers grown on them contain a large number of structural defects. These defects include mostly dislocations of the edge, screw or mixed type, inversion domains (ID) as well as nanopipes.

A schematic diagram after D. Hull and D.J. Bacon²⁴ in fig. 3 shows the basic concept of an edge and screw dislocation.

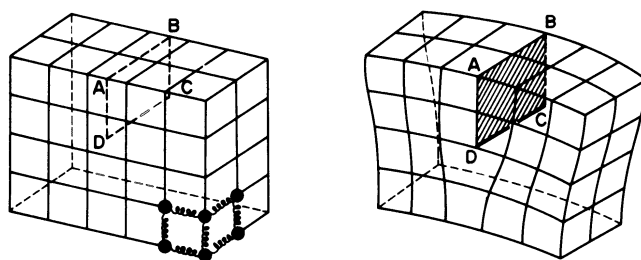


Figure 3: (a) Model of a simple cubic lattice; the atoms are represented by filled circles and bonds between atoms by springs, only a few of which are shown; (b) positive edge dislocation DC formed by inserting extra half-plane of atoms in ABCD. [After D. Hull and D.J. Bacon²⁴]

Figure 3(a) shows an undisturbed lattice; if all the bonds along the ABCD surface were to be broken and an extra half plane was inserted in that position the original surfaces would have been separated by a one-atom spacing (fig. 3(b)). The only place, though, where there would be a large displacement of atoms from their original position is in direct vicinity of the line DC. The line DC is in this configuration called a “positive edge dislocation” and denoted by \cdot . If the extra half plane was inserted below plane ABCD then the line DC would be so called “negative edge dislocation” and labelled \ominus . Arrangement of atoms around a screw dislocation is due to displacement in the AB direction of the crystal on one side of the ABCD plane with respect to the other side, as shown in fig. 4. Parallel planes initially perpendicular to the line DC become a single surface with a spiral nature. If the helix advances when a

clockwise circuit is made around the dislocation line (looking down that line) than the dislocation is called a “right-handed screw” dislocation, otherwise a “left-handed screw” dislocation.

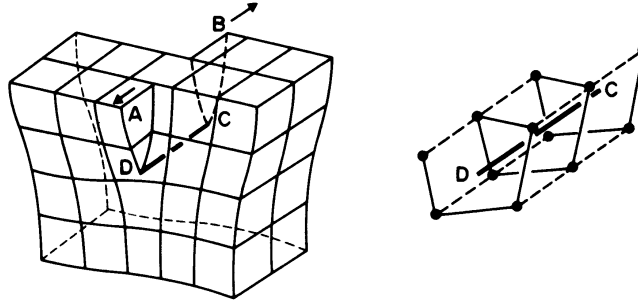


Figure 4: Left-handed screw dislocation DC formed by displacing the faces ABCD relative to each other in direction AB; (b) spiral of atoms adjacent to the line DC. [After D. Hull and D.J. Bacon²⁴]

The technical definition of a dislocation is by means of Burgers vector. It is defined as a vector equal to the difference between Burgers circuit made around a dislocation line and one made around an equivalent undisturbed crystal. Figure 5 shows that Burgers circuit is simply a closed path taken from atom to atom around a certain area. There are two important conclusions to be made based on these facts: the Burgers vector of an edge dislocation is normal to the line of the dislocation, while the Burgers vector of a screw dislocation is always parallel to the dislocation line.

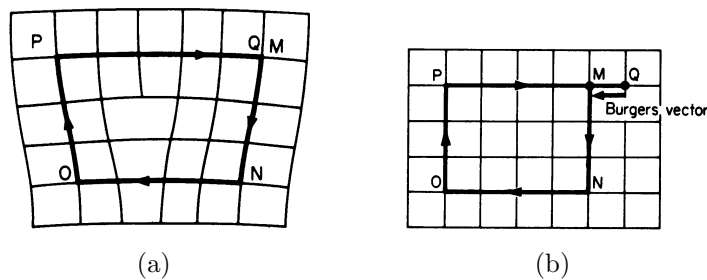


Figure 5: (a) Burgers circuit round an edge dislocation and (b) the same circuit in a perfect crystal; the closure failure is the Burgers vector. [after D. Hull and D.J. Bacon²⁴]

In GaN which has in general wurtzite type structure the geometry is not as simple as for cubic lattices. The smallest translation vectors in the wurtzite

structure are: a – type $\frac{1}{3}\langle\bar{1}2\bar{1}0\rangle$ and c – type $\langle 0001\rangle$. They are also the Burgers vectors of the simplest threading dislocations, i.e. dislocations parallel to the c -axis which penetrate through the thickness of the layer. These simple dislocations are: an edge dislocation with Burgers vector $\mathbf{b}=\mathbf{a}$ and a screw dislocation with $\mathbf{b}=\mathbf{c}$. A mixed dislocation is a linear combination of edge and screw dislocations, e.g. a dislocation in the $[\bar{1}\bar{1}01]$.

$$\begin{aligned} \frac{1}{3}\langle 11\bar{2}0\rangle + [0001] &\rightarrow \frac{1}{3}\langle 11\bar{2}3\rangle \\ \text{edge} + \text{screw} &\rightarrow \text{mixed} \end{aligned}$$

(note that $[\bar{1}2\bar{1}0]$ and $[\bar{2}110]$ are the same type displacements at an angle of 120° to each other).

A detailed description of all dislocations possible within the wurtzite structure can be found elsewhere,^{25,26} while I would like to concentrate on dislocations specific for GaN. They are important not only for their own intrinsic properties but also for the fact that earlier mentioned point defects such as vacancies, interstitials or impurities might be attracted to them. The sum of these defects with their individual properties has a very detrimental effect on the potential device performance. Such dislocations are commonly called “decorated” dislocations.

By far, the most common of the structural defects in GaN layers grown on the mentioned substrates is the threading dislocation. In the initial phase of growth a GaN buffer layer is deposited which role is to release the strain and match the later grown high quality GaN main layer to the substrate.^{27–29} However, the remaining strain still induces a large number of dislocations of the order of 10^9 - 10^{10} cm^{-2} for sapphire substrates³⁰ and one order of magnitude lower for SiC substrates. The quantitative distribution of the different types of defects is usually around the 80 % edge dislocations, 17 % mixed dislocations, 3 % pure screw dislocations. Hino *et al.*³¹ has shown a correlation between etch pits formed after vapor-phase etching in HCl and these kinds of dislocations. His conclusions after TEM, AFM and PL measurements were that dislocations having a screw component act as nonradiative recombination centres whereas the edge dislocations do not show electrical activity. Arslan and Browning³² in their theoretical work argue that there are no localized states present in the gap which could be explained just by the existence of intrinsic dislocation cores. That means that undecorated threading dislocations should not be electrically active. In the same work the authors perform a simulation on a core containing Ga-

vacancies and the results in this case show electrical activity in such case. It is therefore plausible that experimental electrical activity which limits the performance of GaN based devices is a result of aggregation of intrinsic defects as well as dopants and impurities. Further theoretical work, which takes into account doping and growth conditions,³³ proves that the stress field of threading edge dislocations is likely to trap gallium vacancies, oxygen atoms and gallium vacancy-oxygen defect complexes. Experiments show that these as well as mixed dislocations become electrically active and negatively charged in n-type GaN³⁴ while pure screw dislocations show no significant charge but instead turn into localized leakage paths. Direct atomic scale observations³⁵ show that there is a significant difference between different types of screw dislocations. An open core screw dislocation (nanopipe) tends to accumulate Oxygen on its inside edges up to the depth of approximately 20 monolayers. The second type of screw dislocation, a filled nanopipe is an open core screw dislocation which closed up at a later stage of growth, presumably by filling with liquid Ga which later reacted with N to form GaN. This type shows much smaller O aggregation and its distribution suggests that it happened during stage of growth when the dislocation was open. On the other hand, a full core, threading, screw dislocation exhibits no measurable O content. This indicates that open core screw dislocations might be the most detrimental to device operation.

Another factor in the effect of dislocations on the properties of materials is the fact that GaN is a polar material, i.e. the opposing directions along the c-axis are not the same from crystallographic point of view. The strain distribution associated with the dislocations may have impact through an extra piezoelectric effect. According to theoretical calculations such an effect does not occur for pure screw dislocations but is quite pronounced for pure edge dislocations.³⁶ The mixed dislocations are affected to the extent of their edge component. The effect of that is not significant for bulk materials but produces piezoelectrically induced charges localized at intersections of dislocations and surfaces or interfaces. Thus, in addition to impurity effect, multi-layer devices such as HEMTs might suffer additional decrease in performance. Indeed, for a test HEMT a doubling of dislocation density results in $\sim 17\%$ and $\sim 9\%$ decrease of electron mobility at temperatures 77 K and 300 K respectively.³⁷

Apart from the threading dislocations which are parallel to the c-axis, there are also mismatch dislocations parallel to c-plane, usually located close

to the interface of the sample. Transmission Electron Microscopy Cathodoluminescence (TEM-CL) measurements show that edge dislocations both having the same Burgers vector \mathbf{a} but different directions, a case of threading versus mismatch dislocation, have a large difference in recombination rates.³⁸ Where threading edge dislocations have negligible electrical activity, the mismatch kind shows much larger recombination rate. This difference is considered to originate from the difference in dislocation core structures, namely, the nature of dangling bonds at the core. Threading edge dislocation has dangling bonds for both N and Ga atoms while an edge dislocation parallel to the c-plane has dangling bonds for either N or Ga atoms and not for both.

2.3 Planar defects

Adding extra dimensions to the defects described before yields a number of larger defects. These include 2 dimensional or planar defects such as stacking faults, twin boundaries as well as low and high angle boundaries. Precipitates, inclusions, voids and striations constitute volume defects.³⁹

Stacking faults (SF) are errors in the stacking sequence of atomic planes when the perfect order of atomic planes of the crystal is disturbed. The original stacking sequence in the (0001) direction for wurtzite GaN is:

$$\dots\text{AaBbAaBbAaBbAaBb}\dots$$

where capital and lowercase letters correspond to Ga and N atoms, respectively. There are four types of stacking faults possible in such case.⁴⁰

Type-I stacking fault (also called I_1) contains one violation of the stacking rule and is commonly expected to have the lowest formation energy. For this type of fault two stacking sequences can be considered: $\dots\text{AaBbCcBb}\dots$ (as shown in fig. 6(a)) and $\dots\text{AaBbAaCcAaCc}\dots$ but they are equivalent and have the same energy.

Type-II stacking fault (I_2) containing two violations of the stacking rule is shown in fig. 6(b).

Type-III stacking fault is an intrinsic fault in which one of the Aa or Bb layers occupies the wrong Cc position, e.g. $\text{AaBbAaCcAaBb}\dots$; which according to theoretical predictions has the second lowest formation energy.

Extrinsic (E) stacking fault where an extra plane is added between normal atomic layers, e.g. $\dots\text{AaBbCcAaBb}\dots$

The theoretical calculations predict the formation energies of these stacking faults to be 10, 24, 19 and 38 meV for I_1 , I_2 , Type-III and E stacking faults, respectively. There are several high resolution transmission electron microscopy (HRTEM) reports on the existence of I_1 ^{41,42} but also I_2 and E stacking faults can be found.⁴³ Because, for Type-I stacking fault a removal of one double layer is necessary it cannot be the result of splitting a perfect dislocation into partials. Nevertheless, due to its lowest formation energy it is believed to form during the growth process.

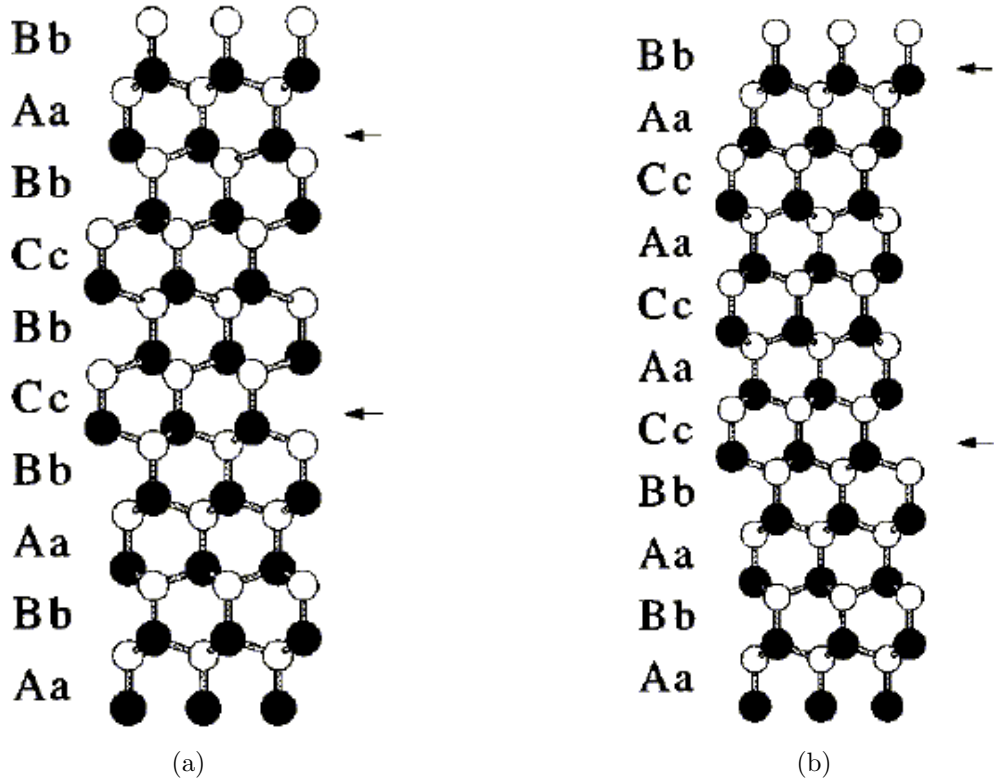


Figure 6: Stacking faults : (a) type I, (b) type II. The arrows indicate the position of the stacking faults and the black and white circles denote cations and anions, respectively.

Type-II, however, can be formed directly by shear or after a dissociation of a pure edge dislocation into two Shockley partial dislocations.

$$\frac{1}{3} \langle 11\bar{2}0 \rangle \rightarrow \frac{1}{3} \langle 10\bar{1}0 \rangle + \frac{1}{3} \langle 01\bar{1}0 \rangle$$

Stacking faults do not generate interface levels in the bandgap, but since they can be regarded as an insertion of zinc-blende (ZB) phase into wurtzite

(WZ) lattice there is a bandgap difference to be expected. Experimental results indicate a luminescence line at 3.40 eV⁴⁴ and theoretical calculations predict it to be due to so called type-II line-up where the electronic states at the conduction band minimum are localized in the ZB region, while those at the valence band maximum are confined to WZ region.

The stacking fault energy is also found to be lowered by impurities such as In, Mg, C and Si.⁴⁵ The most significant effect is due to Si doping and is calculated to be the result of an increase in covalent bonding as silicon is incorporated into lattice.⁴⁶ On the other hand stacking faults have also influence on the segregation of impurities as has been calculated for magnesium atoms. Mg is preferentially incorporated into WZ GaN, so that in a ZB lattice containing stacking fault Mg segregates towards the SF, while in WZ lattice the most stable position is assumed away from the SF.⁴⁷ It is suggested that local strain relief processes are responsible for this behaviour. SFs bound by dislocations (faulted dislocation loops) are frequently observed in Mg-doped GaN single crystals. They can be revealed and analysed both by TEM and selective etching.⁴⁸

A completely different kind of a threading defect is an Inversion Domain (ID). As previously mentioned GaN is a polar material, its growth along the *c*-axis might be oriented in such a way that the surface is terminated either with Ga or N atoms. It is not just a property of the surface, the polarity is determined by the position of Ga and N atoms along the vertical bond in the GaN structure. Therefore a complete sample across its entire thickness might have either Ga- or N-polarity. However, there are local perturbations to this geometry. Small areas at the interface between GaN layer and substrate may give rise to columnar defects which have polarity opposite to the matrix. Therefore there might be N-polar IDs in Ga matrix⁴⁹ or Ga-polar IDs in N-polar matrix.⁵⁰ In the second case it is important to note the existence of two types of IDs, small ones measuring ~ 20 nm in diameter which are quite frequent and large ones with diameters ranging from 500 nm to 3 μm placed in the centers of growth pyramids commonly associated with N-polar growth. The fact that material is inverted should not affect its electrical characteristics to any extent but as with the case of dislocations the problem is the impurity incorporation. In fact if both polarities are grown at the same time, the incorporation of O is much stronger into the N-polar areas.⁵¹ Therefore it is expected that N-polar IDs in Ga-polar matrix will locally have much higher electron concentration.

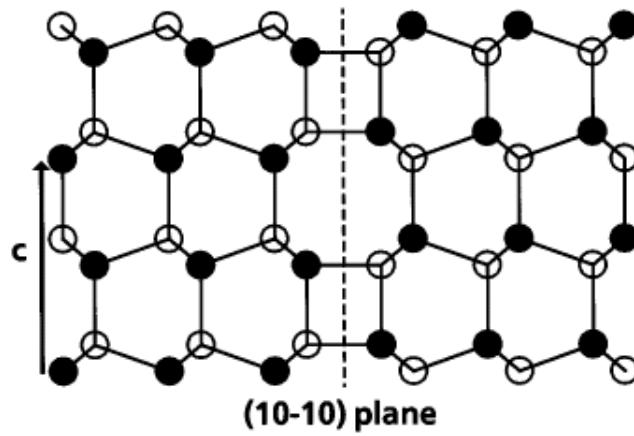


Figure 7: Schematic representation of IDB*. This structure can be formed by translating one side of an IDB by $c/2$ along the $[0001]$ direction. The IDB* structure contains fourfold and eightfold rings of bonds, but there are no Ga-Ga or N-N bonds.

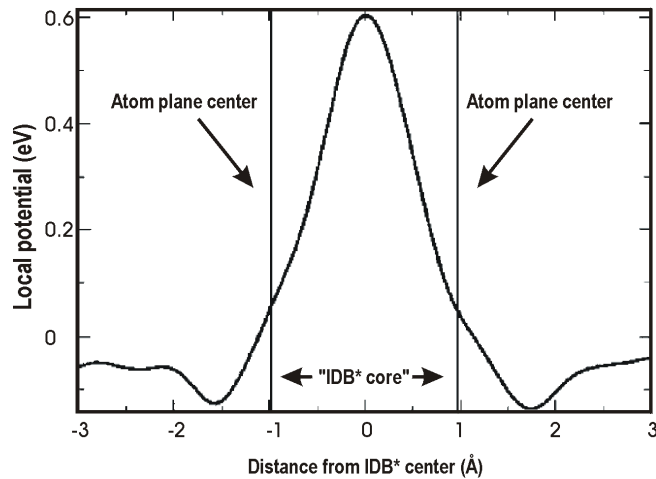


Figure 8: Potential plot of an IDB*; the potential captures holes and leads to accumulation of electrons on both sides resulting in enhanced PL.

Also the interface between Ga- and N-polar materials is very important. A model proposed by Northrup *et al.* postulates a bending of bonds between Ga and N atoms up to a square configuration and shift of the matrix by $c/2$ to allow for Ga-N bonds instead of Ga-Ga and N-N bonds.⁵² Such a configuration, shown in fig. 7, is consistent with a postulate that IDs might nucleate at the surface steps on the substrate, but it is also more energetically

favourable for the inversion domain boundary (IDB) formation.

However, it does not explain the obvious electrical activity which is unique for the IDB and not for the material inside the ID. Such activity is predominantly visible in PL experiments⁵³⁻⁵⁵ and also by defect selective etching.^{50,51} A theoretical study by V. Fiorentini⁵⁶ shows that the local disturbance in the lattice parameters due to the square bonds creates a potential across the IDB which is very efficient at capturing holes between the Ga and N atoms and at the same time accumulates electrons on both sides of the IDB, as shown in fig. 8. This situation causes increased radiative recombination clearly visible in PL.

References

- [1] M.J. Puska, R.M. Nieminen, *Rev. Mod. Phys.* **66**, 841 (1994).
- [2] J. Neugebauer, C.G. Van de Walle, *Appl. Phys. Lett.* **69**, 503 (1996)
- [3] J. Oila, J. Kivioja, V. Ranki, K. Saarinen, D.C. Look, R.J. Molnar, S.S. Park, S.K. Lee, J.Y. Han, *Appl. Phys. Lett.* **82**, 3433 (2003)
- [4] K. Saarinen, T. Suski, I. Grzegory, D.C. Look, *Phys. Rev. B*, **64**, 233201 (2001)
- [5] X.L. Sun, S.H. Gross, L.J. Brillson, D.C. Look, R.J. Molnar, *J. Appl. Phys.* **91**, 6729 (2002)
- [6] J. Oila, V. Ranki, J. Kivioja, K. Saarinen, P. Hautojärvi, J. Likonen, J.M. Baranowski, K. Pakula, T. Suski, M. Leszczynski, I. Grzegory, *Phys. Rev. B* **63**, 45205 (2001)
- [7] A.F. Wright, *J. Appl. Phys.* **90**, 1164 (2001)
- [8] H.P. Maruska, J.J. Tietjen, *Appl. Phys. Lett.* **15**, 327 (1969)
- [9] J. Neugebauer, C.G. Van de Walle, *Phys. Rev. B* **50**, 5067 (1994)
- [10] S. Hautakangas, J. Oila, M. Alatalo, K. Saarinen, L. Liskay, D. Seghier, H.P. Gislason, *Phys. Rev. Lett.* **90**, 137402 (2003)
- [11] C.D. Latham, R. Jones, S. Öberg, R.M. Nieminen, P.R. Briddon, *Phys. Rev. B* **68**, 205209 (2003)
- [12] Q. Yang, H. Feick, E.R. Weber, *Appl. Phys. Lett.* **82**, 3002 (2003)
- [13] D.C. Look, G.C. Farlow, P.J. Drevinsky, D.F. Bliss, J.R. Sizelove, *Appl. Phys. Lett.* **83**, 3525 (2003)
- [14] A.F. Wright, *J. Appl. Phys.* **90**, 6526 (2001)
- [15] K.H. Chow, G.D. Watkins, A. Usui, M. Mizuta, *Phys. Rev. Lett.* **85**, 2761 (2000)

- [16] S. Limpijumnong, C.G. Van de Walle, Phys. Rev. B **69**, 35207 (2004)
- [17] K.H. Chow, L.S. Vlasenko, P. Johannesen, C. Bozdog, G.D. Watkins, A. Usui, H. Sunakawa, C. Sasaoka, M. Mizuta, Phys. Rev. B **69** 45207 (2004)
- [18] D.C. Look, D.C. Reynolds, J.W. Hemsky, J.R. Sizelove, R.L. Jones, R. J. Molnar, Phys. Rev. Lett. **79**, 2273 (1997)
- [19] W. Götz, N.M. Johnson, C. Chen, H. Liu, C. Kuo, W. Imler, Appl. Phys. Lett. **68**, 3144 (1996)
- [20] R. Armitage, W. Hong, Q. Yang, H. feick, J. Gebauer E.R. Weber, S. Hautakangas, K. Saarinen, Appl. Phys. Lett. **82**, 3457 (2003)
- [21] A.F. Wright, J. Appl. Phys. **92**, 2575 (2002)
- [22] C.H. Seager, A.F. Wright, J. Yu, W. Götz, J. Appl. Phys. **92**, 6553 (2002)
- [23] A. Armstrong, A.R. Arehart, B. Moran, S.P. DenBaars, U.K. Mishra, J.S. Speck, S.A. Ringel, Appl. Phys. Lett. **84**, 374 (2004)
- [24] D. Hull, D.J. Bacon, *Introduction to Dislocations*, Pergamon Press 1984
- [25] Y.A. Osibiyani, I.S. Smirnova, Phys. Stat. Sol. **30**, 19 (1968)
- [26] Y.A. Osipyan, I.S. Smirnova, J. Phys. Chem. Solids **32**, 1521 (1971)
- [27] M. Sumiya, N. Ogusu, Y. Yotsuda, M. Itoh, S. Fuke, T. Nakamura, S. Mochizuki, T. Sano, S. Kamiyama, H. Amano, I. Akasaki, J. Appl. Phys. **93**, 1311 (2003)
- [28] T. Kachi, K. Tomita, K. Itoh, H. Tadano, Appl. Phys. Lett. **72**, 704 (1998)
- [29] H.K. Cho, J.Y. Lee, K.S. Kim, G.M. Yang, J.H. Song, P.W. Yu, J. Appl. Phys. **89**, 2617 (2001)
- [30] D. Huang, M.A. Reshchikov, P. Visconti, F. Yun, A.A. Baski, T. King, H. Morkoç, J. Jasinski, Z. Liliental-Weber, C. W. Litton, J. Vac. Sci. Tech. B, **20**, 2256 (2002)
- [31] T. Hino, S. Tomiya, T. Miyajima, K. Yanashima, S. Hashimoto, M. Ikeda, Appl. Phys. Lett. **76**, 3421 (2000)
- [32] I. Arslan, N.D. Browning, Phys. Rev. B **65**, 075310 (2002)
- [33] J. Elsner, R. Jones, M.I. Heggie, P.K. Stitch, M. Haugk, Th. Frauenheim, S. Öberg, P.R. Briddon, Phys. Rev. B, **58**, 12571 (1998)
- [34] B.S. Simpkins E.T. Yu, P. Waltereit, J.S. Speck, J. Appl. Phys. **94**, 1448 (2003)
- [35] I. Arslan, N.D Browning, Phys. Rev. Lett. **91**, 165501 (2003)
- [36] C. Shi, P.M. Asbeck, E.T. Yu, Appl. Phys. Lett. **74**, 573 (1999)

- [37] R.P. Joshi, S. Visvanadha, B. Jogai, P. Shah, R.D. del Rosario, *J. Appl. Phys.* **93**, 10046 (2003)
- [38] N. Yamamoto, H. Itoh, V. Grillo, S.F. chichibu, S. Keller, J.S. Speck, S.P. DenBaars, U.K. Mishra, S. Nakamura, G. Salviati, *J. Appl. Phys.* **94**, 4315 (2003)
- [39] J.L. Weyher, G. Kamler, G. Nowak, J. Borysiuk, B. ucznik, M. Krysco, I. Grzegory, S. Porowski, *J. Crystal Growth – accepted for publication (2005)*
- [40] C. Stampfl, C.G. Van de Walle, *Phys. Rev. B* **57**, R15052 (1998)
- [41] N.E. Lee, R.C. Powell, Y.W. Kim, J.E. Greene, *J. Vac. Sci. Technol. A* **13**, 2293 (1995)
- [42] X.H. Wu, L.M. Brown, D. Kapolnek, S. Keller, B. Keller, S.P. DenBaars, J.S. Speck, *J. Appl. Phys.* **80**, 3228 (1996)
- [43] V. Potin, B. Gil, S. Charar, P. Ruterana, G. Nouet, *Mat. Sci. Eng.* **B82**, 114 (2001)
- [44] M. Albrecht, S. Christiansen, G. Salviati, C. Zanotti-Fregonara, Y.T. Rebane, Y.G. Shreter, M. Mayer, A. Pelzmann, M. Kamp, K.J. Ebeling, M.D. Bremser, R.F. Davis, H.P. Strunk, *Gallium Nitride and Related Materials II*, edited by C.R. Abernathy. H. Amano, J.C Zolper, MRS Symposia Proceedings No. 468 (Materials Research Society, Pittsburgh, 1997), p.293
- [45] J.A. Chisholm, P.D. Bristowe, *J. Crystal Growth* **230**, 432 (2001)
- [46] J.A. Chisholm, P.D. Bristowe, *Appl. Phys. Lett.* **77**, 534 (2000)
- [47] T.M. Schmidt, R.H. Miwa, W. Orellana, H. Chacham, *Phys. Rev. B* **65** 33205 (2002)
- [48] G. Kamler, J. Borysiuk, J.L. Weyher, M. Woniak, I. Grzegory, *EPJ Appl. Phys.* **27**, 247 (2004)
- [49] L.T. Romano, J.E. Northrup, M.A. O’Keefe, *Appl. Phys. Lett.* **69**, 2394 (1996)
- [50] J.L. Weyher, F. D. Tichelaar, H. W. Zandbergen, L. Macht, P. R. Hageman, *J. Appl. Phys.* **90**, 6105 (2001)
- [51] L. Macht, J.L. Weyher, P.R. Hageman, M. Zielinski, *J. Phys.: Condens. Matter* **14**, 13345 (2002)
- [52] J.E. Northrup, J. Neugebauer, L.T. roman, *Phys. Rev. Lett.* **77**, 103 (1996)
- [53] P.J. Schuck, M.D. Mason, R.D. Grober, O. Ambacher, A.P. C. Miskys, R. Dimitrov, M. Stutzman, *Appl. Phys. Lett.* **79**, 952 (2001)

- [54] W.-C. Yang, B.J. Rodriguez, M. Park, R.J. Nemanich, O. Ambacher, V. Cimalla, J. Appl. Phys. **94** 5720 (2003)
- [55] M.A. Reshchikov, D. Huang, F. Yun, P. Visconti, L. He, H. Morkoç, J. Jasinsky, Z. Lilental-Weber, R.J. Molnar, S.S. Park, K.Y. Lee, J. Appl. Phys. **94**, 5623 (2003)
- [56] V. Fiorentini, Appl. Phys. Lett. **82**, 1182 (2003)

Chapter 3

Defects in wide band-gap semiconductors: selective etching and calibration by complementary methods ¹

3.1 Introduction to defect selective etching

Defect-selective etching is a standard method for determining the density and distribution of dislocations in semiconductor crystals. The classical (orthodox) etching is known to reveal dislocations in the form of well defined etch pits, which can be automatically counted.¹ The EPD (etch pit density) value is given as one of the standard characteristic parameters in the specification of all semiconductor substrates. Due to the complex nature of defects in compound semiconductors, more sophisticated etching procedures were developed (e.g. shallow photo-etching, projective etching) and were shown to be effective in studying crystallographic and chemical non-homogeneities in GaAs.^{2,3} For wide gap semiconductors, (especially GaN), the progress in defect-selective etching trailed behind the use of other methods of structural characterization (e.g. TEM), because of the high chemical resistance of this material and polarity-related strong anisotropy.

¹Chapter based on: “Defects in wide band-gap semiconductors: selective etching and calibration by complementary methods”, J.L. Weyher, L. Macht, *Eur. Phys. J. Appl. Phys.* **27**, 37 (2004)

In addition, the most commonly grown hetero-epitaxial GaN layers and structures contain dislocations of very high density (up to 10^{10} cm⁻²) and co-existing with dislocations specific type of defects, such as nano-pipes, pinholes and inversion domains. The combination of these factors makes it difficult to develop a reliable and universal defect-selective etching procedure. SiC bulk single crystals are characterized by much lower dislocation density, but the common defects are micro-pipes, low angle grain boundaries and polytype lamellas. Despite these unfavourable features of the wide band-gap semiconductors, large scale research performed recently resulted in introduction of different etching systems both for GaN and SiC. The aim of this paper is to summarize the data on the defect-selective etching methods used at present for both materials and to emphasize their advantages and limitations.

3.2 Etching of GaN.

GaN and related compounds are resistant to the majority of acids and bases used at temperatures up to 75 ° C.⁴ Until now, two approaches appeared to be useful in revealing defects in this material: (i) etching in acids or bases at elevated temperature (orthodox method) and (ii) room temperature etching activated by the use of light with the energy larger than the band gap.

3.2.1 Orthodox etches.

This group consists of H₂SO₄, H₃PO₄ and the mixture of both (HH etch),⁵⁻¹³ molten KOH, NaOH and their eutectic mixture,^{11,13-20} as well as, vapour phase HCl.³¹ The mechanism of surface reactions has not been studied in detail, but there are arguments that it is purely chemical with surface kinetics as the rate limiting step. As a result preferential dissolution of defects can be expected due to their contribution to the local changes of surface energy. Indeed all these etches result in formation of etch pits on the outcrops of dislocations, i.e. they can be classified as orthodox etches. The assumed reactions during etching are as follows:

- in H₃PO₄: $\text{GaN} + \text{H}_3\text{PO}_4 \rightarrow \text{Ga}^{3+} + \text{PO}_4^{3-} + \text{NH}_3 \uparrow$ ¹⁰
- in molten bases: $\text{GaN} + 3\text{H}_2\text{O} \rightarrow \text{Ga}(\text{OH})_3 + \text{NH}_3 \uparrow$ ²²
- in vapor of HCl: $\text{GaN} + 3\text{HCl}(\text{g}) \rightarrow \text{GaCl}_3(\text{g}) + \text{NH}_3(\text{g})$ ²¹

It has to be remarked that in the second reaction water comes from the environment (KOH is strongly hygroscopic) and from the OH^- ions in the melt.

The pits formed on the Ga-polar (0001) surfaces of GaN by these etches are crystallographic hexagonal-shaped, with the edges of pits parallel to the low index $\{1100\}$ planes. Only on the N-polar surface of GaN single crystals the round-shape pits were observed.^{19,23} This method is particularly suited for quantitative estimation of the density of dislocations in GaN single crystals and epitaxial layers. It can be also used for study of other defects, e.g. stacking faults^{24,25} and micro-defects²⁶ both on basal and on low-index cleavage planes. The resultant etch features are then more complex (e.g. pyramidal hillocks are formed on micro-defects related to Mg-doping²⁶ or complex pits on the faulted dislocation loops²⁵) and depend upon the chemical and crystallographic nature of the defects. Numerous examples of application of these etches for studying defects in GaN single crystals, homo- and hetero-epitaxial layers can be found in the cited references, but especially valuable are these, in which the results of different etching methods have been compared or calibrated by TEM and AFM.^{7, 11, 14, 17, 23, 25, 27, 31}

The reliability in revealing all types of dislocations, including open-core screw dislocations (nanopipes) was the main problem encountered when the new orthodox etches were applied for revealing defects in GaN. The dislocations in the wurtzite GaN lattice are characterized by large differences in the magnitude of the Burgers vector:

edge dislocations: $b_e = a$

screw dislocations: $b_s = 2,66 a$

mixed dislocations: $b_m = 3.66 a$, where a is the lattice constant.

The nanopipes can be considered as screw dislocations with $n \cdot b_s$ ($n=1,2,\dots$) value of Burgers vector.¹⁸ The thermodynamics of the etching process predicts that the change of the chemical potential during formation of the etch pits is inversely proportional to the energy of the defects; therefore, one could expect that defects of larger energy will be etched easier (or at lower temperature). Indeed, first results of etching in hot acids showed that only nanopipes give rise to the formation of etch pits.^{6,7,9} Later it was shown that dislocations are also revealed by this method; however, the density of pits was usually slightly lower than the density of dislocations established using etching by other methods or by TEM analysis.^{12,13,28} This discrepancy can be explained by taking into account the kinetic factor, which is also critical

for the formation of the pits: when the velocity of the horizontal movement of steps around the defect is higher than the nucleation rate of the pits on the low energy dislocations, then some small pits may be “swept” away by the quickly propagating steps of large pits formed on nanopipes, mixed or screw dislocations. Since the low energy edge dislocations prevail in the heteroepitaxial GaN layers, the large pits formed on the high energy defects may remarkably diminish the number of pits related to the edge dislocations and as a consequence result in underestimation of the total density of defects. This reasoning has been confirmed by the author’s own study, in which evidence was found for the “sweeping” effect, which resulted in an EPD after HH etching one order of magnitude lower than the EPD after (E+M) and photo-etching.²⁹ Evidently these acidic etches do not fulfil the kinetic-related conditions for the formation of deep pits on defects in GaN,² i.e. the ratio of pit diameter to depth is too large. In order to overcome this difficulty the optimised etching conditions (temperature and time) have to be employed, as was demonstrated by etching of GaN in another orthodox system.^{11,20} However, for proper selection of a reliable etching technique another factor has to be taken into account, namely the overall density of defects.

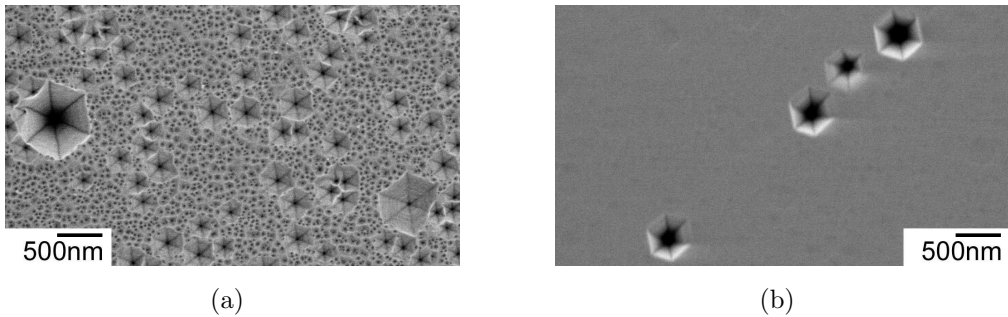


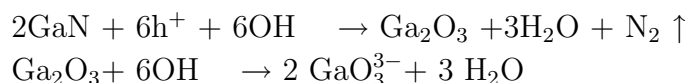
Figure 1: SEM images of defects after etching in molten (E+M) etch (notation after [20]): (a) Four size-grades of pits formed on nanopipes, mixed, screw and edge dislocations in AlGaIn (20%Al) hetero-epitaxial layer and (b) etch pits in the low-defect density homo-epitaxial GaN layer grown by HVPE method.

Figure 1(a) clearly demonstrates that in the material containing a dislocation density in the range $(2-5) \times 10^{10} \text{ cm}^{-2}$ (as established by TEM), the use of optimised orthodox etching will not allow precise estimation of the density of all types of defects: the smallest pits formed on the edge dislocations, though overwhelming in density, are visible only locally between the larger pits formed on nanopipes, screw and mixed type dislocations. In

contrast, any orthodox etching method is particularly suitable for revealing defects in GaN single crystals and HVPE-grown layers, see example in fig. 1(b). This etching technique is also favourable when the density of defects has to be established in resistive or heavily doped material, for which the photo-assisted etching method cannot be used (see comments in the next section).

3.2.2 Photo-etching (photoelectrochemical – PEC or electroless method).

Etching in aqueous KOH solutions with UV light is the best understood and explored method used for studying defects in GaN and related compounds. Youtsey *et al.* were the first to show that this etching system reveals dislocations in the form of protruding whisker-like etch features.^{30,31} The principle of photo-etching method was well recognized and described for GaAs:^{2,32} the photo-generated electron-hole pairs are separated in the space charge layer of n-type semiconductor immersed into the etching solution and the holes take active part in the dissolution process. Based on the electrochemical and spectroscopic studies^{33,34} the decomposition of GaN in aqueous KOH solution proceeds in two steps via oxidation of Ga and dissolution of the oxide:



When a low KOH concentration (in the range 0.002 – 0.01 M) stirred solution is used, the defects are revealed in the form of protruding whiskers, see fig. 2(a). Stirring is necessary in order to perform etching in the kinetically-controlled, instead of mass transport-controlled, mode.³⁵ By analogy to the photo-etching of GaAs it can be assumed, that the defects constitute effective sites for recombination of photo-generated carriers, resulting in formation of a cylinder (around e.g. straight threading dislocation) depleted in holes.

The critical diameter of this cylinder, in which the average number of holes is smaller than that required for dissolution of one GaN molecule (i.e. 3 holes, see reaction (4)), corresponds to the diameter of the unetched whisker, see a hypothetical model in fig. 2(b). For higher KOH concentration, instead of protruding etch features etch pits are formed,^{36,37} but the suggested association of these pits with dislocations was not confirmed by any direct structural method. Among the favourable features of the PEC techniques are:

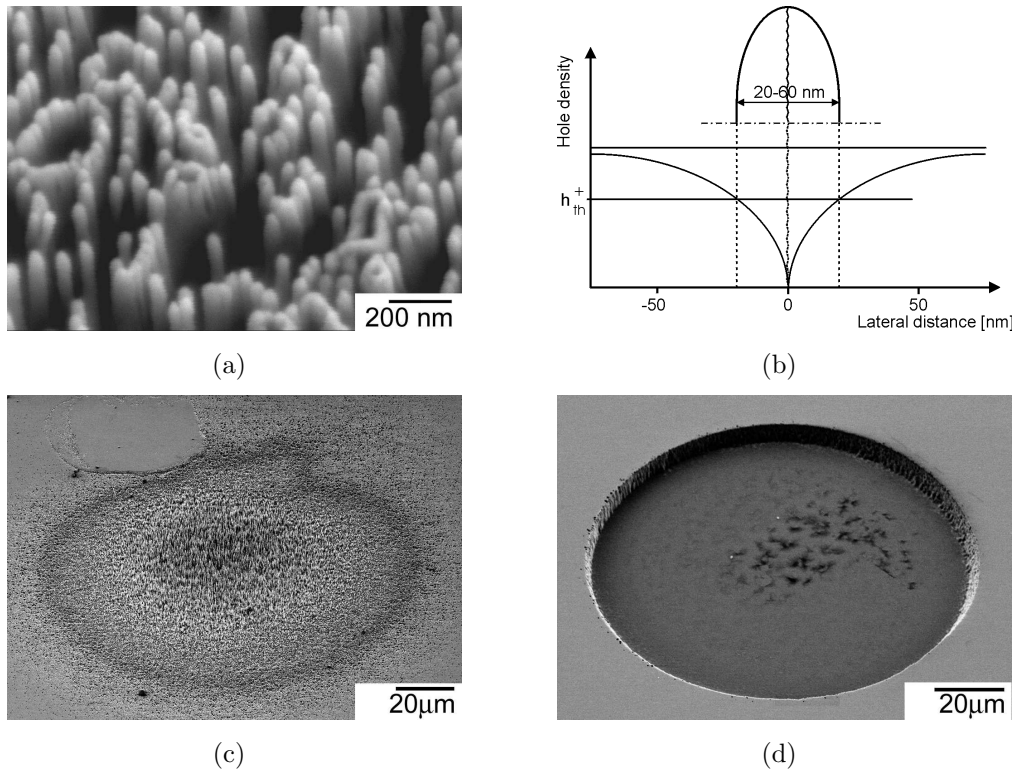


Figure 2: SEM image (a,c,d) of hetero-epitaxial n-type GaN layers after PEC etching in stirred (a,c) and non-stirred (d) 0.004 M KOH solution using 450 W Xe lamp illumination. In (c,d) the surface of GaN sample was locally illuminated through a quartz fibre. (b) Hypothetical model of the formation of a whisker on a linear threading defect during PEC etching of GaN.

(i) the possibility of large area or local etching (only the illuminated surface of the sample undergoes etching as is shown in fig. 2(c)), (ii) easy control of the mechanism of etching, e.g. by stirring (as an example fig. 2(d) shows a GaN layer locally etched in the same solution as used for revealing defects in fig. 2(c), but not stirred: the kinetically-controlled defect-selective etching was changed into diffusion-controlled smooth etching), (iii) revealing of all types of dislocations, inversion domains and inversion domain boundaries, nanowires, micro-defects and chemical inhomogeneities.^{13, 20, 23, 28, 30, 31, 38–41} It is also suitable for defect-selective etching of both N- and Ga-polar samples^{38, 40} and for GaN-related compound materials.²³ The fact, that the defects are preserved in the PEC-etched samples in the form of protruding features constitutes an important advantage of this method over the orthodox

etching technique.

The use of PEC etching is, however, limited to moderately n-type doped materials and always requires Ti contacts for removing electrons from the etched surface. This factor also limits the size of samples to be etched. Recently it was shown that this difficulty might be avoided by adding a strong oxidizing agent to the KOH solution, e.g. peroxydisulfate, which effectively removes electrons from the GaN surface.⁴² The usefulness of this modified etch for revealing defects has yet to be examined. Another drawback of the PEC etching versus the orthodox method is that no differences could be noticed in the morphology of the whiskers formed on different types of dislocation and nanopipes.

The reliability of both orthodox and PEC etching of GaN has been confirmed using different etching techniques on the same material, AFM measurements and direct calibration of the etch features by TEM.

3.3 Etching of Silicon Carbide.

For revealing defects in SiC, molten bases, particularly KOH, have been used for a long time. The results of the old work were summarized by Harris.⁴³ Molten KOH is frequently used as the reference etching method. It reveals different types of dislocations, micropipes and stacking faults, see some selected papers and references therein.⁴⁴⁻⁴⁸ Recently it has been found that the molten eutectic of (KOH+NaOH) with MgO (E+M etch)²⁵ is also effective in revealing defects in SiC,²⁹ see fig. 3. The advantage of this method is that no crucible is needed and that etching can be performed locally. Etching in molten bases is performed in the temperature range from 450 up to 570 °C for several minutes. The vapour of KOH also acts selectively on the defects in SiC but at much higher temperatures (up to 1000 °C).⁴⁹ Some attempts have been done to employ electrochemical etching methods for studying defects in SiC. Both highly concentrated (50 wt %) aqueous solution of KOH,⁵⁰ diluted HF (2 vol.%) and 0.05 M KOH electrolyte⁵¹ were used.

Good correlation was obtained between the etch pits formed during electrochemical etching and subsequent molten KOH etching; however, the differences in the etch pit morphology were attributed to different etching mechanisms. By analogy with GaN, it can be assumed that the dissolution of SiC in molten bases is chemical in nature, while electrochemical etching

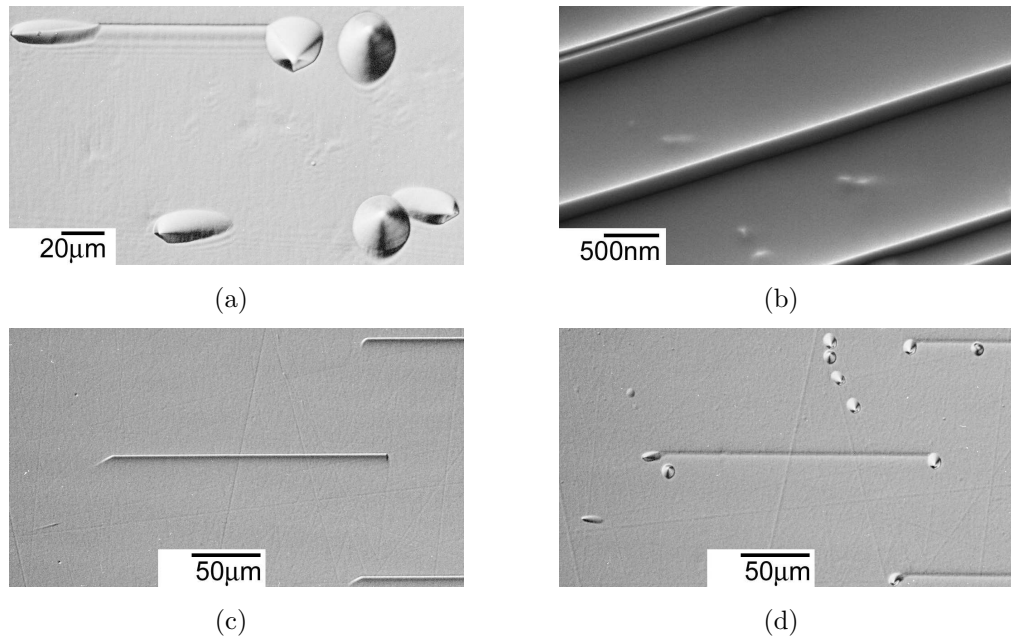
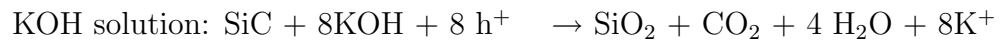
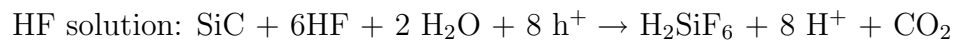


Figure 3: 4H SiC 8° off basal plane (a) and (1-100) cleavage plane (b) after etching in molten E+M at 520 ° C, optical DIC and SEM images, respectively. (c-d) DIC images of the basal plane of the same SiC crystal after: (c) PEC etching in 0.02M KOH solution and Xe lamp illumination and (d) the same sample as in (c) but after additional etching in molten E+M at 520 ° C.

proceeds via electroless oxidation-dissolution reactions, with the critical role of holes:²²



In fact the role of holes during photoelectrochemical etching of SiC in HF solution was already recognized.⁵² Consequently it could be concluded, that by analogy to GaN silicon carbide can be etched without the external source of current, but under UV illumination. Recently performed experiments confirmed the possibility of revealing defects in SiC using a Xe lamp and aqueous solution of KOH.²⁹ Figure 3(c) shows the result of PEC etching of n-type SiC with 8 deg. off basal plane. Subsequent etching of the same sample in molten E+M, as shown in fig. 3(d), clearly demonstrates that both stacking faults and bounding partial dislocations are revealed by PEC etching in the form of protruding etch features. This method requires further experiments in order to establish the optimal etching parameters and the

reliability of PEC method in revealing all types of defects.

References

- [1] N. Toyoda *et al.*, in Proceedings of the International Symposium on Defect Recognition and Image Processing in III-V Compounds, Montpellier, 1985, edited by J.P. Fillard (Elsevier, Amsterdam, 1985), p. 141
- [2] J.L. Weyher, in *Handbook on Semiconductors*, edited by S. Mahajan, Vol. 3 (Elsevier, Amsterdam, 1994), p. 995
- [3] J.L. Weyher, *Inst. Phys. Conf. Ser.* No 146, IOP (1995) 399-408
- [4] S.J. Pearton, J.C. Zolper, R.J. Shul, F. Ren, *Appl. Phys. Rev.* **86**, 1 (1999)
- [5] A. Shintani, S. Minagawa, *J. Electrochem. Soc.* **123**, 706 (1976)
- [6] M. Iwaya *et al.*, *Jpn. J. Appl. Phys.* **37**, L316 (1988)
- [7] S.K. Hong, B.J. Kim, H.S. Park, Y. Park, S.Y. Yoon, T.I. Kim, *J. Cryst. Growth* **191**, 275 (1998)
- [8] D.A. Stocker, E.F. Schubert, J.M. Redwing, *Appl. Phys. Lett.* **73**, 2654 (1998)
- [9] Y. Ono, Y. Iyechika, T. Takada, K. Inui, T. Matsue, *J. Cryst. Growth* **189/190**, 133 (1998)
- [10] M.G. Mynbaeva *et al.*, *Electrochem Sol.-State Lett.* **2**, 404 (1999)
- [11] J.L. Weyher *et al.*, *J. Cryst. Growth* **210**, 151 (2000)
- [12] J. Jasinski *et al.*, *Appl. Phys. Lett.* **78**, 2297 (2001)
- [13] P. Visconti *et al.* *Appl. Phys. Lett.* **77**, 3532 (2000)
- [14] T. Kozawa, T. Kachi, T. Ohwaki, Y. Taga, N. Koide, M. Koike, *J. Electrochem. Soc.* **143**, L17 (1996)
- [15] P. Hacke, A. Kuramata, K. Domen, K. Horino, T. Tanahasi, *phys. stat. sol. (b)* **216**, 639 (1999)
- [16] J.L. Rouviere, J.L. Weyher, M. Seelmann-Eggebert, S. Porowski, *Appl. Phys. Lett.* **73**, 668 (1998)
- [17] K. Shiojima, *J. Vac. Sci. Technol. B* **18**,) 37 (2000)
- [18] S.K. Hong, T. Yao, B.J. Kim, S.Y. Yoon, T.I. Kim, *Appl. Phys. Lett.* **77**, 82 (2000)
- [19] J.L. Weyher, *et al.*, *Mat. Sci. Eng.* **B80**, 318 (2001)
- [20] G. Kamler, J.L. Weyher, I. Grzegory, E. Jezierska, T. Wosinski, *J. Cryst. Growth* **246**, 21 (2002)

- [21] T. Hino *et al.*, Appl. Phys. Lett. **76**, 3421 (2000)
- [22] J.J. Kelly (private communication)
- [23] J.L. Weyher, L. Macht, G. Kamler, J. Borysiuk, I. Grzegory, phys. stat. sol. (c) **0**, 821 (2003)
- [24] T.L. Chu, K. Ito, R.K. Smeltzer, S.S.C. Chu, J. Electrochem. Soc. **121**, 159 (1974)
- [25] G. Kamler, J. Borysiuk, J.L. Weyher, A. Presz, M. Wozniak, I. Grzegory, DRIP !!!!!
- [26] I. Grzegory *et al.* phys. stat. sol. (b) **216**, 537 (1999)
- [27] M. Albrecht *et al.*, J. Appl. Phys. **92**, 2000 (2002)
- [28] P. Visconti *et al.* Mat. Sci. Eng. **B93**, 229 (2002)
- [29] J.L. Weyher, (unpublished)
- [30] C. Youtsey, L.T. Romano, I. Adesida, Appl. Phys. Lett. **73**, 797 (1998)
- [31] C. Youtsey, L.T. Romano, R.J. Molnar, I. Adesida, Appl. Phys. Lett. **74**, 3537 (1999)
- [32] J.L. Weyher, C. Frigeri, S. Müller, in: *Microprobe characterization of optoelectronic materials*, edited by J. Jimenez, (Taylor and Francis, New York, London, 2003), p. 595
- [33] G. Nowak *et al.* J. Cryst. Growth **222**, 735 (2001)
- [34] D. Li *et al.* J. Appl. Phys. **90**, 4219 (2001)
- [35] E. Harush, S. Brandon, J. Salzman, Y. Paz, Semicond. Sci. Technol. **17**, 510 (2002)
- [36] J.T. Hsieh *et al.*, Electrochem. Sol.-State Lett. **3**, 395 (2000)
- [37] C.H. Ko *et al.*, Mat. Sci. Eng. **B96**, 43 (2002)
- [38] J.L. Weyher *et al.*, J. Appl. Phys. **39**, 6105 (2001)
- [39] L. Macht *et al.*, J. Phys.: Condens. Matter **14**, 13345 (2002)
- [40] J.L. Weyher *et al.*, Mat. Sci. Eng. **B91-92**, 280 (2002)
- [41] S. Lazar, J.L. Weyher, L. Macht, F.D.Tichelaar, H.W. Zandbergen, DRIP !!!!!
- [42] J.A. Bardwell, J.B. Webb, H. Tang, J. Fraser, S. Moisa, J. Appl. Phys. **89**, 4142 (2001)
- [43] G.L. Harris, in: *Properties of Silicon Carbide*, edited. By G.L. Harris, (INSPEC, London, UK, 1995) p. 133
- [44] R. Yakimova *et al.*, Diamond and Rel. Mat. **6**, 1456 (1997)
- [45] J. Takahashi, N. Ohtani, M. Katsuno, S. Shinoyama, J. Cryst. Growth **181**, 229 (1997)
- [46] I. Kamata, H. Tsuchida, T. Jikimoto, K. Izumi, Jpn. J. Appl. Phys. **39**,

- 6496 (2000)
- [47] M. Syväjärvi, R. Yakimova, E. Janzén, J. Electrochem. Soc. **147**, 3519 (2000)
- [48] E.K. Sanchez *et al.* J. Appl. Phys. **91**, 1143 (2002)
- [49] R.T. Bondokov *et al.*, Jpn. J. Appl. Phys. **41**, 7312 (2002)
- [50] M. Kato, M. Ichimura, E. Arai, P. Ramasamy, J. Electrochem. Soc. **150**, C208 (2003)
- [51] M. Kabyambaki *et al.*, J. Electrochem. Soc. **147**, 2744 (2000)
- [52] J.S. Shor, A.D. Kurtz, J. Electrochem. Soc. **141**, 778 (1994)

Chapter 4

Surface termination of dislocations in HVPE ZN:GaN; Morphology and Etching ¹

4.1 Introduction to etch pits

The research on Gallium Nitride over the past decades have been extremely extensive resulting in large numbers of optoelectronic and high-power, high frequency devices.¹ In view of the existence of operational GaN light emitting diodes (LEDs), laser diodes (LDs) and other devices,² it is hard to believe that there are still fundamental problems in the production of GaN thin films. However, the lack of commercially available free standing GaN substrates makes hetero-epitaxy on sapphire or silicon carbide (SiC) wafers an unwelcome necessity. Due to the differences in lattice constants and thermal expansion coefficients the resultant layers are characterized by large number of dislocations and other structural defects.

For a long time transmission electron microscopy (TEM) was used for dislocation counting and general verification of the dislocation structure. Unfortunately, a time-consuming and difficult specimen preparation and the need for expensive equipment make TEM unsuitable for routine use. Defect-selective etching constitutes an attractive alternative for fast assessment of the defect density. Two approaches have been successfully used for this purpose: photoenhanced wet etching and etching in molten bases.³⁻⁵ The

¹Chapter based on a paper in preparation

former method has a major drawback, namely its applicability depends upon the electrical characteristics of the etched material. However, etching in molten KOH or NaOH has no such limitations and can be used for the whole spectrum of GaN samples with no regard to the method of growth or doping densities. This etching method is not only anisotropic with regard to crystallographic directions⁶ but shows high selectivity for structural defects such as dislocations and nanopipes.^{7,8}

In fact, this technique has been successfully used to establish the dislocation density for various heteroepitaxial samples.^{9,10} Although not particularly suited for etching of single crystals, which exhibit both Ga and N polarities, it has been later modified to allow etching of single side of a sample.¹¹

Nevertheless, not all of those reports agreed on the suitability of etching in molten bases for dislocation counting. In some cases the etch pit density (EPD) differed significantly from the dislocation density as shown by other methods, e.g. TEM or atomic force microscopy (AFM). The differences might be due to various etching parameters used by different groups, such as different temperatures of etching and different etchants used, e.g. KOH, NaOH or eutectic mixture of these two, as well as, solutions of these compounds in water or other solvents. Furthermore, some groups reported using molten KOH etching at temperatures at which KOH should not have melted, which suggests contamination with water due to hygroscopic properties of KOH.

This report tries to set a standard by using a eutectic mixture of KOH and NaOH for defect selective etching of vapour phase grown GaN layers. The effect of varying the etching temperature on the selectivity and etch rate is studied consistently.

4.2 Eutecting etching of GaN:Zn

The samples have been grown by Hydride Vapour Phase Epitaxy (HVPE) technique on sapphire substrates and have a thickness of about 40 μm . They were doped with Zn to obtain semi-insulating behaviour. All etching experiments were performed in eutectic mixture of KOH and NaOH in a heated platinum crucible. The temperature varied between 300 °C and 500 °C and heating was provided by a semi-spherically shaped heater ensuring constant distribution of temperature. The temperature sensor has

been mounted in an aluminium ring fit to the outside of the crucible below the level of liquid KOH-NaOH mixture. Such a set-up ensures the best possible heat transfer between the large body of heated etchant and a thermocouple. The temperature thus measured should not differ by more than 2-3 K from the actual temperature of the etchant.

The morphology of samples after etching was examined by scanning electron microscopy (SEM) and atomic force microscopy (AFM) in the tapping mode. The morphology of as-grown samples was inspected by both differential interference contrast (DIC) optical microscopy and AFM.

4.3 The significance of etch pits

4.3.1 Etching results

Figure 1 shows an SEM micrograph of a sample surface after typical etching in eutectic mixture of KOH and NaOH. Three different size-grades of etch pit sizes can be distinguished. The smaller two grades have average diameters of 120 nm and 300 nm, respectively, with very little variation in size over the whole sample area and the largest kind can have diameters ranging from 500 nm to over 1 μm .

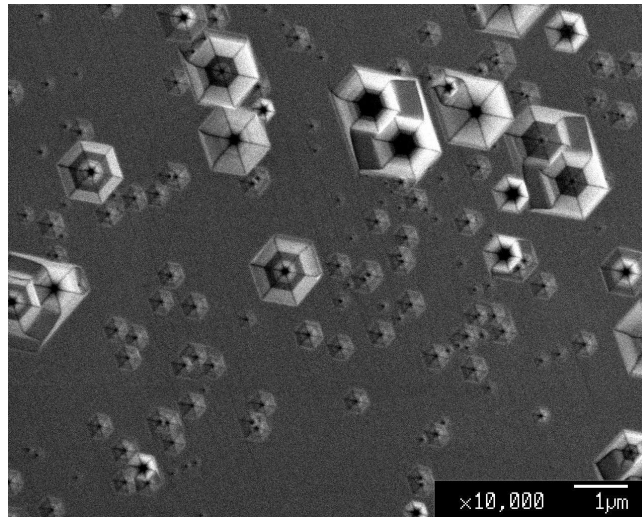


Figure 1: SEM micrograph showing a sample etched in “eutectic” at 420 ° C for 2 minutes. The morphology is typical for such etching and the distinguishable grades of pit sizes are observed for both MOCVD and HVPE grown samples.

The EPD obtained from SEM measurements is usually sufficient for basic characterization of defect density. However, the etch pits differ not only in lateral size but also the depth and consequently the angle of the side walls. Figure 2.(a) & (b) presents an AFM images showing both the depth and deflection views. AFM has a unique advantage over SEM in that the image is in fact a morphology map of the surface and therefore it is possible to derive from it all the surface feature data such as roughness or slope angle as well as precise dimensions. The labels in fig. 2.(b) designate examples of different grades of pits with A being the smallest and C – the largest.

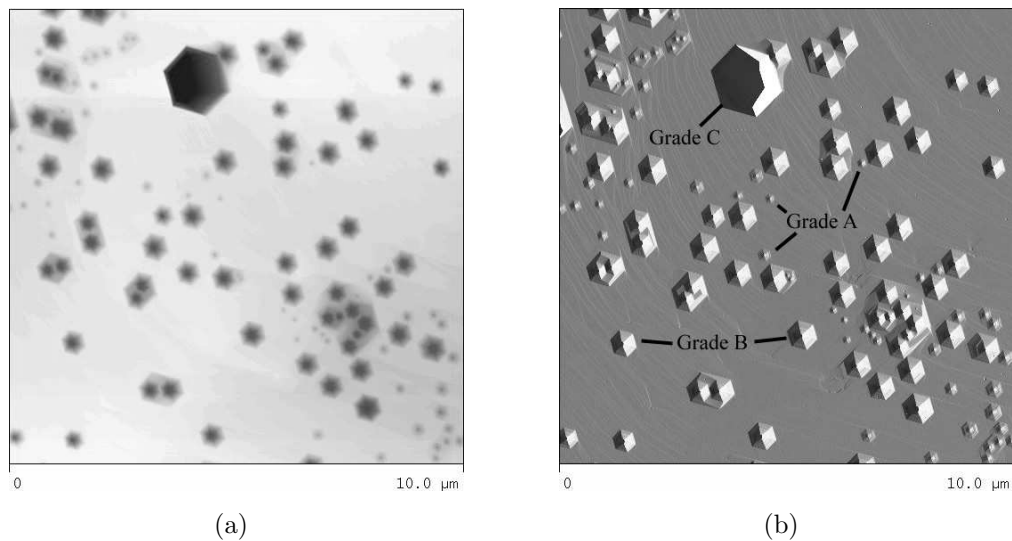


Figure 2: (a) AFM image showing height map of a sample etched in “eutectic” at 400 °C for 8 minutes. The depth of the largest pits exceeds 500 nm. (b) AFM image showing deflection map of the same sample. Deflection mode allows for accurate visualization of morphology details

The size of the etch pits is strongly dependent on the temperature of the etchant and on the time of etching. Table 4.1 shows the results for lateral dimensions and angle of the slopes of the etch pits as well their density. The etching time has been optimised to obtain etch pits which would not overlap thereby obscuring their accurate density. The table data is based upon statistical measurements of over 200 pits and the error is represented by the value of standard deviation. The area used for measurement is 200 μm² for each sample. The largest grade of pits is not included in this statistics because the variation of the size of these pits was too large to enable any statistical approach; the reason for this variation will be discussed later.

However, the angle of the slopes of such pits stays reasonably consistent within 38° to 54° range with no clear connection to the temperature of etching and the average density of these pits is 2 orders of magnitude lower than for other grades.

There are at least two factors which might influence the size and morphology of dislocation-related etch pits. These are: (i) energy of dislocations represented by their Burgers vector and (ii) interactions with point defects (dopants, impurities) represented by decoration effect and/or Cottrell atmosphere. The dislocations in the wurtzite GaN lattice are characterized by large differences in the magnitude of the Burgers vector:

- edge dislocations: $b_e = a$
- screw dislocations: $b_s = 2,66 a$
- mixed dislocations: $b_m = 3.66 a$, where a is the lattice constant.

The nanopipes can be considered as screw dislocations with $n \cdot b_s$ ($n=1,2,3 \dots$) value of Burgers vector.^{8,12} The thermodynamics of the etching process predicts that the change of the chemical potential during formation of the etch pits is inversely proportional to the energy of the defects; therefore, one could expect that defects of larger energy will be etched easier (or at lower temperature). This effect in conjunction with the data from table 1 seems to suggest that at $T=300^\circ\text{C}$ the defects responsible for grade A pits have activation energy which is too small to facilitate etching.⁵ On the other hand, the density of grade B pits is almost constant throughout the whole range of temperatures and the total EPD is constant from 350°C upwards. Therefore it might be concluded that 350°C is a threshold temperature for successful “eutectic” etching of GaN.

The slope of the pits which is relatively constant at different temperatures for both grades of pits stems from the interplay of vertical and horizontal etch rates, as shown in fig. 3. The vertical etch rate is the rate of nucleation of the pit and theoretically it should be proportional to the energy of dislocations. The horizontal etch rate is the rate of etch step propagation which in an ideal situation should be only dependent on the etching temperature.

Figure 4 presents TEM image of a cross section of grade C pits. From contrast analysis it is concluded that this type of pits originates on screw dislocations. As shown later, one of the reasons for these etch pits to

Table 4.1: Statistical characteristics of the etch pits.

Temp (C)	Etch time (min)	Grade A diameter (nm)	Grade A slope angle	Grade A density (cm^{-1})	Grade B diameter (nm)	Grade B slope angle	Grade B density (cm^{-1})	Overall pit density (cm^{-1})
300 ° C	120	51.4±1.9	10.0±1.9	5.5x10 ⁶	176.1±24.6	16.9±1.9	4.8x10 ⁷	5.8x10 ⁷
350 ° C	40	114.3±25.0	8.6±1.8	4.3x10 ⁷	241.0±33.1	19.8±2.2	5.3x10 ⁷	9.8x10 ⁷
400 ° C	8	202.5±22.5	9.8±1.0	4.5x10 ⁷	392.3±32.6	16.5±1.1	6.6x10 ⁷	1.1x10 ⁸
450 ° C	3	238.9±33.0	12.3±1.6	3.7x10 ⁷	407.1±51.6	23.0±2.4	5.0x10 ⁷	8.8x10 ⁷
500 ° C	2	301.5±55.7	14.1±2.2	3.0x10 ⁷	563.1±65.0	21.3±1.9	7.0x10 ⁷	1.0x10 ⁸

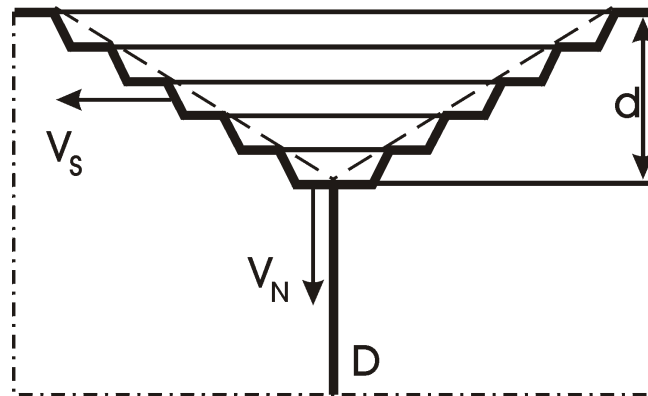


Figure 3: Schematic drawing of an etch pit originating on a dislocations (D). It can be characterized by slope which is the result of the ratio of nucleation rate (V_N) and step propagation velocity (V_S).

significantly vary in size and depth over the sample is the fact that they can originate on screw dislocations with $2c$ component or on dislocation dipoles.

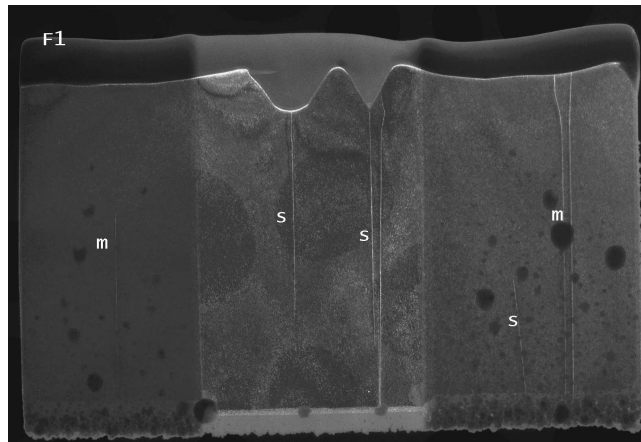


Figure 4: TEM cross sectional image showing two of the grade C pits originating on screw and mixed dislocations.

4.3.2 Morphology

The morphology of as-grown sample is dominated by large hillocks with typical dimensions ranging from $5 \mu\text{m}$ to $30 \mu\text{m}$, as shown in fig. 5. Detailed AFM analysis shows that the surface exhibits a clear step-flow pattern with

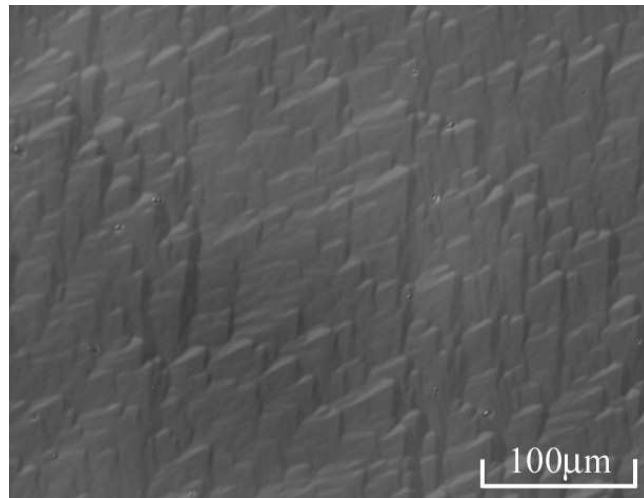


Figure 5: DIC optical microscopy image showing the typical morphology of an HVPE grown GaN layer. The characteristic hillocks vary in diameter over the surface of the sample.

the most efficient sources of steps originating at the top of the hillocks. The outcrops of dislocations can be divided into 3 categories:

- a small nano-pit generating either two steps in one direction or one step with 2-monolayer height, but not influencing the general step flow at the surface of the sample. This type is later referred to as X-type outcrop. (fig. 6.(a))
- a small nano-pit located in the middle of a v-shaped feature, which is also an origin of one or two steps but at the same time causes pinning of the general step-flow. This type is later referred to as Y-type outcrop. (fig. 6.(b))
- a larger nano-pit which is an origin of a total of 3-4 steps. This type is later referred to as Z-type outcrop. (fig. 7.(a) & (b))

From the perspective of dislocation termination it is clear that both X and Y dislocation outcrops originate on dislocations having a Burgers vector with c component. It is possible that they might have differing components of Burgers vector in the a -related directions (which represent an edge component of dislocations), however AFM measurements cannot resolve this issue.

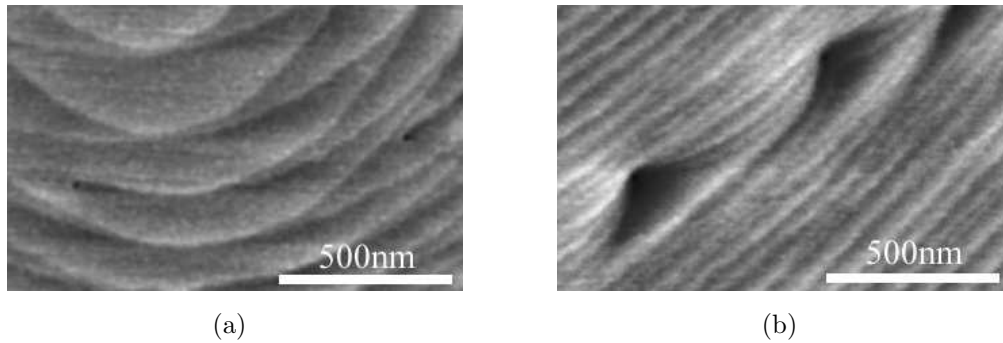


Figure 6: (a) An AFM image of an X-type dislocation outcrop generating two surface steps but no disruption in general step-flow. (b) An AFM image of an Y-type dislocation outcrop generating two surface steps and pinning the general step-flow.

Z-type dislocations originate only at the top of the hillocks and are, most probably, the source of the hillocks' rapid growth rate. There were two types of those outcrops found:

- a single pit being an origin of 4 spiral steps (fig. 7.(a)) with the height of each step close to $c/2$ value for GaN lattice.
- two pits within a short distance: one causing a total of 4 spiral steps and the other causing 2 spiral steps with the opposite direction. (fig. 7.(b))

In the first instance it is clear that the Burgers vector of such a dislocation has a $\pm 2c$ component resulting in generation of 4 spiral steps in the clockwise or counter clockwise direction. In the second instance the actual defect is a complex of two dislocations, one with $\pm 2c$ component and the other with opposite c component resulting in annihilation of two of the four steps. This behaviour has been confirmed on several hillocks. The particular outcrop depicted in fig. 7.(b) shows only 3 visible steps, but AFM analysis proved that while the two "free" spiral steps have heights of the order of 2.3 \AA , the step that is terminated at the second dislocation has a height of 4.7 \AA , which is close to the value of c lattice parameter (5.18 \AA).

Edge dislocations can also be visualized by AFM method; the resulting outcrops have a form of small pits with no steps generated at the surface. However, no such pits were found which suggests that edge dislocations are scarce in this type of samples. At the various temperatures that have been

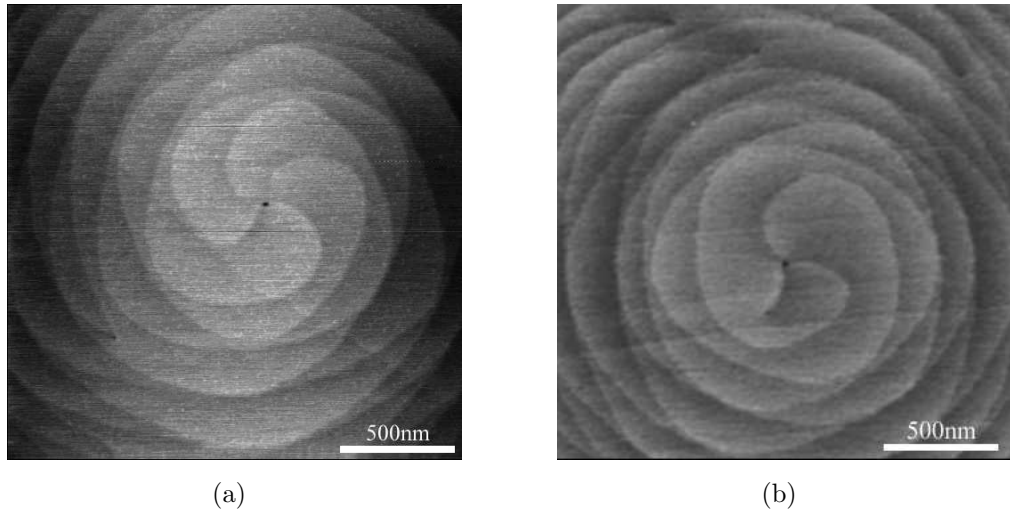


Figure 7: (a) An AFM image of a single Z-type, $\pm 2c$ dislocation, outcrop generating four spiral surface steps. (b) An AFM image of a complex Z-type outcrop, featuring a $\pm 2c$ dislocation generating three spiral surface steps two of which annihilate on the neighbouring $\pm c$ dislocation of the opposite sign. The step connecting the two dislocations is double the height of the “free” steps, hence the total step height for the $\pm 2c$ dislocation is four monolayers.

used for the etching experiments it is highly improbable that edge dislocations would remain unetched. However, the total density of dislocations as measured by AFM on as-grown samples is comparable to the total density of all etch pits. This fact suggests that in HVPE grown GaN:Zn, the creation of edge dislocations is inhibited and all the dislocations have a screw component. Also other researchers report that the ratio of *edge:mixed:screw* dislocations can vary depending on the growth method and the type of the sample.^{13,14}

By correlating the statistically determined density of dislocation outcrops from AFM measurements of as-grown samples with the densities of various grades of etch-pits, the etch pits can be tentatively attributed to dislocations with specific types of outcrops. Thus the smallest grade A pits correlate with the X-type dislocations creating two steps but no disruption in the step-flow. The medium sized grade B pits have a comparable density to the Y-type dislocations which result in creation of two surface steps and pinning of the general step-flow.

Grade C pits in the etched samples seem to be more numerous than the Z-type dislocation outcrops. However, this can be explained by the fact

that they occur singularly at the top of the hillocks and the hillock size varies considerably over the surface of sample. The structure of the Z-type dislocations consisting either of a single dislocation with large Burgers vector or two dislocations one of which has a large Burgers vector suggests that indeed they should be the origin of the largest type of pits. Hence, grade C etch pits can be tentatively assigned to Z-type dislocations.

4.3.3 Activation energy calculations

The unresolved issue of the type of dislocations responsible for grade A and B etch pits and X- and Y-type outcrops can be further investigated by calculation of the activation energy of etch pit nucleation for these types of defects.

In order to determine the temperature dependence of GaN etching velocity it has been assumed that the process is controlled by a rate-controlling step much slower than the other processes. The temperature dependence of the velocity of the slow process is described by Arrhenius formula:

$$v = v_o \exp\left(-\frac{\Delta E}{k_B T}\right) \quad (4.1)$$

where v_o is a constant, ΔE is the energy barrier, k_B and T are Boltzmann constant and the temperature, respectively. In eq. 4.1 it is assumed that v_o is a slowly varying function of temperature so that its variation can be neglected. It was also assumed that the temperature variation of the other processes will not change them to the point where they can have comparable rate to the selected, rate determining process. From the van t'Hoff plot of the logarithm of the etch rate vs. inverse of the temperature, the energy barrier can be deduced as follows

$$\Delta E = k_B T \ln\left(-\frac{v}{v_o}\right) \quad (4.2)$$

Figure 8 presents a plot of the vertical etch velocity for grade A and grade B etch pits. This rate is essentially equivalent to the rate of the exposition of the new layers at the dislocation core.

- $\Delta E = 122.6 \pm 8.8$ kJ/mole - for grade A pits
- $\Delta E = 110.6 \pm 6.9$ kJ/mole - for grade B pits

The resulting approximate lines were also plotted in fig. 8. It follows then that the etch processes are characterized by different energy barriers for different pits. Because both types of pits originate on dislocations having a $\pm c$ component in Burgers vector the actual difference in their activation energy can be attributed to surface termination and differences in decoration

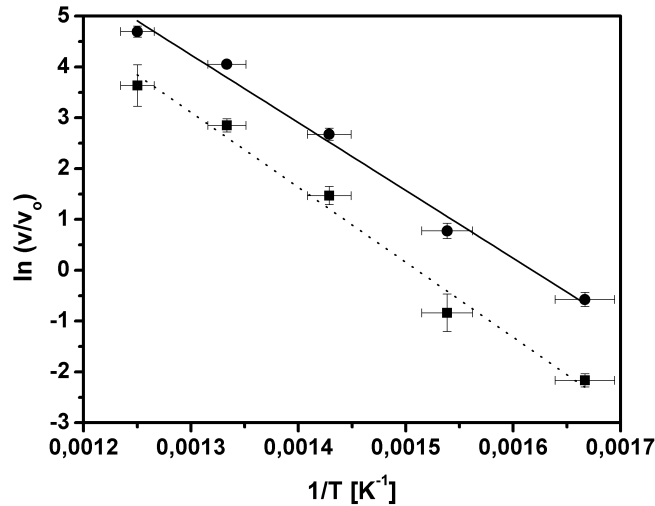


Figure 8: Experimentally determined temperature dependence of the vertical growth rate on the inverse of the etching temperature: squares – A pits, circles – B pits. The error bars correspond to the error in the temperature (x-axis) and the rate (y-axis). The dashed and solid lines correspond to approximate activation energy rate obtained using eq. 4.1 for A and B pits, respectively. The energy barrier was determined by the minimization of the standard deviation of the approximate line and the experimental points. From the above procedure the following activation energies were obtained:

The horizontal etching velocity may be treated in a similar manner. As shown in fig. 9, the experimental etch rates may be successfully approximated by the single barrier rate. The following rate barriers were obtained:

- $\Delta E = 113.1 \pm 8.7$ kJ/mole - for grade A pits
- $\Delta E = 104.4 \pm 8.2$ kJ/mole - for grade B pits

It may be noted that the difference between the activation energies of the grade A and grade B pits is smaller. As before, the larger barrier is observed for smaller pits.

The differences in activation energies are not significant which suggests that there are no fundamental differences in the Burgers vector size. The edge

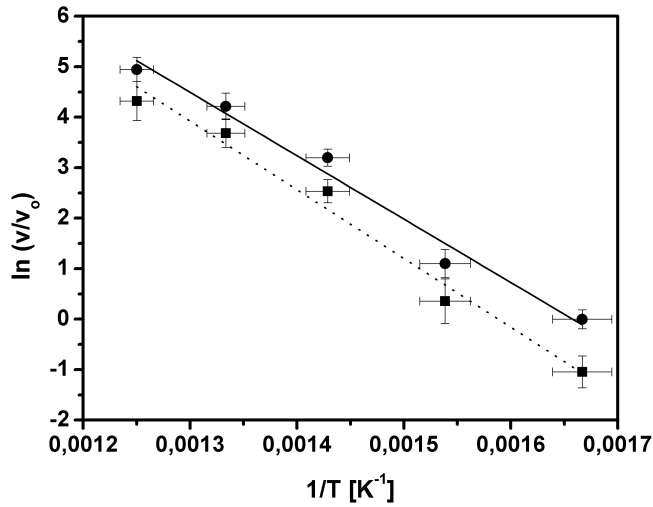


Figure 9: Experimentally determined temperature dependence of the horizontal growth rate on the inverse of the etching temperature: squares – A pits, circles – B pits. The error bars correspond to the error in the temperature (x-axis) and the rate (y-axis). The dashed and solid lines correspond to approximate activation energy rate obtained using eq. 1 for A and B pits, respectively.

component which cannot be resolved by AFM measurements might play a role but it would not explain the reason for pinning of the step-flow. Pure edge dislocations for other GaN samples do not cause step-flow pinning, therefore it is unlikely that a difference of an edge component in a mixed dislocation should do so. Consequently, the difference in structure of X- and Y-type outcrops and resulting difference in etching characteristics can be attributed to the decoration effect.

4.4 Conclusions

For successful examination of dislocation density, proper care must be taken to ensure sufficiently high etching temperature. For etching in a eutectic of KOH-NaOH, temperatures below 350 °C might result in EPD significantly lower than the actual dislocation density.

The size of the pits and the angle of their slopes is dependent on the type of dislocations. However, the values for those will not give direct answer as to type of the dislocations on which the pits originate. The types of dislocations populating the sample will strongly depend on the growth method used, e.g.

HVPE or MOCVD, as well as type of doping.

In HVPE grown GaN:Zn all of the measured dislocations have a screw component; there were no indications of any pure edge dislocations terminating at the surface of the sample. AFM measurements and activation energy calculations show that 98% of all dislocations originate randomly in the matrix generating two kinds of surface features and creating two different kinds of etch pits with clearly defined activation energy.

The difference in the activation energy is not large which suggests that it is caused by differences in dislocation decoration and not in fundamental changes of the Burgers vector. Further cross sectional TEM study with statistical measurement of the dislocations could explain this problem in a more detailed manner.

The remaining 2% of the dislocations are either screw type with $\pm 2c$ components in the Burgers vector generating 4 spiral surface steps, or dislocation dipoles: one $\pm 2c$ dislocation combined with one $\pm c$ but of the opposite direction resulting in a generation of 4 spiral surface steps of which 2 are annihilated at the neighbouring dislocation. These types of dislocations/dislocation complexes are the sources of spiral step-flow and the high local growth rate which results in hillocks commonly populating HVPE grown samples.

References

- [1] H. Morkoç, *Nitride Semiconductors and Devices* (Springer, Berlin, 1999)
- [2] S. J. Pearton, J. C. Zolper, R. J. Shul, F. Ren, *J. Appl. Phys.* **86**, 1 (1999)
- [3] C. Youtsey, L.T. Romano, R.J. Molnar, I. Adesida, *Appl. Phys. Lett.* **74**, 3537 (1999).
- [4] P. Visconti, K.M. Jones, M.A. Reshchikov, R. Cingolani, H. Morkoç, R.J. Molnar, *Appl. Phys. Lett.* **77**, 3532 (2000)
- [5] J.L. Weyher, P.D. Brown, J.L. Rouvire, T. Wosiski, A.R.A. Zauner, I. Grzegory, *J. Crys. Growth* **210**, 151 (2000)
- [6] D.A. Stocker, E.F. Schubert, J.M. Redwing, *Appl. Phys. Lett.* **76**, 2654 (1998)
- [7] K. Shiojima, *J. Vac. Sci. Technol. B* **18**, 37 (2000)
- [8] S.K. Hong, T. Yao, B.J. Kim, S.Y. Yoon, T.I. Kim, *Appl. Phys. Lett.* **77**, 82 (2000)

- [9] P. Visconti, K.M. Jones, M.A. Reshchikov, R. Cingolani, H. Morkoç, *Appl. Phys. Lett.* **77**, 3532 (2000)
- [10] P. Visconti, D. Huang, M.A. Reshchikov, F. Yun, R. Cingolani, D.J. Smith, J. Jasiski, W. wider, Z. Liliental-Weber, H. Morkoç, *Mat. Sci. Eng.* **B93**, 229 (2002)
- [11] G. Kamler, J.L. Weyher, I. Grzegory, E. Jeziarska, T. Wosiski, *J. Crys. Growth* **246**, 21 (2002)
- [12] J.L. Weyher, F. D. Tichelaar, H. W. Zandbergen, L. Macht, and P. R. Hageman, *J. Appl. Phys.* **90**, 6105 (2001)
- [13] Z. Liliental-Weber, unpublished report.
- [14] F. Tichelaar, unpublished report.

Chapter 5

An electrochemical study of photoetching of heteroepitaxial GaN: kinetics and morphology ¹

5.1 Introduction to PEC etching

In the last decade enormous progress has been made in both the growth and the characterization of gallium nitride. Products based on GaN are already available on the commercial market; these include light-emitting diodes, laser diodes, detectors and even a completely new standard for Home Entertainment – Blu-Ray. AlGaIn/GaN based high electron mobility transistors (HEMTs), having extremely high breakdown voltage and superior thermal and chemical stability, offer performance significantly better than that of GaAs based devices. Despite all these advances, the scientific community still cannot say unequivocally that it has mastered the fabrication of GaN based devices in all its aspects. The main reason remains the lack of a suitable growth substrate which is lattice matched to GaN. The production of single crystals, although possible, is still not efficient on a scale large enough to meet the market needs. The resultant crystals are not perfect; they

¹Chapter based on: “An electrochemical study of photoetching of heteroepitaxial GaN: kinetics and morphology”, L. Macht, J.J. Kelly, J.L. Weyher, A. Grzegorzczuk, P.K. Larsen, *J. Crystal Growth*, **273**, 347 (2005)

have small dimensions and high intrinsic carrier concentration. Therefore, sapphire and silicon carbide (SiC) remain the substrates of choice for growth of GaN layers. Due to differences in lattice constants and thermal expansion coefficients the layers grown on these substrates contain a large number of threading dislocations. The average density for thin films grown on sapphire is around 10^9 - 10^{10} cm^{-2} while it is an order of magnitude lower for samples grown on SiC. Despite this high dislocation density, manufactured devices function satisfactorily but their electrical and optical properties could be improved. The race for the perfect lattice is not over yet!

The only exact method for dislocation counting and general verification of the dislocation structure is still transmission electron microscopy (TEM). Unfortunately, a time-consuming and difficult specimen preparation and the need for expensive equipment make TEM unsuitable for routine use. Defect-selective etching constitutes an attractive alternative for fast assessment of the defect density. Two approaches have been successfully used for this purpose: photoenhanced wet etching^{1,2} and etching in molten bases. The former method has a major drawback, namely its applicability depends upon the electrical characteristics of the etched material.

It was first shown by Minsky *et al.*³ that n-type GaN, when illuminated, could be rapidly etched in KOH solution; no etching occurs in the dark. They suggested an etching process similar to that of GaAs, i.e. photogenerated holes cause oxidation and dissolution of GaN. Subsequently, in a series of articles, Youtsey *et al.*^{1,4,5} showed that etching could result in both smooth and rough morphologies and they suggested a simplified reaction for the dissolution process. They also found a direct correlation between the surface morphology after etching and the concentration of the KOH solution. In addition, they showed that the resultant “whiskers” are, in fact, formed on dislocations. Weyher *et al.*⁶ subsequently established a one-to-one correlation between whiskers and dislocation sites for Ga-polar layers and they also showed that whiskers are formed on narrow inversion domains in N-polar layers. In 2000, Rotter *et al.*⁷ suggested a two-step process for etching of n-type GaN thin films grown by MOCVD on sapphire and a year later Nowak *et al.*⁸ suggested the same mechanism for dissolution of GaN single crystals.

Much of the recent work on photoetching of n-type GaN in alkaline solution has been performed with a counter electrode (generally platinum) but without potentiostatic control of the semiconductor potential; a voltage

source and reference electrode were, in general not used.⁹ An exception is the work of Borton *et al.*¹⁰ and Huygens *et al.*¹¹

Various factors are important in determining the etching kinetics and, thus, the surface morphology of the etched solid. These include the electrochemical potential of the semiconductor, the photon flux, the OH⁻ concentration in solution and the hydrodynamics of the system. If the potential of the semiconductor is not well defined then it is difficult to draw conclusions with regard to etching mechanisms and morphologies.

In the present work we have studied the influence of the parameters listed above on the photoelectrochemical (PEC) etching of n-type GaN epitaxial films. These measurements allow us to define different etching regimes and their corresponding surface morphologies. In addition we try to relate this “potentiostatic” approach to the more commonly used “open-circuit” photoenhanced etching and we emphasize important differences between the two approaches. Finally, we indicate the range of dopant density for which photoetching of GaN is considered feasible.

5.2 Growth parameters and PEC methods

A set of four GaN samples was grown by MOCVD on c-plane sapphire substrates. The substrates were first cleaned in HCl:HNO₃ solution outside the reactor and later annealed in N₂ atmosphere in the reactor while the temperature was ramped down from 1100 °C to 950 °C. A 90 nm low-temperature buffer layer was grown first at 525 °C, followed by the main GaN layer at 1175 °C. All the samples were Si-doped. Hall experiments, performed at room temperature, gave carrier densities of 1.5x10¹⁷, 2.3x10¹⁸, 4.6x10¹⁸ and 9.3x10¹⁸ cm⁻³ (samples A, B, C and D, respectively). Ohmic contacts to the GaN were made by evaporating a Ti layer, 100 nm thick without any additional heat treatment. All the samples used in this study had a Ga-polar face.

Electrochemical measurements were performed in a three-electrode cell with a platinum counter electrode and a saturated calomel electrode (SCE) as reference. Potentials are given with respect to SCE; its potential is +0.24 V with respect to that of the standard hydrogen electrode (SHE). A potentiostat was used to measure current density – potential curves (*j*-*U*) in the dark and under illumination. In most of the experiments the potential was scanned at a constant rate (10 mV/s) and the (photo)current

was measured as a function of potential. For details of such electrochemical measurements see ref.¹² The light source was a UV-enhanced xenon lamp with a power density of ~ 300 mW/cm² fitted with a water filter. It is important to note that this value was measured by an absorptive power meter in the whole emission range of the lamp while photoetching makes use only of the energy above the bandgap of GaN. Aqueous KOH solutions with a concentration varying from 0.001 to 0.05 M were used. Unless otherwise stated, the electrolyte solution was stirred during the experiment. For the measurement of the oxygen reduction current, the GaN working electrode was replaced by a Pt electrode.

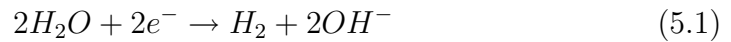
For the photoenhanced etching experiments the GaN working electrode was connected via an ammeter to the counter electrode, a platinum-coated plate. The etch rate and the morphology were studied as a function of carrier density and KOH concentration (0.001 – 0.5 M). The etching time was 20 minutes for all samples and, unless otherwise stated, the solution was stirred. All experiments described in this paper were performed at room temperature.

5.3 Results and discussion

5.3.1 Kinetics

Figure 1 shows typical current density - potential plots for an n-type epitaxial GaN electrode with carrier concentration of 1.5×10^{17} cm⁻³ in 0.004 M KOH solution at room temperature. In the dark (curve (a)) diode characteristics are observed.

At negative potentials (range I) a cathodic current due mainly to hydrogen evolution results from the reduction of water by conduction band electrons.^{11,13}



The flat-band potential is located in this range ($U_{fb} = -1.4$ V), so that the electron concentration at the surface is high.

At positive potentials the current is very low. Under illumination, electron-hole pairs are generated. In the potential range I the band bending is small and the electric field is not sufficiently strong to separate the electrons and holes; they recombine both in the bulk and at the surface and, consequently, no photocurrent is observed.

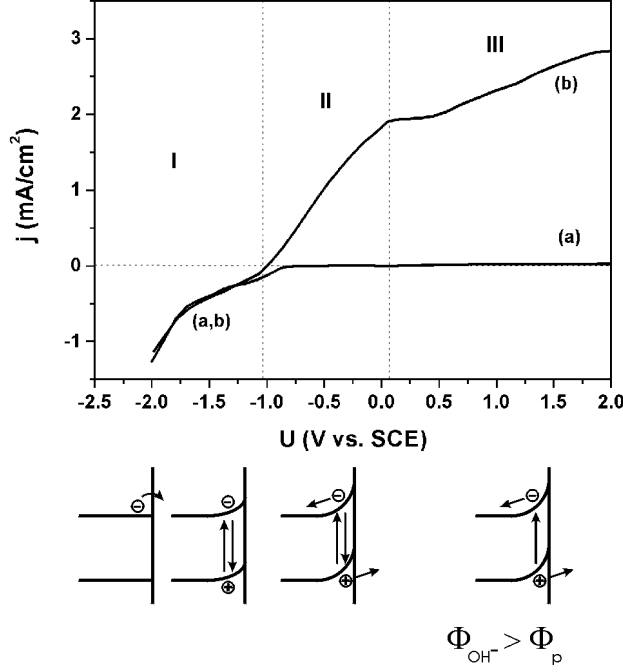
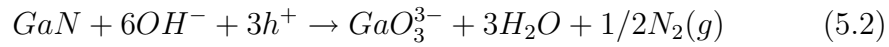
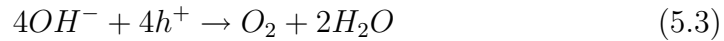


Figure 1: Typical current density – potential plots for an n-type epitaxial GaN electrode: with a carrier concentration of $1.5 \times 10^{17} \text{ cm}^{-3}$ in 0.004 M KOH solution (a) in the dark, (b) under illumination. The corresponding energy band diagrams are also shown.

At more positive potential (stronger band bending in range II) a partial spatial separation of the charge carriers occurs. The holes driven to the surface can cause one of two electrochemical reactions: the oxidation of GaN,



or the formation of oxygen,



Previous work¹¹ has shown that dissolution of the semiconductor is the predominant reaction. The electrons are detected as a photocurrent in the external circuit (at the counter electrode they give rise to a reduction reaction e.g. hydrogen evolution). It is clear that in this potential range not all the photogenerated holes contribute to the photocurrent. Since the band bending is moderate, the surface electron concentration is still rather high

and some recombination occurs. As the potential is made more positive, the recombination rate of electrons and holes decreases due to increase in the electric field and the photocurrent increases. In range III the photocurrent begins to level off. In fig. 2 this photocurrent at 0.2 V is plotted as a function of the light intensity for a number of OH^- concentrations. At a given OH^- concentration (0.003 M for example) the photocurrent first increases linearly with light intensity and then becomes independent of the photon flux. This constant value at high intensity increases with increasing OH^- concentration. These results suggest that the photocurrent can be controlled in one of two ways. From equation (5.2) it is clear that OH^- ions are essential for the photoanodic reaction. If the flux of OH^- (Φ_{OH^-}) to the surface is larger than the flux of photogenerated holes to the surface (Φ_p), i.e. $\Phi_{OH^-} > \Phi_p$, then the photocurrent is determined by the light intensity.

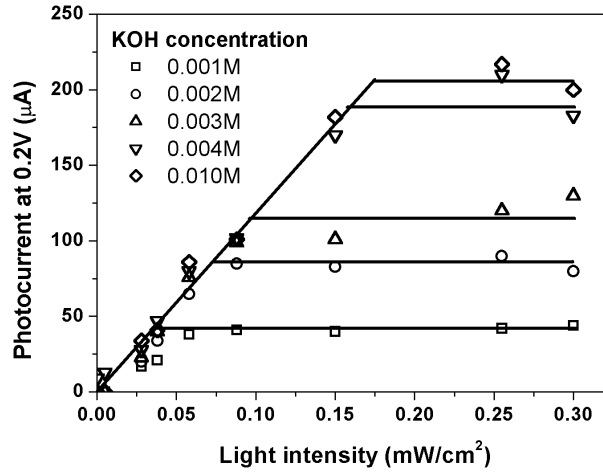


Figure 2: The dependence of the photocurrent at 0.2 V on illumination intensity for different KOH concentrations. The electron density of the sample was $1.5 \times 10^{17} \text{ cm}^{-3}$. Light intensity was measured for the full spectrum of the Xe lamp, however, only the range above bandgap energy of GaN can be used for photoetching.

In this case the number of holes transferred across the semiconductor/solution interface per absorbed photon is high. This case corresponds to normal depletion, i.e. a change in applied potential (ΔU) results in a corresponding change of the space-charge layer potential ($\Delta U \approx \Delta U_{SC}$). If, on the other hand, the photon flux is high ($\Phi_{OH^-} < \Phi_p$), the OH^- ions at the surface will be depleted. In this case the rate of the surface reaction is

determined by mass transport of OH^- ions and the limiting photocurrent depends on the pH of the solution and the hydrodynamics of the system. For example, if the solution is not stirred then a considerably lower photocurrent is observed. Since the rate of photogeneration of holes is higher than the rate of their reaction at the surface, considerable electron – hole recombination must occur, even in the limiting photocurrent range. The surface reaction is kinetically limited and the space-charge layer potential becomes independent of the applied potential ($\Delta U_{SC} = constant$); because of accumulation of positive charge at the interface, the potential changes across the Helmholtz layer in solution ($\Delta U = \Delta U_H$).¹⁴

When the KOH concentration is raised above 0.004 M only a slight increase in the photocurrent is observed at high intensity (see 0.01 M KOH in fig.2). An even higher OH^- concentration does not lead to a higher photocurrent. This result is very likely due to the formation of a sparingly soluble oxide.¹¹

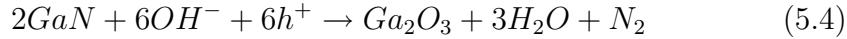
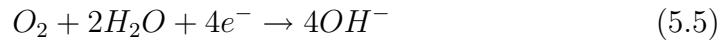


Figure 3 shows current-potential curves for n-type GaN electrodes with three dopant densities. The result for the lowest dopant density ($1.5 \times 10^{17} \text{ cm}^{-3}$) has been discussed above. The results for the two higher dopant densities resemble those shown in fig. 1. There are, however, two striking differences. An additional cathodic dark current is found with an onset at a potential more positive than that for hydrogen evolution. The process, which is more pronounced for the highest dopant density, is due to oxygen reduction by conduction band electrons.



At a potential of $U \approx -0.75 \text{ V}$ a well-defined diffusion-limited current is clear in the case of the $4.6 \times 10^{18} \text{ cm}^{-3}$ sample. The second difference with respect to the result for the lowest doped sample is the value of the onset potential for photocurrent: a shift to positive potentials is observed with increasing dopant density.

This effect is caused by the difference in depletion layer width of the differently doped samples. During photoetching the excitation light is absorbed in a layer defined by the absorption coefficient and independent of the dopant density. Holes taking part in etching are generated either

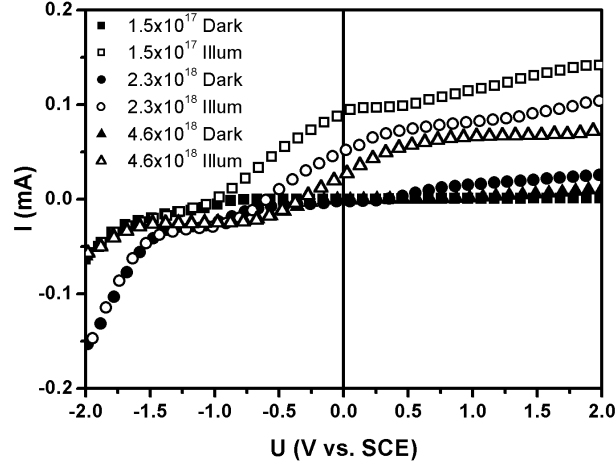


Figure 3: Current-potential curves measured for three samples with different electron densities in the dark and under illumination in 0.004 M KOH solution.

within the depletion layer itself or beyond the depletion layer but not further from the edge than the hole diffusion length.¹⁵ The dopant density which controls the depletion layer width, thus controls the depth in the material from which photogenerated holes can take part in the etching and contribute to photocurrent. Therefore, at constant potential, a higher doped sample having a narrower depletion layer yields smaller photocurrent.

5.3.2 Open-circuit photoetching kinetics

In the experiments described in the previous section, the potential of the GaN electrode was fixed by the voltage source (potentiostat) and measured with respect to the reference electrode. In an open-circuit photoetching experiment (see fig. 4(a)) the potential of the GaN is determined by the kinetics of the reactions occurring at both the semiconductor and the counter electrode. With short-circuited electrodes and no Ohmic losses in the system the Fermi level is constant (fig. 4(b)). Holes produced by illumination of the semiconductor can either recombine with electrons or cause oxidation of the semiconductor. In the latter case the electrons pass to the counter electrode where a reduction reaction occurs.

To maintain electroneutrality, the rate of the electrochemical reaction involving holes at the GaN/solution interface must be equal to the rate of

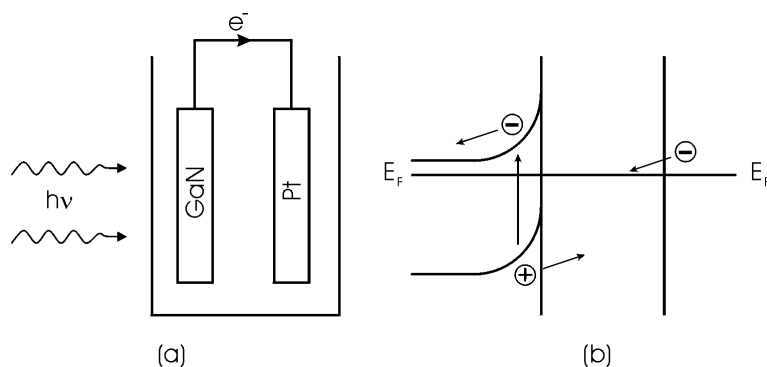


Figure 4: Schematic representation of open-circuit photoetching (a) and of the energy bands and Fermi level of the GaN and Pt electrodes (b) under illumination.

reduction via electrons at the metal. The latter reaction is important in determining what happens at the GaN. In aqueous solution there are two possibilities for the reaction at Pt, the reduction of water (eq. 5.1) or of oxygen (eq. 5.5). For open-circuit photoetching to be possible, the onset of the reduction reaction must be at potential more positive than that of the photoanodic oxidation of GaN (-1.0 V in the case of low-doped sample, fig. 1).

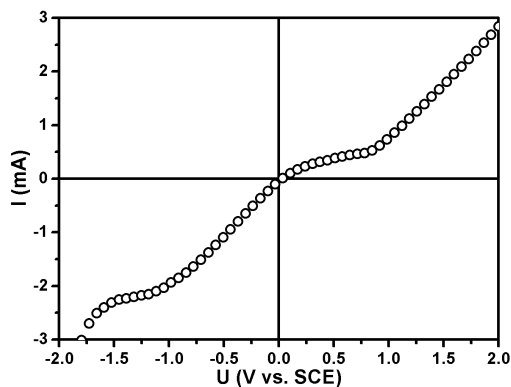


Figure 5: Current-potential curve measured with a Pt working electrode in an aerated 0.004 M KOH solution. The solution was stirred.

To obtain information on which reduction reactions will be important we show in fig. 5 the cathodic current-potential curve measured under potentiostatic conditions at a Pt electrode in stirred 0.004 M KOH solution.

Oxygen reduction starts at 0 V, which is well positive of the photocurrent onset (see fig. 5). The oxygen reduction current eventually becomes independent of potential since the reaction rate becomes mass-transport controlled. At more negative potential (-1.6 V) the cathodic current increases further; this is due to hydrogen evolution (eq. 5.1). This potential is more negative than the onset potential for photocurrent. Consequently hydrogen evolution is not important for photoetching under these conditions.

With regard to the counter electrode two factors are important: the electrocatalytic activity of the metal and the electrode area relative to that of the exposed GaN. To illustrate the latter aspect we consider two cases, depicted schematically in fig. 6. Curve (a) is the photoanodic current-potential curve for an illuminated GaN electrode. Curves (b) and (c) represent oxygen reduction at a Pt counter electrode. In case (c) the mass-transport conditions are more favourable and/or the area of Pt is larger than in case (b). In the steady state the rates of oxidation and reduction must be equal. This defines the open-circuit potential of the system. From fig. 6 it is clear that this potential can either be in the rising part of the photocurrent curve (U_b) or in the limiting current range (U_c), depending on the area of the metal electrode, the kinetics of oxygen reduction at the metal and the hydrodynamics of the system. To illustrate the importance of surface area figure 7 shows results of photocurrent measurements as a function of time for an 8 minute etching process using two different Pt electrodes, a thin wire with a surface area much smaller than that of the GaN electrode and a Pt-coated plate with an area roughly 50 times larger than that of the GaN sample. The results clearly illustrate the importance of counter electrode size on the photocurrent and therefore on the etch rate.

If there is a series resistance involved (for example, a poor Ohmic contact to GaN) the open-circuit situation becomes more complicated. There is an Ohmic potential drop across the resistance (see fig. 8a) and the Fermi levels in semiconductor and counter electrode are no longer the same (fig. 8b). This has consequences for the photoetching rate as is obvious from the schematic figure 9, which corresponds to the situation for curve (c) shown in fig. 6. The etching rate is decreased markedly with respect to the resistance-free case. In fact, the potential of the semiconductor may be shifted substantially with a resulting change in etching mechanism (the Ohmic resistance displaces the potential from the limiting to the rising photocurrent range).

Clearly, the latter effect may have consequences for the etching morphol-

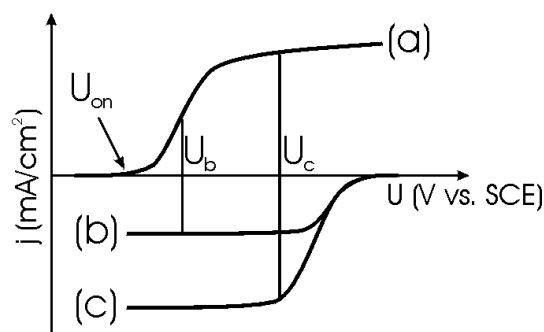


Figure 6: Schematic current-potential curves illustrating the role of the counter electrode size in open-circuit photoetching. Curve (a) is the photocurrent-potential curve for GaN with onset potential U_{on} . Curves (b) and (c) refer to oxygen reduction at the counter electrode; the current in case (c) is larger than in (b) because of a larger surface area and/or more favourable mass transport condition. the corresponding open-circuit potentials are indicated by U_b and U_c .

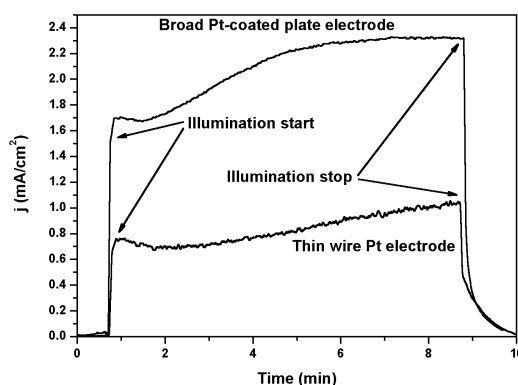


Figure 7: The influence of counter electrode size on the measured photocurrent density for open-circuit photoetching.

ogy.

A comparison of fig. 3 and fig. 5 shows that the dopant density can be expected to influence the open-circuit etching rate. In fact, the measured etch rate is inversely proportional to the carrier concentration and amounts to $4\mu\text{m/h}$, $2.2\mu\text{m/h}$, 300nm/h and less than 100nm/h for the samples with electron concentrations 1.5×10^{17} , 2.3×10^{18} , 4.6×10^{18} and 9.3×10^{18} , respectively. This is due to the fact that at higher dopant density the onset of photocurrent is shifted considerably to the more positive

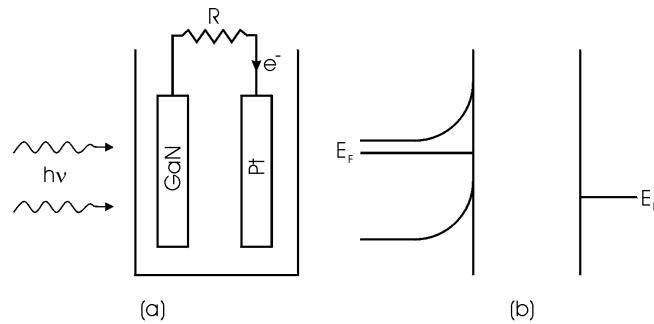


Figure 8: Schematic representation of open-circuit photoetching (a) and the energy bands and Fermi level of the GaN and Pt electrodes (b) in the case of an additional Ohmic resistance (such as a low-quality contact to the GaN electrode).

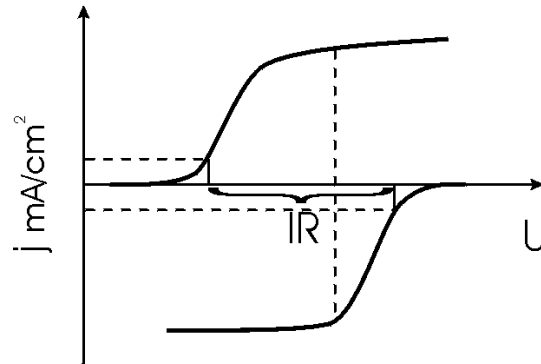


Figure 9: Schematic current-potential curves illustrating the influence of an additional Ohmic resistance on open-circuit photoetching. The ohmic drop (IR) shifts the potential of the GaN to a more negative value, thereby decreasing the photoetching rate.

potentials and the “overlap” between the anodic and cathodic curves becomes less favourable. This results in a lower open-circuit photoetching rate. The rate of $4\mu\text{m/h}$ for the most favourable case (the lowest electron density) agrees reasonably well with that expected on the basis of the corresponding limiting photocurrent density ($3.5\mu\text{m/h}$).

5.3.3 Morphology

The rate-determining step of the dissolution reaction generally decides the morphology of the etched surface.¹⁶ In GaN photoetching one can clearly distinguish two main etching regimes: on the one hand, strong

defect selectivity results in the formation of “needles” and, on the other hand, a uniform polishing of the surface is possible.¹⁷ Past experience with (photo)etching of III-V and other semiconductors helps us to relate surface morphology to the kinetics of the etching reaction. Recombination of photogenerated holes with electrons reduces the dissolution rate at surface defects. This mechanism is responsible for the formation of needles at threading dislocations in GaN. Clearly these conditions correspond to potential range II of fig. 1. Mass transport control of etching by species in solution usually results in polishing. Surface reactivity is not important. Since diffusion to protruding parts of surface is more effective than to recessed parts, a levelling action occurs. Polishing of GaN is expected in the limiting photocurrent range (III) when the flux of OH^- ions is rate-determining ($\Phi_{OH^-} < \Phi_p$). If oxide solubility is a problem, as at high photocurrent densities, then etching may become non-uniform due to local differences in the thickness and etching properties of the oxide.

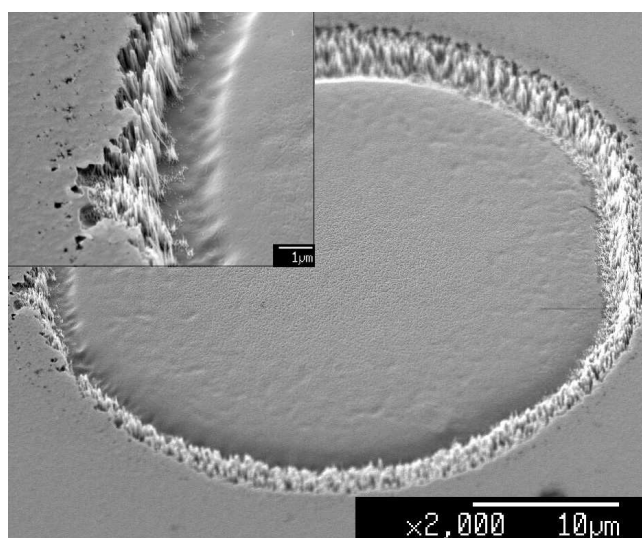


Figure 10: A SEM micrograph demonstrating the results of open-circuit etching via fiberguide. Kinetically controlled etching near the edge reveals dislocations in the form of needles while the centre of the spot remains smooth as a result of mass-transport controlled etching.

The result shown in figure 10 gives a nice illustration of how morphology can be determined. A fiberguide, placed close to the GaN surface, was used to photoetch a GaN sample under open-circuit conditions. A low KOH concentration (0.004 M) was used and the solution was not stirred. At the

centre of the illuminated area the photon flux was clearly higher than the OH^- ion flux and smooth etching occurs. On the other hand defect selective etching, clear from the appearance of needles, occurs at the edge of the illuminated area. This is due to an enhanced supply of OH^- ions from the surrounding non-etching area (outside the light spot) and, possibly, to a reduction of light intensity as a result of the Gaussian distribution in the beam. Improved hydrodynamics gives rise to a larger etch rate at the edge, as indicated by the deeper groove at the perimeter of the illuminated area (this is referred to as the negative crown effect).

Figure 11 shows a series of SEM micrographs detailing defect-selective features for open-circuit etching with a range of KOH concentrations and GaN electron densities. Each micrograph shows an area of the sample that was partially covered by wax during etching. The wax has been subsequently removed to show the contrast between the morphology of etched and unetched areas. Two trends are clear. At constant KOH concentration (see, for example, 0.004 M) the etch rate drops with increasing electron density and defect selectivity is lost for the highest doped sample; the upper limit for open circuit photoetching is roughly $5 \times 10^{18} \text{ cm}^{-3}$. For a given electron density a clear change in morphology is observed on going to higher KOH concentration.

This is very likely related to the limitation of the photocurrent observed in fig. 2 at high KOH concentration ($>0.004 \text{ M}$). Oxide formation seems to prevent uniform etching of the surface and localized pits are formed, not related to defects. The lower limit of carrier concentration is less easily defined. In the case of resistive samples uniform etching does not take place. In such a situation it is clear that the distance from the titanium contact will have an impact on the etch rate since the total resistance “seen” by the electrons is proportional to the distance travelled. The effect is similar to that introduced by a low quality Ohmic contact (see fig. 4) The practical lower limit of carrier concentration for uniform etching is roughly 10^{16} cm^{-3} . However, samples having an even lower carrier concentration can be PEC etched in narrow area near the Ti contact. This area is usually sufficient for a quick verification of dislocation density but it does not allow for a thorough study.

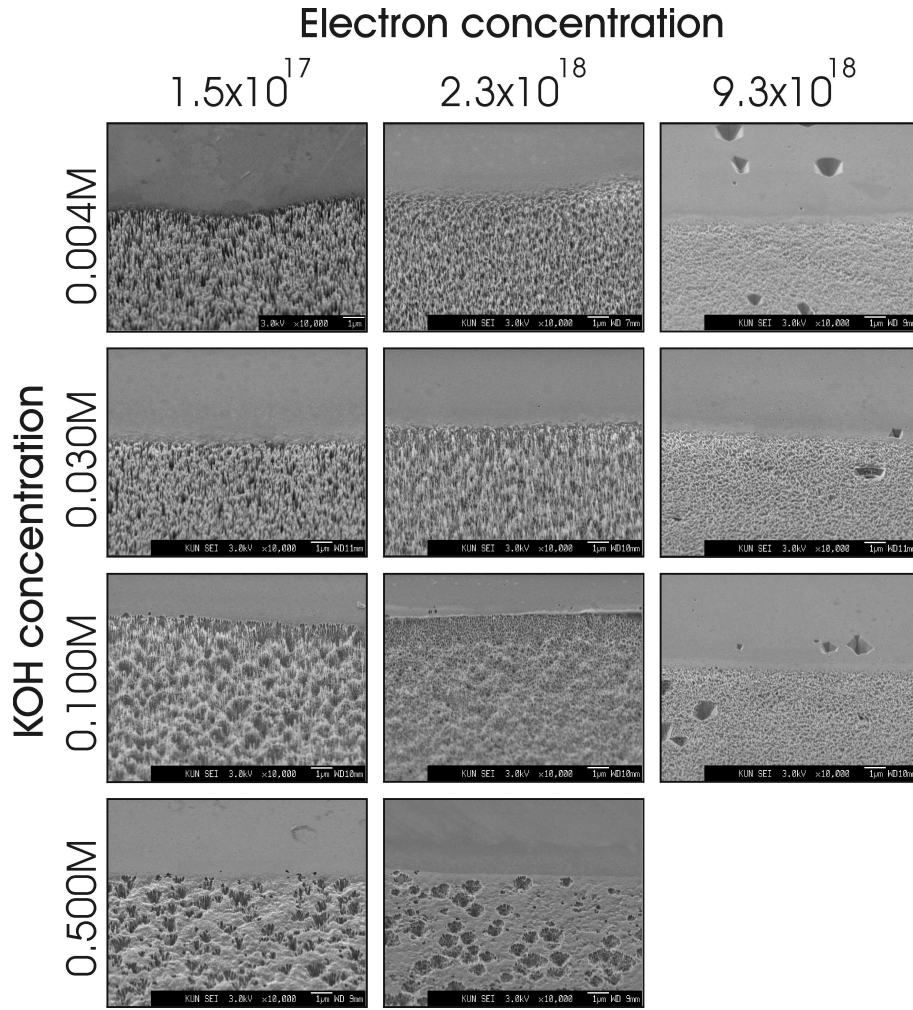


Figure 11: PEC etching features as a function of electron concentration and KOH molar fraction.

5.4 Conclusions

Electrochemical experiments have shown that the anodic photocurrent of GaN can be controlled either by the photon flux or the OH^- ion diffusion rate. For sufficiently large KOH concentration, photocurrent and etch rate are linearly dependent on the intensity of absorbed light. However, if the KOH concentration is low then diffusion of OH^- ions rate becomes the limiting step and a further increase of light intensity does not yield a higher photocurrent or etch rate. In the first case we have a defect-selective regime since local depletion of holes at recombination centres such as dislocations leads to the

creation of needles. The latter case leads to polishing-like behaviour and defect selectivity is lost. A transition between the two regimes can be realized by changing the KOH concentration and illumination intensity.

In the case of open circuit experiments, matching of the anodic photocurrent at the GaN electrode with the cathodic current at the counter electrode sets the open-circuit potential. For samples with higher electron concentration this potential is in the rising part of the current-potential plot which limits the photocurrent and etch rate. In addition, a low quality ohmic contact or small-area counter electrode can introduce an extra series resistance in the circuit; this decreases the current and further lowers photoetch rate.

The practical range of electron concentration that can be expected to give valuable data falls between 10^{16} cm^{-3} and $5 \times 10^{18} \text{ cm}^{-3}$. This also happens to be the natural electron concentration for unintentionally doped samples.

References

- [1] C. Youtsey, L.T. Romano, R.J. Molnar, I. Adesida, *Appl. Phys. Lett.* **74**, 3537 (1999).
- [2] P. Visconti, K.M. Jones, M.A. Reshchikov, R. Cingolani, H. Morkoç, R.J. Molnar, *Appl. Phys. Lett.* **77**, 3532 (2000)
- [3] M.S. Minsky, M. White, E.L. Hu, *Appl. Phys. Lett.* **68**, 1531 (1996).
- [4] C. Youtsey, I. Adesida, G. Bulman, *Appl. Phys. Lett.* **71**, 2151 (1997).
- [5] C. Youtsey, L.T. Romano, I. Adesida, *Appl. Phys. Lett.* **73**, 797 (1998).
- [6] J. L. Weyher, F. D. Tichelaar, H. W. Zandbergen, L. Macht, P. R. Hageman. *J. Appl. Phys.* **90**, 6105 (2001)
- [7] T. Rotter, D. Mistele, J. Stemmer, F. Fedler, J. Aderhold, J. Graul, V. Schwegler, C. Kirchner, M. Kamp, M. Heuken, *Appl. Phys. Lett.* **76**, 3923 (2000).
- [8] G. Nowak, X.H. Xia, J.J. Kelly, J.L. Weyher, S. Porowski, *J. Crystal Growth* **222**, 735 (2001)
- [9] L.-H. Peng, C.-W. Huang, J.-K. Ho, C.-N. Huang, C.-Y. Chen, *Appl. Phys. Lett.* **72**, 939 (1998)
- [10] J.E. Borton, C. Cai, M.I. Nathan, P. Chow, J.M. Van Hove, A. Wowchak, H. Morkoç, *Appl. Phys. Lett.* **77**, 1227 (2000)
- [11] I.M. Huygens, K. Strubbe, W.P. Gomes, *J. Electrochem. Soc.* **147**, 1797 (2000)

- [12] P.H. Reiger, *Electrochemistry*, Prentice-Hall (Englewood Cliffs, NJ), 1987, chapter 4 (section 4.2)
- [13] J.D. Beach, R.T. Collins, J.A. Turner, *J. Electrochem. Soc.* **150**, A899 (2003)
- [14] J.J. Kelly, P.H.L. Notten, *J. Electrochem. Soc.* **130**, 2452 (1983)
- [15] W.W. Gartner, *Phys. Rev.* **116**, 84 (1959)
- [16] P.H.L. Notten, J.E.A.M. van den Meerakker, J.J. Kelly, *Etching of III-V Semiconductors: an Electrochemical Approach*, Elsevier Advanced Technology, Oxford (1991)
- [17] C. Youtsey, I. Adesida, L.T. Romano, G. Bulman, *Appl. Phys. Lett.* **72**, 560 (1998)

Chapter 6

Statistical photoluminescence of dislocations and associated defects in MOCVD-grown heteroepitaxial GaN ¹

6.1 Dislocation related luminescence

Gallium nitride research and technology has progressed enormously over the past two decades resulting in large number of optoelectronic and high-power, high frequency devices.¹ Despite the existence of operational GaN light emitting diodes (LEDs), laser diodes (LDs) and other devices,² the III-Nitride system is not yet flawless. Lack of commercially available free standing GaN substrates makes it necessary to use foreign ones such as sapphire or silicon carbide (SiC). Therefore, the resultant layers are characterized by large quantities of dislocations and other defects. Particular interest is concentrated around the origin of defect related luminescence bands, as they are natural competitors of the band-edge luminescence utilized in all GaN-based optoelectronic devices.

The bands in question are yellow luminescence (YL) centred around 2.2 eV and blue luminescence (BL) centred around 2.9 eV. The first of the two

¹Chapter based on: “Statistical photoluminescence of dislocations and associated defects in MOCVD-grown heteroepitaxial GaN” L. Macht, A.P. Grzegorzczuk, J. Weyher, P.K. Larsen, Phys. Rev. B **71**, (2005)

is quite commonly observed but it has never been attributed to any specific defect with certainty. Electron irradiation studies seem to suggest that the origin of YL is a gallium vacancy (V_{Ga}),³ or a V_{Ga} -Ga_I Frenkel pair.⁴ Many reports suggest shallow donor – deep acceptor recombination as the cause of YL with the V_{Ga} as the deep acceptor^{5–7} and an oxygen substitutional atom on a nitrogen site (O_N) as shallow donor.^{8–10} The most commonly accepted cause for YL is thus a donor-acceptor recombination of V_{Ga} - O_N defect. BL is not as commonly observed and as such its origins have not been studied in sufficient detail. Kang *et al.* suggest the same V_{Ga} - O_N defect complex to be responsible for BL.¹¹ Li *et al.*, on the other hand, suggest a free electron to deep acceptor transition.¹² Similar blue bands can be observed also in intentionally doped samples, but in that case their origin is believed to be of different nature.¹³

There are also theoretical reports suggesting preferential incorporation of V_{Ga} - O_N complexes into dislocation cores.¹⁴ Such an effect should result in YL or BL originating at dislocations, as was previously suggested by Ponce *et al.* for YL.¹⁵ The association of oxygen related defects with nano-pipes has also been predicted theoretically¹⁶ and confirmed experimentally.¹⁷

In this paper we present luminescence data for GaN samples which have been etched in a defect selective manner. The etching results in creation of nanocolumns which are formed around dislocation cores. By comparing the data obtained from unetched and etched samples we can verify the direct influence of dislocations on all photoluminescence bands.

6.2 Samples and measurements

The samples used in this investigation were Ga-polar, nominally undoped GaN layers, which were grown on c-plane sapphire by MOCVD in a horizontal geometry reactor. The substrate was first cleaned in an HCl:HNO₃ solution outside the reactor, followed by an anneal in the reactor in a N₂ atmosphere at 500 mbar and at a temperature about 1000 °C. After this nitradation of the sapphire surface the substrate was cooled to 525 °C at which temperature a 20 nm GaN nucleation layer was grown at 500 mbar, followed by growth of the main n-type GaN layer at 1130 °C and 50 mbar. Trimethyl gallium and ammonia were used as precursors. The thickness of the GaN layers was typically about 2.5 μm with a carrier concentration of 6.5x10¹⁶ cm⁻³ and a resistivity of 3.0 Ohm/cm, as obtained from Hall measurements. The overall

crystalline quality is described by the FWHM of X-ray rocking curves and these were typically 259 arcsec and 136 arcsec for the (0002) and (0105) peaks, respectively.

The photoetching setup used in this study was an open-circuit version similar to that of Youtsey *et al.*¹⁸ The sample's area was approximately 0.5 cm², thereby ensuring homogenous illumination. Ohmic contacts to the GaN surface were made by evaporation of a 100 nm Ti layer covering area of 10-20% of the total surface area. No additional heat treatment of the contacts was applied. The counter electrode was a PT coated plate with a surface area 50 times larger than that of the GaN electrode. The electrolyte used was a stirred KOH solution with a concentration of 0.004 M. The illumination was provided by 450 W UV enhanced Xe lamp equipped with water IR filter. The resultant power density was measured to be 300 mW/cm⁻². It is important to note that only wavelengths below ~ 360 nm, i.e. the room temperature bandgap of GaN, will contribute to photoetching. The photocurrent, which is a rough measure of the etch rate, was measured by a multimeter. As function of time the photocurrent is rather constant (or slightly decreasing) until eventually a current collapse occurs. In this case the GaN layer (except the nanocolumns, see section III) has been etched completely away. From integration of the photocurrent vs. time plots of fully etched sample, time values for intermediate stages of etching, e.g. 1/4, 1/2 or 3/4 of the total layer can be estimated.

The morphology of samples after etching was examined by diffraction interference contrast (DIC) optical microscopy and scanning electron microscopy (SEM).

All PL measurements were performed at 4.4 K in a cold-finger continuous flow cryostat. Excitation was provided by the 325 nm line of HeCd laser with power density of 300 W/cm⁻². Luminescence was analyzed using a 1 m long, Spex 1704 monochromator and a Jobin-Yvon back-illuminated UV-enhanced CCD detector.

6.3 The origins of YL and BL bands

In order to recognize the origin of luminescence in this study, the effect of defect selective etching has to be understood. A sample submerged in a weak KOH solution equipped with a contact is illuminated by light with energy higher than that of the GaN bandgap. The resultant photo carriers

are spatially separated by the electric field at the interface between the semiconductor and the electrolyte. In the case of n-type material the holes are forced towards the surface while electrons are forced away from it. Holes then take part in the etching process while electrons move through the sample and wiring to the counter electrode where they complete the circuit by oxygen reduction.¹⁹

Any kind of surface recombination will impede the etching by decreasing the number of available holes. Therefore, dislocations, which act as recombination centers, will not etch at all, leaving a sharp featured morphology. These nanocolumns have been proven to represent dislocations and nanopipes and their immediate vicinity.^{20,21} Figure 1 shows an SEM micrograph of the sample which has been etched for 1/4 of the time needed to etch the GaN layer completely. Each “whisker” represents a threading dislocation which might be either a screw, a mixed or an edge type as has been already proven by TEM measurements.²² The dislocation density measured for this sample is estimated at $6 \times 10^9 \text{ cm}^{-1}$, which is in line with usual dislocation density for our samples and it is also comparable to the etch pit density (EPD) resulting from defect selective etching in molten KOH-NaOH mixture.

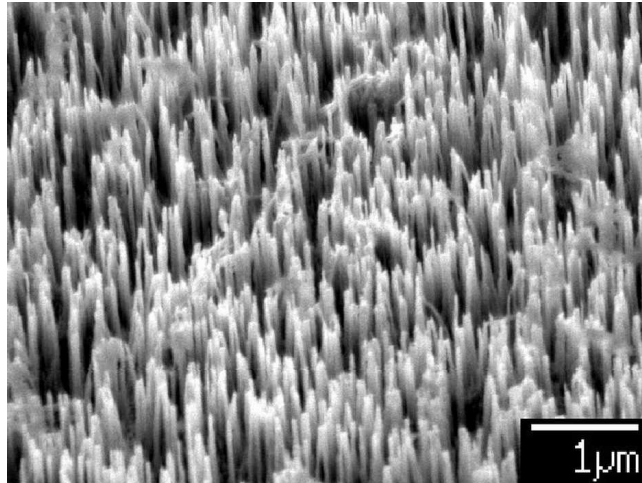


Figure 1: Typical nanocolumns created on dislocations during photoetching. Each nanocolumn represents one dislocation of either screw, mixed or edge type.

PL measurements have been performed with a spot diameter in the order of 30-50 μm , which is much larger than the average distance and diameter of individual nanocolumns. In this manner we obtain statistical PL data over a comparably large area. Figure 2 shows PL results for the band edge

spectral range. The PL intensity is plotted in logarithmic scale to show low intensity features. The unetched sample shows a clear donor-bound exciton (DBE) peak at 3.481 eV and free excitons A and B at 3.488 eV and 3.497 eV respectively. Two peaks attributed to excitons bound on acceptors are visible at 3.460 eV and 3.466 eV. All these values are slightly shifted towards higher energies from the commonly known energies. This shift is attributed to the fact that at $2.5 \mu\text{m}$ thickness, the samples are compressively strained.

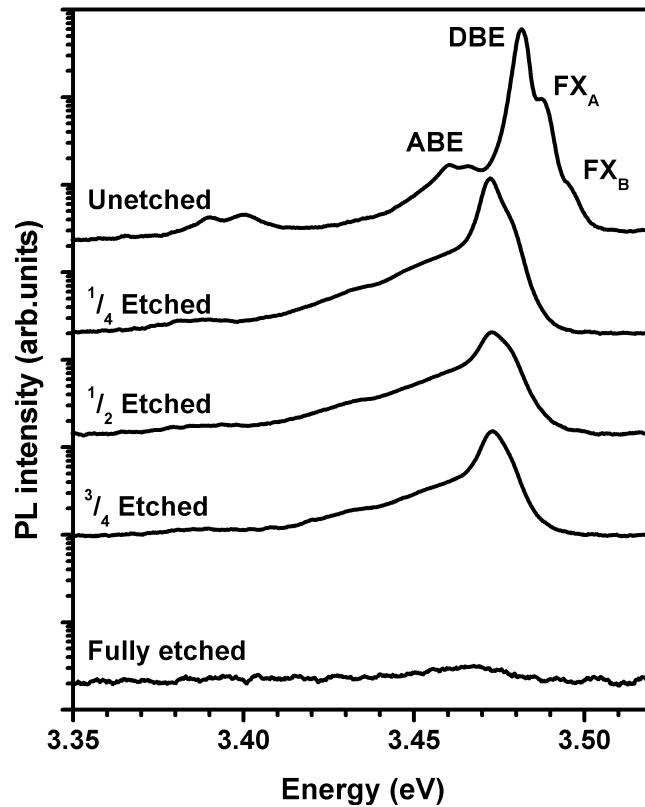


Figure 2: PL spectra taken at 4.4 K of the band edge region for etched and unetched samples.

The largest difference between the PL signal between the unetched and fully etched sample is the fact that all of the band edge luminescence is quenched. This is a clear proof that dislocations are sources of ruinous recombination which is competitive to UV luminescence used for LED and LD operation. The samples etched partially retain their band edge luminescence to a considerable degree with visible redshift. The luminescence is not quenched proportionally to the etched amount due to the fact that the

absorption depth for excitation wavelength is only ~ 250 nm. After removal of some GaN during etching the remaining thickness remains larger than the absorption depth except for the fully etched sample. The signal thus obtained is therefore not considerably weaker than that from the unetched sample. The redshift of the luminescence peaks is caused by the fact that the etch rate is highest in the areas furthest away from dislocations. This results in the formation of nanocolumns and also rough morphology at their bases, causing, relaxation of strain and the visible lowering of emission energies.

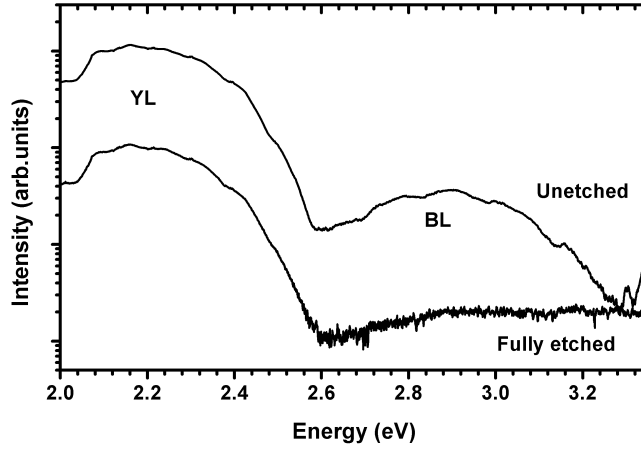


Figure 3: PL spectra taken at 4.4 K for the fully etched and unetched samples in the yellow and blue luminescence spectral range.

Figure 3 shows full emission spectra of the unetched and the fully etched samples in the range 1.9 eV to 3.35 eV. The unetched sample shows, apart from the previously mentioned band edge components, also a considerable blue luminescence (BL) centred around 2.9 eV and a strong yellow luminescence (YL) centred around 2.2 eV. After etching the BL is completely extinguished while the YL considerably diminished. We have estimated that the complete etching removes between 85% and 95% of the material. The decrease in the YL intensity matches the decrease in the amount of GaN.

It has been suggested previously that the origin of yellow luminescence might be the $V_{Ga}-O_N$ defect complexes, which are predicted to accumulate at threading dislocation cores. Results described in this paper show that the YL has no correlation with threading dislocations other than that it is not quenched by non-radiative recombination occurring at dislocation sites. This indicates that defect centers responsible for YL are point defects

homogenously distributed through the GaN layer and that they possess a higher recombination rate than that of dislocations. Therefore, either $V_{Ga}-O_N$ defects do not incorporate preferentially into dislocation cores, or such incorporation terminates their optical activity. Complete quenching of BL upon etching can be explained in two ways; either defects responsible for BL are not incorporated into the vicinity of dislocations or their recombination rate is much lower than that of dislocations and YL defect centres.

It has been previously reported, that BL and YL are involved in so called “bleaching” effect.²³⁻²⁵ A slow decay of the BL intensity under excitation is observed, accompanied by gradual increase of the YL intensity. Figure 4 shows such behaviour for our samples with the BL decay matching the YL strengthening, suggesting a direct transfer of charge between the two defect complexes responsible for these PL bands. In agreement with other publications²⁶ this metastable effect can be reversed by cycling the sample to room temperature within the confines of cryostat.

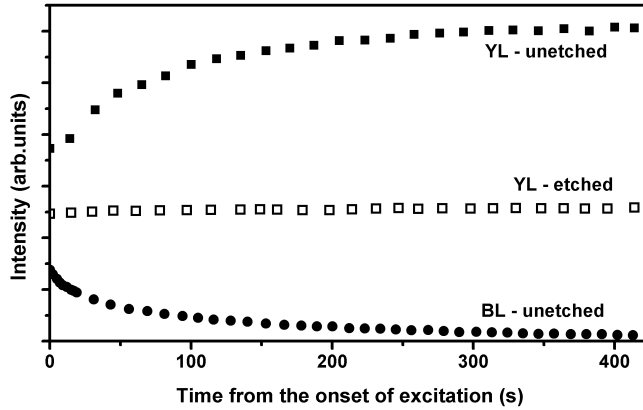


Figure 4: Evolution of YL and BL in time taken at 4.4 K for both etched and unetched samples.

It is important to note that this behaviour, in our case, is valid for as-grown samples, as opposed to H_3PO_4 -etched ones described by Reshchikov *et al.* The bleaching times are much shorter compared to other reports, but it can be attributed to the fact that the excitation intensity used in this study was considerably higher, and according to Reshchikov *et al.* it should have direct influence on the decay rate. No bleaching effect has been observed for the etched sample; lack of measurable BL being one of the reasons. However, YL in the same regime showed a completely constant intensity over time (see

fig. 4). This is another evidence that YL and BL are interconnected, most probably by different charge states of the same defect. However, the data collected does not allow us to state unambiguously which defects could be responsible.

6.4 Conclusions

Measured PL data indicates that the presence of dislocations is destructive to the band-edge optical activity. Furthermore it suggests that there is no spatial correlation between dislocations and yellow luminescence and that the YL is in fact caused by point-like defects homogenously distributed in the GaN layer.

As mentioned in the Introduction the YL is commonly believed to originate from $V_{Ga}-O_N$ complexes. Additionally it has been suggested that these complexes incorporate preferentially into dislocations and in their vicinity. However, our results imply that YL is not directly related to the presence of dislocations. It is merely not diminished by their presence. One possible explanation is that the same $V_{Ga}-O_N$ defects have a different electronic signature when incorporated into dislocation free GaN matrix in comparison with those incorporated into dislocation sites. In that case it is possible that they are indeed incorporated preferentially into dislocations but such an incorporation quenches their optical activity.

Defect centres responsible for the BL are either incorporated into the dislocation free areas of the sample or they have a much lower recombination rate than that of non-radiative recombination on dislocation cores. The collected data also suggests a direct connection between YL and BL defect centres making it quite probable that they are different charge states of the same defect complex.

It is our belief that additional cathodoluminescence mapping and time resolved photoluminescence studies would further contribute to answering the questions of spatial distribution and recombination rate of the defects responsible for YL and BL

References

- [1] H. Morkoç, *Nitride Semiconductors and Devices* (Springer, Berlin, 1999)
- [2] S. J. Pearton, J. C. Zolper, R. J. Shul, F. Ren, J. Appl. Phys. **86**, 1 (1999)
- [3] K. Kuriyama, H. Kondo, M. Okada, Solid State Commun. **119**, 559, (2001)
- [4] Y. Hayashi, T. Soga, M. Umeno, T. Jimbo, Physica B **304**, 12 (2001)
- [5] H. Lei, H.S. Leipner, J. Schreiber, J.L. Weyher, T. Wosinski, I. Grzegory, J. Appl. Phys. **92**, 6666 (2002)
- [6] R. Armitage, W. Hong, Q. Yang, H. feick, J. Gebauer E.R. Weber, S. Hautakangas, K. Saarinen, Appl. Phys. Lett. **82**, 3457 (2003)
- [7] C.H. Seager, D.R. Tallant, J. Yu, W. Gotz, J. Lum.**106**, 115 (2004)
- [8] K. Michael, U. Rogulis, F.K. Koschnick, Th. Trösner, J.-M. Spaeth, B. Beaumont, P. Gibart, Physica B, **308**, 85 (2001)
- [9] H.Z. Xu, A. Bell, Z.G. Wang, Y. Okada, M. Kawabe, I. Harrison, C.T. Foxon, J. Crystal Growth, **222**, 96 (2001)
- [10] M.A. Reshchikov, H. Morkoç, S.S. Park, K.Y. Lee, Appl. Phys. Lett. **81**, 4970 (2002)
- [11] J. Kang, Y. Shen, Z. Wang, Mat. Sci. Eng. **B91-92**, 303 (2002)
- [12] S. Li, F. Jiang, G. Fan, L. Wang, C. Xiong, X. Peng, H. Mo, J. Lum. **106**, 219 (2004)
- [13] U. Kaufmann, M. Kunzer, M. Maier, H. Obloh, A. Ramakrishnan, B. Santic, P. Schlotter, Appl. Phys. Lett. **72**, 1326 (1998)
- [14] J. Elsner, R. Jones, M.I. Heggie, P.K. Sitch, M. Haugk, Th. Frauenheim, S. Öberg, P.R. Briddon, Phys. Rev. B, **58**, 12571 (1998)
- [15] F.A. Ponce, D.P. Bour, W. Gotz, P.J. Wright, Appl. Phys. Lett. **70**, 1983 (1997)
- [16] J. Elsner, . Jones, M. Haugk, R. Gutierrez, Th. Frauenheim, M.I. Heggie, S. Öberg, P.R. Briddon, Appl. Phys. Lett. **73**, 3530 (1998)
- [17] I. Arslan, N.D. Browning, Phys. Rev. Lett. **91**, 165501-1 (2003)
- [18] C. Youtsey, I. Adesida, G. Bulman, Appl. Phys. Lett. **71**, 2151 (1997)
- [19] L. Macht, J.J. Kelly, J.L. Weyher, A. Grzegorzcyk, P.K. Larsen, J. Crystal Growth, **273**, 347 (2005)
- [20] J. L. Weyher, F. D. Tichelaar, H. W. Zandbergen, L. Macht, P. R. Hageman. J. Appl. Phys. **90**, 6105 (2001)
- [21] S. Lazar, J.L. Weyher, L. Macht, F.D. Tichelaar, H.W. Zandbergen, to

- be published in EPJ Appl. Phys. **27**, (2004)
- [22] C. Youtsey, L.T. Romano, I. Adesida, Appl. Phys. Lett. **73**, 797 (1998)
 - [23] B. Kim, I. Kuskovsky, I.P. Herman, D. Li, G.F. Neumark, J. Appl. Phys. **86**, 2034, (1999)
 - [24] M.A. Reshchikov, P. Visconti, H. Morkoç, Appl. Phys. Lett. **78**, 177 (2001)
 - [25] B.J. Ryan, M.O. Henry, E. McGlynn, J. Fryar, Physica B, **340-342**, 452, (2003)
 - [26] S. Dhar, S. Ghosh, Appl. Phys. Lett. **80**, 4519 (2002)

Chapter 7

Micro photoluminescence mapping of laterally overgrown MOCVD GaN layers on patterned Si (111) substrates ¹

7.1 Patterned Si as alternative substrate

Despite extensive research into the growth of gallium nitride (GaN), there are still no industrially available free standing GaN wafers. This fact enforces the use of foreign substrates and therefore results in layers exhibiting large numbers of dislocations. Among the possible substrates, silicon offers some potential advantages as a substrate for GaN; these include: low cost, large-scale availability and well-established processing technology. Additionally, growth of non-polar r-plane GaN layers can be realized on Si (001) by careful control of the nucleation layer.¹ However, silicon's large lattice mismatch with GaN (17%) and additionally their difference in thermal expansion coefficients makes it very challenging to grow GaN layers of high enough quality to ensure proper operation of devices. Apart from a high density of dislocations (in the order of 10^{10} cm⁻²) created at the substrate-layer interface, the thermal expansion coefficient mismatch leads to generation of

¹Chapter based on: "Micro photoluminescence mapping of laterally overgrown MOCVD GaN layers on patterned Si (111) substrates" L. Macht, P.R. Hageman, S. Haffouz, P.K. Larsen, accepted for publication in Appl. Phys. Lett.

cracks for layers thicker than $1\ \mu\text{m}$.² Several methods of growth optimization can be used to improve these unfavorable characteristics, for instance various modifications to the AlN nucleation layer.³ An additional SiN_x layer,⁴ or AlGaN/GaN superlattice structures⁵ also serve to release strain and lower the overall dislocation density. A significant improvement can be obtained by using epitaxial lateral overgrowth (ELO) technique.⁶ In fact dislocation densities as low as $5 \times 10^7\ \text{cm}^{-2}$ have been obtained.⁷ However, these techniques require complicated and costly *ex-situ* processing during an interruption of the GaN growth.

The present paper reports on the photoluminescence (PL) characteristics of ELO GaN epilayers on (111) Si substrates patterned with hole openings. The results are discussed in terms of strain distribution and dislocation density as shown by photo electrochemical (PEC) etching. According to PL results these layers exhibit characteristics favourable for growth of low cost LED structures and are therefore industrially feasible.

7.2 Growth parameters and measurement configuration

Prior to the growth of the GaN layers, the Si substrates were etched in a hole pattern creating $4\ \mu\text{m}$ deep circular holes with diameter of $1.5\ \mu\text{m}$ and center to center distance of $3.5\ \mu\text{m}$, arranged in a hexagonal plan. The etching was done in a series of dry etching steps: inductively coupled plasma (ICP) etching followed electron cyclotron resonance (ECR) plasma etching. First an oxide mask was deposited in an ICP C_4F_8 plasma, subsequently RIE-oxygen plasma etching was used to remove the organic residues and finally the actual etching of Si substrate was carried out in SF_6/O_2 ECR plasma. Under these conditions the etch rate is estimated to be $300\ \text{nm}/\text{min}$. The depth of $4\ \mu\text{m}$ is chosen to prohibit nucleation of GaN layer inside the holes or at the ridges. A more extensive description of the etching process is provided by Haffouz *et. al.*⁸

The GaN layers have been grown by MOCVD on the patterned (111) Si substrates. Trimethylgallium (TMGa), trimethylaluminum (TMAI) and ammonia (NH_3) were the precursors for gallium, aluminum and nitrogen, respectively. An optimized AlN nucleation layer needed for correct growth is deposited first at $850^\circ\ \text{C}$. Later the sample is heated to $1170^\circ\ \text{C}$ to commence

the growth of the main GaN layer of Ga-polarity.⁸ Figure 1 shows an SEM micrograph of the cleaved GaN layer on top of the patterned Si substrate. It can be clearly seen that nucleation occurred on the unetched surfaces and that the growth then proceeded laterally and vertically. Lateral growth resulted in closing of the holes etched in the substrate creating crystallographically oriented inverted pyramidal shapes with the slopes made of $\langle 10\bar{1}1 \rangle$ planes.

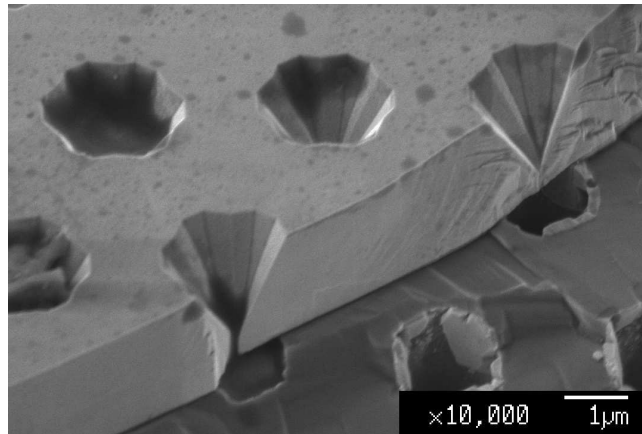


Figure 1: SEM micrograph at 45° inclination of the GaN layer overgrowing the pits in the substrate. Complete coalescence can be observed, however, the growth run was too short for complete smoothing of the surface; (b)

Schematic drawing of the growth process is presented in fig. 2; the arrows indicate both lateral and vertical growth directions, the solid line represents sample's surface at the end of the growth run, dotted lines represent sample surface during growth and the dashed line corresponds to the expected surface if the growth had been continued. At the growth thickness of 2-2.3 μm the holes are on the threshold of being completely overgrown, however the surface exhibits hexagonally shaped pits. This sample, as shown in fig. 1 has been used in all the PL measurements.

μ -PL mapping measurements were performed at room temperature on a custom built set-up. HeCd laser provided excitation at 325 nm with power of 20 mW; the laser beam was routed into an diffraction-limited aspheric lens by means of a dichroic mirror. The same lens was used to collect photoluminescence which after passing through the same dichroic mirror was collected into a CoherentTM liquid light guide. The luminescence was analyzed by a 1-m Spex 1704 monochromator equipped with a back illuminated UV-enhanced CCD camera by Jobin Yvon. The spectral

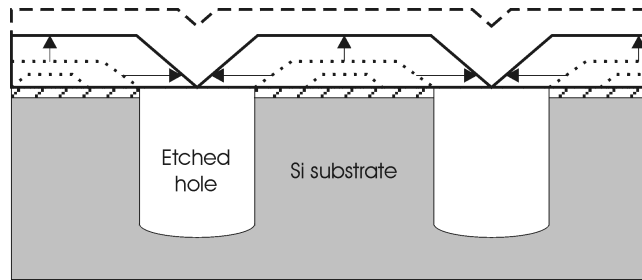


Figure 2: Schematic drawing of the overgrowth process. The arrows indicate lateral and vertical growth directions and solid line indicates the sample surface at the end of the growth run. The dotted lines show growth surfaces during the growth and the dashed line shows projected surface if the growth run had been continued

resolution was measured to be less than 0.3, and the spatial resolution was measured to be $0.8 \mu\text{m}$, which is quite satisfactory taking into account that the theoretical diffraction limit for the lens used (numerical aperture 0.6) is $0.66 \mu\text{m}$.

PEC etching was employed to visualize the threading dislocations and to give an estimate of the dislocation density. It was performed in a stirred aqueous KOH solution (0.004 M) at room temperature. The UV illumination was provided by a 450W UV-enhanced XE-lamp. The nature and physical background of PEC etching can be found elsewhere.⁹

7.3 Results and Discussion

Figure 3 shows the GaN layer after PEC etching. Due to its nature PEC etching reveals dislocations of edge, mixed and screw type as well as narrow inversion domain boundaries. Because the sample exhibits Ga-polarity formation of inversion domains does not seem probable.

Therefore all the whiskers visible on the figure are attributed to dislocations and the density is calculated to be $\sim 8 \times 10^9 \text{ cm}^{-2}$. No whiskers can be seen in the overgrown areas. There are two reasons for that. Firstly, as shown in ref.,⁸ the dislocations which nucleated at the edge of a hole in Si substrate tend to bend towards the center and either annihilate or become basal plane dislocations. Secondly, no new dislocations are generated in the overhanging GaN layer. The dislocations are known to suppress band edge luminescence¹⁰ and this is clearly reflected in fig. 4. Figure 4.(a) shows a map

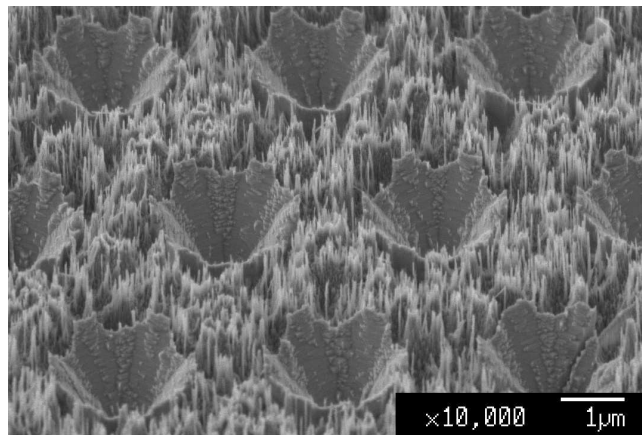


Figure 3: SEM micrograph at 45 inclination of the GaN layer after PEC etching. Single whiskers represent threading dislocations.

of luminescence intensity at the spectral position of the peak for a $15 \times 15 \mu\text{m}$ area. This peak position is not constant and it varies from spot to spot, the intensity of luminescence is taken at the actual spectral position of the peak for each point and not at an arbitrary energy. Thus measured intensity of overgrown areas is, on average, 5 times higher than intensity measured in the areas directly over the substrate. On the figure the bright circular areas represent over-the-void layer.

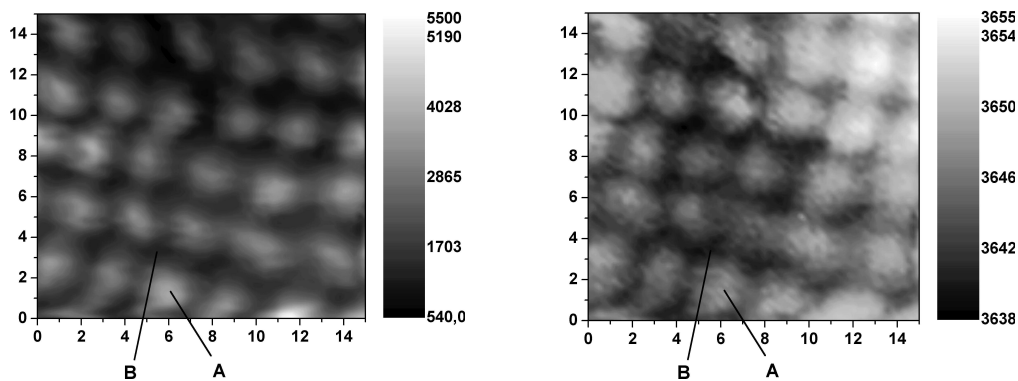


Figure 4: (a) A μ -PL map of a $15 \times 15 \mu\text{m}$ area the parameter mapped is intensity at the position of the peak. The position of the peak shifts depending on the location. (b) a μ -PL map of a $15 \times 15 \mu\text{m}$ area, the parameter mapped is the spectral position of the peak. Emission wavelength is presented in \AA .

A corresponding map of the same area shown in fig. 4.(b) shows peak

emission energy. The luminescence from the overgrown areas of GaN layer have markedly lower energy than those from areas above the Si substrate and the values are 3.400 eV and 3.405 eV, respectively. Figure 5 shows PL spectral data from two points designated A and B on fig. 3. The scans show the difference between luminescence intensity as well as the spectral position of the peaks. The latter value is consistent with value of 3.406 eV reported elsewhere for GaN/Si layers.⁵ For comparison: GaN/Sapphire which is believed to be in small compressive strain at RT emits at 3.424 eV¹¹ while completely unstrained GaN emits light at 3.420 eV.

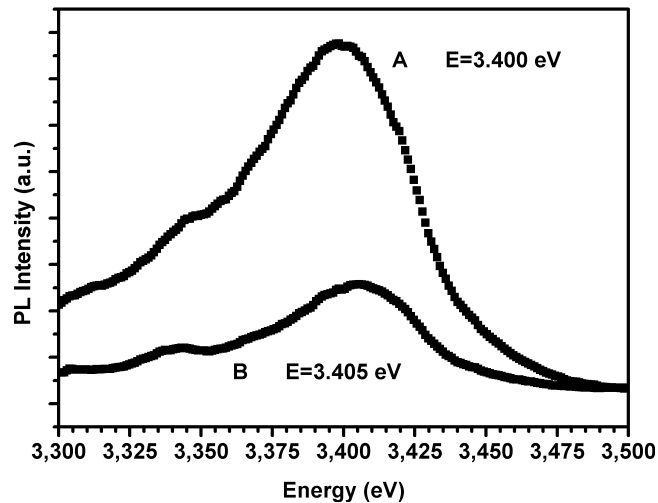


Figure 5: Spectral scans of PL at the points designated A and B on the PL maps.

GaN layers grown on Si substrates are believed to be in tensile strain at room temperature resulting in emission wavelength shifted towards lower energies. This is also the case for our samples as can be seen by lower emission energies than those for relaxed GaN. It is also believed that layers grown over a mask in the ELOG process or, in this case, over a void should be relaxed and therefore have emission at comparably higher energy. Figure 3.(b) shows exactly the opposite behaviour, as spots corresponding to areas grown over the voids show even lower emission energy than those directly over the substrate.

The reason for such an effect can be explained by the dislocation formation mechanism and the strain relaxing properties of dislocations. There are two major reasons for existence of dislocations. One is the fact that growth is usually started as 3D growth and the layers coalesce at

a later time which induces creation of low angle grain boundaries at the spots of coalescence, creating rows of dislocations. The second reason is the differences in thermal expansion coefficients which induce stress upon cooling of the sample and dislocations appear post-growth as means of relaxing that stress. Differences between the density of GaN nucleation islands result in the general differences of statistical dislocation density between GaN layers grown on different substrates.

In the case of this sample the PL results shown in fig. 3.(b) suggest that GaN areas grown over a void have higher tensile stress than the ones over Si substrate. This can be explained by the fact that the areas over Si have very high in-grown dislocation density. Those dislocations relax strain, whereas much lower dislocation density in the areas over the voids does not present such an opportunity. The mismatch in the thermal expansion coefficients between Si and GaN induces tensile strain when the sample is cooled down to room temperature, which can be partially relaxed by the grown-in dislocations directly over substrate but will be much less relaxed over the void due to the lack of dislocations.

7.4 Conclusions

In summary, it has been shown that GaN layers can be grown on patterned Si substrates exhibiting locally much lower dislocation density and better structure quality. This enhancement is accompanied by a large increase in luminescence intensity and a slight shift of luminescence peak towards lower energies. This red-shift indicates higher levels of tensile stress which is caused by a locally lower density of dislocations.

Micro PL mapping has been used to study local optical properties of the samples and it is proved to be a suitable tool for local strain mapping of GaN layers.

References

- [1] F. Schulze, A. Dadgar, J. Bläsing, A. Krost, *Appl. Phys. Lett.* **84** (2004) 4747
- [2] A. Dadgar, J. Bläsing, A. Diez, A. Alam, M. Heuken, A. Krost, *Jpn. J. Appl. Phys.* **39** (2000) L1183

- [3] A. Krost, A. Dadgar, J. Bläsing, A. Diez, T. Hempel, S. Petzold, J. Christen, R. Clos, *Appl. Phys. Lett.* **85** (2004) 3441
- [4] P.R. Hageman, S. Haffouz, V. Kirilyuk, A. Grzegorzcyk, P.K. Larsen, *phys. stat. sol. (a)* **188** (2001) 523
- [5] S.H. Jang, C.R. Lee, *J. Crystal Growth* **253** (2003) 64
- [6] H. Marchand, N. Zhang, L. Zaho, Y. Golan, S.J. Rosner, G. Girolami, P.T. Fini, J.P. Ibbetson, S. Keller, S. DenBaars, J.S. Speck, U.K. Mishra, *MRs Internet J. Nitride Semicond. Res.* 4 (1999) 2
- [7] E. Feltin, B. Beaumont, P. Venngues. M. Vaille, P. Gibart, T. Riemann, J. Christen, L. Dobos, B. Pecz, *J. Appl. Phys.* **93**, 182 (2003)
- [8] S. Haffouz, A. Grzegorzcyk, P.R. Hageman, P. Venngus, E.W.J.M. van der Drift, P.K. Larsen, *J. Crystal Growth.* **248**, 568 (2003)
- [9] L. Macht, J.J. Kelly, J.L. Weyher, A. Grzegorzcyk, P.K. Larsen, *J. Crystal Growth*, **273**, 347 (2005)
- [10] L. Macht, J.L. Weyher, A. Grzegorzcyk, P.K. Larsen, *accepted in PRB*
- [11] M. Smith, J. Y. Lin, H. X. Jiang, M. Asif Khan, *Appl. Phys. Lett.* **71**, 635 (1997)

Chapter 8

Direct influence of polarity on structural and electro-optical properties of heteroepitaxial GaN ¹

8.1 Introduction

The application of GaN for blue light emitting devices has driven and still drives the research of both material properties as well as growth methods. The most common one of them to date is Metal-Organic Chemical Vapour Deposition (MOCVD), most frequently used for heteroepitaxial growth on sapphire substrates. GaN layers of both Ga- and N-polarity ((0001) or (000 $\bar{1}$), respectively) can be grown by this method. One of the most obvious features of the two polarities of GaN is dissimilar morphology of the Ga- and N-polar samples, accompanied by remarkable differences in their resistance to chemical etching.^{1,2} The origin of this phenomenon can be traced back to the surface reconstruction of the material during growth, which is completely different for the two polarities, as shown by A.R. Smith *et al.*³⁻⁵ The distinction between the two different polarities can be made by convergent beam electron diffraction (CBED),^{2,6} ion channelling,⁷ and coaxial impact

¹Chapter based on: “Direct influence of polarity on structural and electro-optical properties of heteroepitaxial GaN” L. Macht, J.L. Weyher, P.R. Hageman, M. Zielinski and P.K. Larsen, J. Phys.: Condens. Matter 14 (2002) 13345-13350

collision ion scattering spectroscopy (CAICISS).⁸

The initial nitridation of the sapphire substrate and buffer layer growth have been identified as the source of differences in polarity of the GaN films.⁹⁻¹¹ Variations in optical properties and impurity incorporation also originate from the difference in polarity of GaN layers.^{12,13}

However, all of these reports describe two or more samples that were grown during different processes with unequal growth parameters after which the relevant sample properties were measured. The variations in the growth processes give rise to an uncertainty about attributing differences of sample properties to polarity or merely to changes of growth conditions. In this paper a heteroepitaxial GaN layer is presented which exhibits both polarities. The sample consists of MOCVD grown GaN on a sapphire substrate with a very thin buffer layer. Such a structure allowed for the creation of both polarities in one process, which ensured the identicalness of all growth parameters. Therefore, all the differences in optical or structural properties must be the result of polarity and not of dissimilar growth conditions.

8.2 Experimental details

The GaN epilayer was grown by MOCVD using a horizontal reactor. Trimethylgallium (TMG) and ammonia (NH_3) were used as precursors with H_2 as carrier gas. A two-inch polished (0001) sapphire wafer with a misorientation within $\pm 0.01^\circ$ was used as a substrate. The substrate was first cleaned in organic solvents, etched in aqua regia, rinsed with deionised water and blown dry with filtered N_2 gas. It was then placed on a SiC coated susceptor that was heated by RF and which contains a rotating disk to obtain optimum uniformity during the growth process. The rotation of the susceptor disc is driven by a flow of hydrogen gas. The discharge of this flow causes a small temperature decrease on the growing surface from the centre to its periphery. The first growth step consisted of nitridation of the substrate surface, carried out in a NH_3/N_2 gas stream at gradually changing temperature between 1100 and 950 °C. Then the temperature was lowered to 525 °C and a $\sim 5\text{nm}$ GaN buffer was deposited. This thickness of the nucleation layer was found to be the boundary condition between Ga- and N-polar growth environments. Finally the main 2.75 μm GaN layer was grown at 1170 °C.

Initial differential optical contrast (DIC) microscopy confirmed the

existence of areas with two distinct types of surface morphology. Hall measurements were performed at room temperature on pieces of both polarities in the van der Pauw configuration. Photoluminescence (PL) spectra were measured for both polarities at 4 K using a 100 cm long SPEX 1704 monochromator and ISA CCD camera for detection and HeCd laser for excitation.

SIMS analysis has been applied to verify the amounts of foreign atoms in pieces of both polarities. Particularly, the concentration of O, C and Si has been assessed.

Two etching methods have been used for defect visualisation and analysis: photo enhanced chemical (PEC) etching in a weak KOH solution and wet chemical etching in a mixture of concentrated H_2SO_4 and H_3PO_4 , further referred to as HH solution.

The main characteristic of PEC is the fact that only defect free material is etched away while all structural flaws that induce carrier recombination are left untouched. The carriers generated by UV source are separated due to band bending at the interface of GaN and KOH solution, electrons are carried away while holes take part in a dissolution process described by G. Nowak et al.¹⁴

Thus, any defects such as dislocations, stacking faults or inversion domain boundaries,¹⁵ which are sites of recombination, will not be etched due to lack of holes. The exact nature and details of PEC method can be found elsewhere.¹⁶ Samples of both polarities have been subjected to 20 min. etching in 0.004M KOH solution in H_2O illuminated by Xenon lamp with a power density of $250 \text{ mW}\cdot\text{cm}^{-2}$. Etching in HH solution, which is a classical type of wet chemical etching, is designed to utilize internal energy of structural defects and thus open them up for etching. The combination of those two methods gives very detailed information about the defect composition in any given sample.

8.3 Influence of polarity on GaN properties

The as-grown sample, clearly displayed two different kinds of surface morphology. DIC microscopy revealed that hexagonal pyramids populate N-polar part taking up roughly 60% of the surface and concentrate in the centre of sample. The diameter of the pyramids in this section varied from 10 to 30 μm in diameter. Near the edges the surface remained flat with RMS

roughness of ~ 0.4 nm on a $1 \mu\text{m}$ square, as confirmed by AFM measurements. The rough and smooth areas were separated by ~ 2 mm transition region where the pyramids were gradually spaced further apart until they were completely replaced by smooth surface.

Hall measurements showed an average resistivity of $246 \text{ m}\Omega\cdot\text{cm}$ for the Ga-polar area and $3 \text{ m}\Omega\cdot\text{cm}$ for N-polar. The free carrier concentration was $5.2 \times 10^{17} \text{ cm}^{-3}$ and $1.1 \times 10^{20} \text{ cm}^{-3}$ for Ga-polar and N-polar pieces, respectively. The mobility of the carriers was of comparable magnitude for both polarities, being $48.6 \text{ cm}^2\cdot\text{V}^{-1}\cdot\text{s}^{-1}$ and $20.4 \text{ cm}^2\cdot\text{V}^{-1}\cdot\text{s}^{-1}$ respectively. The actual results for N-polar piece have to be taken as approximate values due to thickness variations. Hall samples are prepared in the Van der Pauw configuration with the distance between contacts of 5 mm and a middle area of around 1 mm^2 in size, which is large compared to the size of pyramids.

PL results as seen on fig. 1, clearly show different optical properties for both polarities. Ga-polar GaN exhibits a well-defined spectrum showing a donor bound exciton (D^0X) peak at 3.478 eV with FWHM of 4.3 meV, which indicates a good, but not outstanding optical quality. The free exciton A (X_A) at 3.484 eV and the free exciton B (X_B) at 3.492 eV are also clearly visible supporting the view about the quality of the material. The less prominent peak at 3.455 eV is attributed to recombination of the neutral – acceptor bound exciton (A^0X).

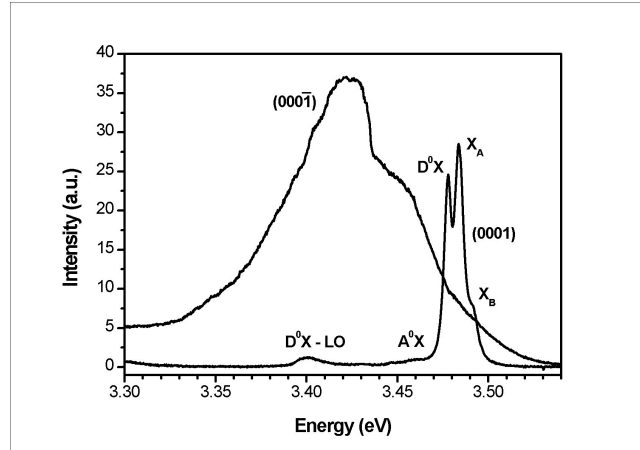


Figure 1: PL spectra for both (0001) and (000 $\bar{1}$) growth directions.

On the other hand, a PL spectrum from the N-polar GaN is completely featureless showing extremely broad peak centred on 3.42 eV with high

overall intensity. The PL luminescence is very inhomogeneous for the N-polar area, mainly due to fact that the surface can modulate the emitted radiation by interference. The variation in PL spectrum for Ga-polar piece across the surface is only in respect to the intensity ratio between D^0X and X_A peaks and their respective FWHM.

SIMS analysis performed on both kinds of polarity with respect to O, C, Si and H is shown on fig. 2 (a) and (b). The difference in the Ga and N profile near the interface at the depth of about $3 \mu\text{m}$ stems from the fact that surface is not smooth. The ion beam does not strike the interface at a single moment but uncovers it in a more gradual manner. The SIMS profile of the N-polar part exhibits much higher concentration of O atoms than the Ga-polar part while the C and H atoms concentration is slightly lower.

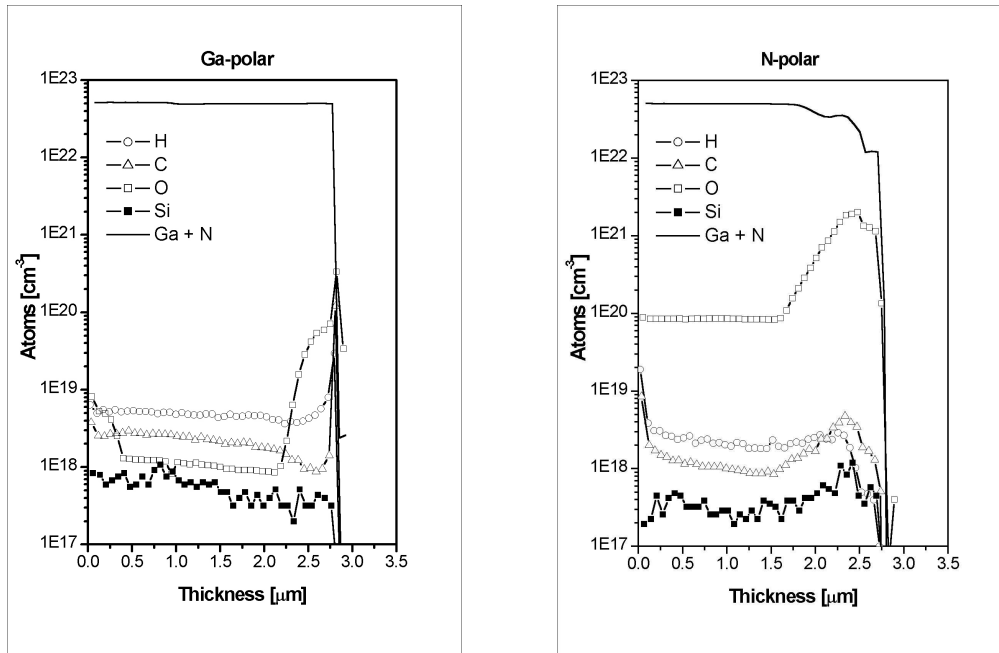


Figure 2: SIMS results for both Ga-polar (a) and N-polar (b) areas.

Fig. 3 shows an SEM image of Ga-polar piece after PEC etching. The “whisker” structure is very regular and predictable for that kind of samples. Every whisker represents a dislocation and is terminated at the surface of the sample. Some whiskers join together and may annihilate before reaching the surface.

Figure 4 shows an SEM image of N-polar, PEC etched (a) and HH etched

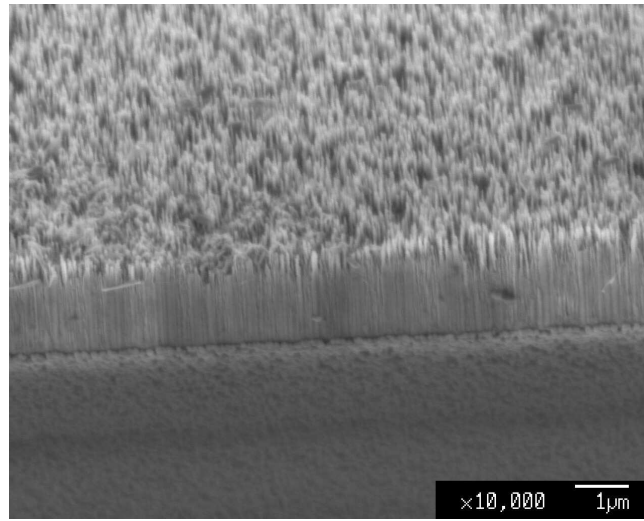


Figure 3: SEM image of PEC etched Ga-polar area.

piece (b). The first one shows that the pyramids have been etched away in a peculiar fashion.

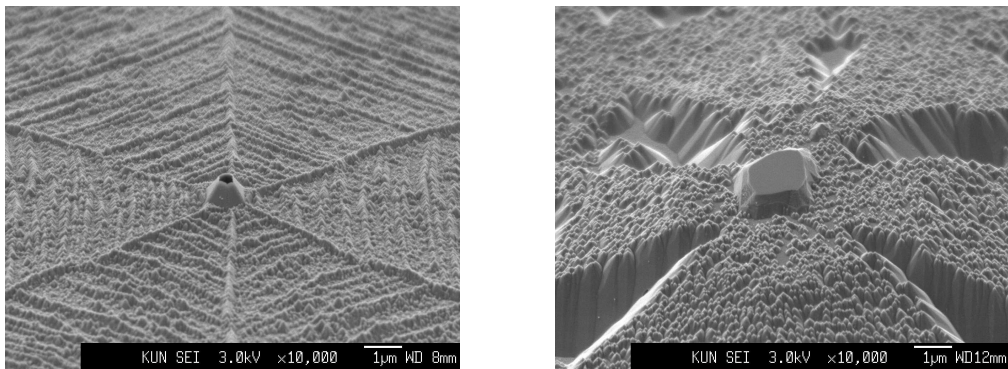


Figure 4: SEM images of N-polar area after PEC etching (a), and HH etching (b).

All pyramids have a single inversion domain (ID) in the centre, which has been etched away quicker than the surrounding material. PEC etching is very sensitive to the carrier concentration; material with a higher carrier concentration etches slower and at values of about 10^{20} cm^{-3} etching stops completely. Intensifying the power of UV radiation or increasing the KOH concentration may raise this limit but not significantly. Thus, etched ID leads to believe that the carrier concentration inside is much lower than outside what agrees with the results from macroscopic Hall measurements.^{17,18}

The edges of all pyramids remained less etched than the rest of surrounding material what again suggests that they are recombinative sites. This is due to easier incorporation of impurities such as Si or O^{19,20} and also due to the existence of stacking faults. Another feature is formed by the ridges perpendicular to lines bisecting the angle between pyramid edges, which also etches less than the surrounding material. Those ridges are not visible on the as-grown sample. When the Ga-polar ID grows within N-polar matrix, all impurities that are incorporated into the surface close to it are swept away along the step flow direction. Their further advance is stopped on a macrostep where they are included in ridge-like structures and serve as recombination sites. The nature and origin of macrosteps is as yet unknown. The second part of the same picture shows similar pyramid etched in HH solution. The mechanism of etching is based on releasing stored energy of structural defects and releasing it in the process of etching. In this case it can be seen that edges of pyramids have etched much more than the surrounding material while the ID in the middle remained unetched. This result is complementary to one obtained from PEC etching. Incorporated impurities and structural defects concentrate in the pyramid edges.

8.4 Conclusions

It is certain that the buffer layer is crucial for growth of GaN on sapphire and is the selecting factor for growth of Ga- or N-polar samples. Thus, by careful control of buffer layer's thickness we can obtain any of the two polarities.

All experimental results show very large differences in carrier concentration, resistivity and impurity incorporation between these two polarities. It has also been demonstrated that preferential incorporation of oxygen in N-polar part is the reason for peculiar effect of PEC etching on large IDs. The fact that growth of N-polar and Ga-polar material occurred in the same process guarantees that polarity is the factor responsible for those differences.

References

- [1] M. Seelman-Eggebert, J.L. Weyher, H. Obloh, H. Zimmermann, A. Rar and S. Porowski, *Appl. Phys. Lett.* **71**, 2365, (1997).

- [2] J.L. Rouviere, J.L. Weyher, M. Seelmann-Eggebert, and S. Porowski, *Appl. Phys. Lett.* **73**, 668 (1998).
- [3] A.R. Smith, R.M. Feenstra, D.W. Greve, M.-S. Shin, M. Skowronski, J. Neugebauer and J.E. Northrup, *Appl. Phys. Lett.* **72**, 2114 (1998).
- [4] A.R. Smith, R.M. Feenstra, D.W. Greve, J. Neugebauer, and J.E. Northrup, *Phys. Rev. Lett.* **79**, 3934 (1997)
- [5] X.Q. Shen, T. Ide, S.H. cho, M. Shimizu, S. Hara and H. Okumura, *Appl. Phys. Lett.* **77**, 4013 (2000).
- [6] F.A. Ponce , D.P. Bour, W.T. Young, M. Saunders, and J.W. Steeds, *Appl. Phys. Lett.* **69**, 337 (1996).
- [7] B. Daudin , J.L. Rouvire, and M. Arlery, *Appl. Phys. Lett.* **69**, 2480 (1996).
- [8] M. Sumiya, M. Tanaka, K. Ohtsuka, S. Fuke, T. Ohnishi, I. Ohkubo, M. Yoshimoto, H. Koinuma, and M. Kawasaki, *Appl. Phys. Lett.* **75**, 674 (1999).
- [9] S. Fuke, H. Teshigawara, K. Kuwahara, Y. Takano, T. Ito, M. Yanagihara, and K. Ohtsuka, *J. Appl. Phys.* **83**, 764 (1998).
- [10] M. Sumiya, K. Yoshimura, T. Ito, K. Ohtsuka, S. Fuke, K. Mizuno, M. Yoshimoto, H. Koinuma, A. Ohtomo and M. Kawasaki, *J. Appl. Phys.* **88**, 1158 (2000).
- [11] D. Huang, P. Visconti, K.M. James, M.A. Reshchikov, F. Yun, A.A. Baski, T. King and H. Morkoc, *Appl. Phys. Lett.* **78**, 4145 (2001).
- [12] S.F. Chichibu, A. Setoguchi, A. Uedono, K. Yoshimura and M. Sumiya, *Appl. Phys. Lett.* **78**, 28 (2001).
- [13] M. Sumiya, K. Yoshimura, K. Ohtsuka and S. Fuke, *Appl. Phys. Lett.* **76**, 2098 (2000).
- [14] G. Nowak, X.H. Xia, J.J. Kelly, J.L. Weyher and S. Porowski, *J. Crystal Growth* **222**, 735 (2001).
- [15] J.L. Weyher, F.D. Tichelaar, H.W. Zandbergen, L. Macht, and P.R. Hageman, *J. Appl. Phys.* **90**, 6105 (2001).
- [16] C. Youtsey, I. Adesida, and G. Bulman, *Appl. Phys. Lett.* **71**, 2151 (1997).
- [17] J. Elsner, Th. Frauenheim, M. Haugk, R. Gutierrez, R. Jones and M.I. Heggier, *Mater. Res. Soc. Symp. Proc.* **G3**, 29/7 (1999).
- [18] J.A. Chisholm and P.D. Bristowe, *MRS Internet J. Nitride Semicond. Res.* **5S1**, W3.72 (2000).
- [19] P. Prystawko, M. Leszczynski, B. Beaumont, P. Gilbert, E. Frayssinet,

- W. Knap, P. Wisniewski, M. Bockowski, T. Suski and S. Porowski, *Phys. Status Solidi B* **210**, 437 (1998).
- [20] M. Mayer, A. Pelzmann, H.Y. Chung, M. Kamp and K.J. Ebeling, *J. Crystal Growth* **201/202**, 318 (1999).

Summary

GaN is a semiconductor belonging to the III-V group. Its most interesting characteristic is its wide, direct bandgap (E_g) of 3.42 eV, which allows for efficient light generation at wavelengths of about 365 nm and can therefore be used for generation of light in the ultra violet (UV) part of the spectrum. The possibility to grow ternary or quaternary alloys with gallium, indium, aluminium, as well as other III-N compounds allows bandgap engineering and extends the emission spectrum from deep UV to yellow. The wide bandgap of GaN and AlGaN is very valuable for high temperature electronics because the ratio of bandgap to the thermal energy kT is much higher than for other common semiconductors such as Si ($E_g = 1.1$ eV). The high drift velocity and breakdown voltage of these nitride compounds are furthermore very valuable for high frequency – high power electronic devices.

These valuable electrical and optical properties are further augmented by high thermal stability, physical hardness and high chemical stability. While the thermal stability of GaN allows freedom for high temperature applications and processing, its chemical stability presents a technological challenge. However, the high thermal stability makes the growth of GaN impossible by common methods, which results in lack of free-standing GaN wafers. Additionally, growth on foreign substrates leads to formation of various structural defects, most notably dislocations, due to lattice constant mismatch and differences in thermal expansion coefficients between GaN and the substrate.

This thesis is aimed at answering some questions concerning formation and characteristics of defects in GaN, particularly through the use of defect selective etching methods and various approaches to photoluminescence. To help the reader get acquainted with defects found in GaN, chapter 2 describes all kinds of defects in reasonable detail followed by a review of defect selective etching methods and their results in chapter 3.

Defect-selective etching is a standard method for determining the density and distribution of dislocations in semiconductor crystals. The classical (orthodox) etching is known to reveal dislocations in the form of well defined etch pits, and the etch pit density (EPD) value is given as one of the standard characteristic parameters in the specification of all semiconductor substrates. Due to the complex nature of defects in compound semiconductors, more sophisticated etching procedures were developed and were shown to be effective in studying crystallographic and chemical non-homogeneities in GaAs. For GaN, the progress in defect-selective etching trailed behind the use of other methods of structural characterization (e.g. TEM), because of the high chemical resistance of this material and polarity-related strong anisotropy. In addition, the most commonly grown hetero-epitaxial GaN layers and structures contain dislocations in very high densities (up to 10^{10} cm^{-2}) which are co-existing with specific types of defects, such as nano-pipes, pinholes and inversion domains (IDs).

One of the two most prominent methods of defect-selective etching is etching in a eutectic mixture of KOH and NaOH. For successful examination of dislocation density, proper care must be taken to ensure sufficiently high etching temperature, temperatures below 350°C might result in EPD significantly lower than the actual dislocation density.

The size of the pits and the angle of their slopes are dependent on the types of dislocations and the types of dislocations populating the sample will strongly depend on the growth method used, e.g. HVPE or MOCVD, as well as type of doping.

As shown in chapter 4, for HVPE grown GaN:Zn all of the measured dislocations have a screw component; there were no indications of any pure edge dislocations terminating at the surface of the sample. AFM measurements and activation energy calculations show that 98% of all dislocations originate randomly in the matrix, generating two kinds of surface features and creating two different kinds of etch pits with clearly defined activation energy.

The difference in the activation energy is not large which suggests that it is caused by differences in dislocation decoration and not in fundamental changes of the Burgers vector. The remaining 2% of the dislocations are either screw type with $\pm 2c$ components in the Burgers vector generating 4 spiral surface steps, or dislocation dipoles: one $\pm 2c$ dislocation combined with one $\pm c$ but of the opposite direction resulting in a generation of 4 spiral

surface steps of which 2 are annihilated at the neighbouring dislocation. These types of dislocations/dislocation complexes are the sources of spiral step-flow and the high local growth rate which results in hillocks commonly populating HVPE grown samples.

Another type of etching frequently utilized during this study is photo-electrochemical etching (PEC) as described in detail in chapter 5. Electrochemical experiments have shown that the anodic photocurrent of GaN can be controlled either by the photon flux or the OH^- ion diffusion rate. For sufficiently large KOH concentration, photocurrent and etch rate are linearly dependent on the intensity of absorbed light. However, if the KOH concentration is low then the diffusion rate of OH^- ions becomes the limiting step and a further increase of light intensity does not yield a higher photocurrent or etch rate. In the first case we have a defect-selective regime since local depletion of holes at recombination centres such as dislocations leads to the creation of needles. The latter case leads to polishing-like behaviour and defect selectivity is lost. A transition between the two regimes can be realized by changing the KOH concentration and illumination intensity. In addition, a low quality ohmic contact or small-area counter electrode can introduce an extra series resistance in the circuit; this decreases the current and further lowers the photo-etch rate.

As shown in chapter 6 statistical PL data indicates that the presence of dislocations is destructive to the band-edge optical activity. Furthermore it suggests that there is no spatial correlation between dislocations and yellow luminescence (YL) and that the YL is in fact caused by point-like defects homogenously distributed in the GaN layer.

The YL is commonly believed to originate from $V_{\text{Ga}}\text{-O}_{\text{N}}$ complexes. Additionally it has been suggested that these complexes incorporate preferentially into dislocations and in their vicinity. However, our results imply that YL is not directly related to the presence of dislocations. It is merely not diminished by their presence. One possible explanation is that the same $V_{\text{Ga}}\text{-O}_{\text{N}}$ defects have a different electronic signature when incorporated into a dislocation free GaN matrix in comparison with those incorporated into dislocation sites. In that case it is possible that they are indeed incorporated preferentially into dislocations but such an incorporation quenches their optical activity.

Defect centres responsible for the blue luminescence (BL) are either incorporated into the dislocation free areas of the sample or they have a

much lower recombination rate than that of non-radiative recombination on dislocation cores. The collected data also suggests a direct connection between YL and BL defect centres making it quite probable that they are different charge states of the same defect complex.

Using micro PL it has been shown in chapter 7 that GaN layers can be grown on patterned Si substrates exhibiting locally much lower dislocation density and better structure quality. This enhancement is accompanied by a large increase in luminescence intensity and a slight shift of luminescence peak towards lower energies. This red-shift indicates higher levels of tensile stress which is caused by a locally lower density of dislocations.

Chapter 8 shows that the buffer layer is crucial for growth of GaN on sapphire and is the selecting factor for growth of Ga- or N-polar samples. Thus, by careful control of buffer layer's thickness we can obtain any of the two polarities.

All experimental results show very large differences in carrier concentration, resistivity and impurity incorporation between these two polarities. It has also been demonstrated that preferential incorporation of oxygen in the N-polar part is the reason for the peculiar effect of PEC etching on large IDs. The fact that growth of N-polar and Ga-polar material occurred in the same process guarantees that polarity is the factor responsible for those differences.

Samenvatting

GaN is een halfgeleider die tot de III-V groep behoort. De meest interessante eigenschap van GaN is de grote, directe bandgap (E_g) van 3.42 eV, die een efficiënte generatie van licht met een golflengte van ongeveer 365 nm mogelijk maakt. GaN kan daarom gebruikt worden voor het genereren van licht in het ultraviolette (UV) deel van het spectrum. De mogelijkheid om drievoudige en viervoudige legeringen met gallium, indium, aluminium, alsook andere III-N mengsels te groeien, maakt bandgap bewerking mogelijk, waardoor het emissiespectrum uitgebreid kan worden van het diep UV tot geel. De grote bandgap van GaN en AlGaIn is erg waardevol voor hoge-temperatuur elektronica, omdat de verhouding tussen bandgap en thermische energie kT veel hoger is dan bij gebruikelijke halfgeleiders zoals Si ($E_g = 1.1$ eV). De hoge driftsnelheid en doorslagspanning van deze nitridecomponenten zijn verder erg waardevol voor hoogfrequent – hoogvermogen elektronische onderdelen.

De waardevolle elektrische en optische eigenschappen worden verder nog aangevuld door een hoge thermische stabiliteit, een grote hardheid en een sterke chemische stabiliteit. Terwijl de thermische stabiliteit van GaN zorgt voor vrijheid in hoge temperatuur toepassingen and verwerking, leidt de chemische stabiliteit tot technische uitdagingen. De hoge thermische stabiliteit leidt er echter toe dat de groei van GaN onmogelijk is met conventionele methodes, waardoor er een gebrek is in vrijstaande GaN substraten. Bovendien leidt groei van GaN op vreemde substraten tot de formatie van verschillende structurele defecten. Dislocaties, ontstaan vanwege een verschil in roosterconstante en verschillen in thermische expansie coëfficiënten tussen GaN en het substraat, vallen het meeste op.

Dit proefschrift is gericht op het beantwoorden van een aantal vragen betreffende de formatie en de karakteristieken van defecten in GaN, in het bijzonder door het gebruik van defect-selectieve etsmethoden en verschillende vormen van fotoluminescentie. Om de lezer bekend te maken met de defecten

die specifiek in GaN voorkomen, worden in hoofdstuk 2 alle soorten defecten in redelijk detail beschreven. Hierna volgt een overzicht van defect-selectieve etsmethodes en hun resultaten in hoofdstuk 3.

Defect-selectief etsen is een standaard methode om de dichtheid en verdeling van dislocaties in halfgeleider kristallen te bepalen. Het klassieke (orthodoxe) etsen maakt dislocaties zichtbaar in de vorm van goed gedefiniëerde etsputjes, en de etsput dichtheid (EPD) wordt gebruikt als een van de standaard karakteristieke parameters in de specificatie van alle halfgeleider substraten. Vanwege de complexe aard van defecten in samengestelde halfgeleiders was het nodig om meer geavanceerde etsmethodes te ontwikkelen; deze methodes bleken effectief te zijn in de bestudering van kristallografische en chemische inhomogeniteiten in GaAs. Voor GaN bleef de voortgang in defect-selective etsmethodes achter bij andere methodes van structurele karakterisatie (bijvoorbeeld TEM), omdat GaN een hoge chemische stabiliteit en een polariteit gerelateerde anisotropie bezit. Daarbij komt ook nog dat de typische gegroeide hetero-epitaxiale GaN lagen en structuren dislocaties in zeer hoge dichtheden bevatten (tot wel 10^{10} cm^{-2}). Deze dislocaties komen tegelijk voor met specifieke defecten zoals nanopijpen, pinholes en inversie-domeinen (ID).

Een van de twee meest gebruikte methodes van defect-selectief etsen is etsen in een eutectisch mengsel van KOH en NaOH. Om de dislocatiedichtheid goed te kunnen onderzoeken moet goed zorg gedragen worden voor een voldoende hoge etstemperatuur; temperaturen onder de 350°C kunnen resulteren in een EPD die significant lager ligt dan de werkelijke dislocatiedichtheid.

De grootte van de etsputjes en de hoek van hun helling hangt af van het soort dislocatie, en de soorten dislocaties die aanwezig zijn in het sample hangen sterk af van de groeimethode, bijvoorbeeld HVPE of MOCVD, en ook van het type dotering.

In hoofdstuk 4 wordt aangetoond dat de dislocaties in HVPE gegroeid GaN:Zn allen een schroef component hebben; er waren geen aanwijzingen dat er zuivere rand-dislocaties, die eindigen aan het oppervlak van het sample, aanwezig zijn. Metingen met AFM en activeringsenergie berekeningen laten zien dat 98% van alle dislocaties op willekeurige plaatsen in de matrix ontstaan, waardoor twee verschillende oppervlaktekenmerken en twee soorten etsputjes met een duidelijk gedefiniëerde activeringsenergie ontstaan.

Het verschil in de activeringsenergie is niet groot, wat doet vermoeden

dat het verschil veroorzaakt wordt door verschillen in decoratie van de dislocatie en niet door fundamentele veranderingen van de Burgers vector. De overgebleven 2% van de dislocaties zijn of schroef-type dislocaties met $\pm 2c$ componenten in de Burgers vector, waardoor vier spiraalvormige oppervlaktestappen ontstaan, of dislocatie dipolen: een $\pm 2c$ dislocatie, gecombineerd met een $\pm c$ maar in tegengestelde richting, waardoor vier spiraalvormige oppervlaktestappen ontstaan waarvan er twee tenietgedaan worden in de aangrenzende dislocatie. Deze types dislocaties of dislocatie complexen zijn de bron van spiraalvormige stapverplaatsing en van de hoge lokale groeisnelheid die resulteert in de veel voorkomende heuveltjes op samples die met HVPE gegroeid zijn.

Een andere etstechniek die veel gebruikt is in dit onderzoek is foto-elektrochemisch (FEC) etsen, zoals beschreven in detail in hoofdstuk 5. Elektrochemische experimenten hebben aangetoond dat de anodische fotostroom van GaN zowel gecontroleerd kan worden door de foton flux als door de diffusiesnelheid van de OH^- ionen. Bij een voldoende hoge KOH concentratie geldt dat de fotostroom en de etssnelheid lineair afhankelijk zijn van de intensiteit van het geabsorbeerde licht. Als de KOH concentratie echter laag is, wordt de diffusiesnelheid van de OH^- ionen de beperkende stap en een verdere verhoging van de lichtintensiteit leidt in deze gevallen niet tot een hogere fotostroom of een hogere etssnelheid. In het eerste geval zitten we in het defect-selectieve regime, omdat een lokale vermindering van gaten bij recombinatieplaatsen zoals dislocaties leidt tot het ontstaan van naalden. Het tweede geval leidt tot een soort polijstgedrag en de defect-selectiviteit gaat verloren. Een overgang tussen de twee regimes kan bereikt worden door de KOH concentratie en de verlichtingsintensiteit te variëren. Een Ohms contact van lage kwaliteit of een tegenelektrode met een klein oppervlak kunnen verder nog een extra serieweerstand in het circuit introduceren; hierdoor wordt de stroom gereduceerd en wordt de foto-etssnelheid verder verlaagd.

In hoofdstuk 6 wordt door middel van statistische fotoluminescentie data aangetoond dat de aanwezigheid van dislocaties destructief werkt op de optische activiteit van de rand van de bandgap. Verder wordt er in dit hoofdstuk geopperd dat er geen ruimtelijke correlatie is tussen dislocaties en gele luminescentie (GL) en dat de GL in feite veroorzaakt wordt door punt-achtige defecten, die homogeen verdeeld zijn in de GaN laag.

Over het algemeen wordt er gedacht dat GL afkomstig is van $V_{\text{Ga}}\text{-O}_{\text{N}}$ complexen. Ook wordt er gesuggereerd dat deze complexen bij voorkeur

ingebouwd worden in dislocaties en in de omgeving hiervan. Onze resultaten laten echter zien dat GL niet direct gerelateerd is aan de aanwezigheid van dislocaties. GL wordt hoogstens niet verminderd door de aanwezigheid van dislocaties. Een mogelijke verklaring is dat dezelfde $V_{\text{Ga-O}_N}$ defecten een verschillende elektronische signatuur hebben wanneer ze ingebouwd zijn in een GaN matrix, vrij van dislocaties, in vergelijking met defecten die ingebouwd zijn in dislocatieplaatsen. In dat geval is het mogelijk dat ze inderdaad bij voorkeur in dislocatieplaatsen worden ingebouwd, maar dat een dergelijke inbouw hun optische activiteit onderdrukt.

De defect centra die verantwoordelijk zijn voor blauwe luminescentie (BL) zijn ingebouwd in de gedeeltes van het sample die vrij zijn van dislocaties, of ze hebben een veel lagere recombinatiesnelheid dan de niet-stralende recombinatie aan de dislocatie kernen. De verzamelde data suggereert een directe connectie tussen GL en BL defect centra, waardoor het waarschijnlijk is dat ze beiden een verschillend energieniveau van hetzelfde defect complex zijn.

In hoofdstuk 7 wordt door middel van micro-fotoluminescentie aangetoond dat GaN lagen kunnen worden gegroeid op Si substraten die van patronen voorzien zijn. De GaN lagen laten lokaal een veel lagere defectdichtheid en een betere kwaliteit van de structuur zien. Deze verbetering gaat samen met een grote toename in luminescentie intensiteit en een kleine verschuiving van de luminescentiepiek naar de lagere energieën. Deze roodverschuiving is een aanwijzing voor grotere trekspanning die veroorzaakt wordt door een lokaal lagere dislocatiedichtheid.

Hoofdstuk 8 laat zien dat de bufferlaag cruciaal is voor de groei van GaN op saffier en dat deze laag de bepalende factor is voor de groei van Ga- of N-polaire samples. Het is dus mogelijk om door een zorgvuldige controle van de dikte van de bufferlaag te bepalen welke van de twee polariteiten gegroeid zal worden.

Alle experimentele resultaten laten zeer grote verschillen in ladingsdragerconcentraties, weerstand en inbouw van onzuiverheden zien tussen de twee polariteiten. Het is ook aangetoond dat de voorkeur voor de inbouw van zuurstof aan de N-polaire kant de oorzaak is voor het aparte effect van FEC etsen op grote ID's. Het feit dat groei van N-polair en Ga-polair materiaal heeft plaatsgevonden in hetzelfde proces garandeert dat polariteit de factor is die verantwoordelijk is voor deze verschillen.

Publications list

1. “Improvement of the optical properties of MOCVD grown GaN on sapphire by an in-situ SiN treatment”, S. Haffouz, V. Kirilyuk, P.R. Hageman, L. Macht, J.L. Weyher and P.K. Larsen, *Appl. Phys. Lett.* 79 (2001) 2390-2392
2. “Improvement of the optical and structural properties of MOCVD grown GaN on sapphire by an in-situ SiN treatment”, P.R. Hageman, S. Haffouz, V. Kirilyuk, L. Macht, J.L. Weyher, A. Grzegorzcyk, and P.K. Larsen, *Phys. Stat. Sol. A* 188 (2001) 659 – 662
3. “Investigation of optical and structural properties of GaN grown by hydride vapor-phase epitaxy”, V. Kirilyuk, P.R. Hageman, P.C.M. Christianen, W.H.M. Corbeek, M. Zielinski, L. Macht, J.L. Weyher and P.K. Larsen, *phys. stat. sol. (a)* 188 (2001) 473-476.
4. “Selective photo-etching and TEM study of defects in hetero-epitaxial GaN”, J.L. Weyher, F.D. Tichelaar, H.W. Zandbergen, L. Macht and P.R. Hageman, *J. Appl. Phys.* 90 (2001) 6105-6109
5. “Direct influence of polarity on structural and electro-optical properties of heteroepitaxial GaN” L. Macht, J.L. Weyher, P.R. Hageman, M. Zielinski and P.K. Larsen, *J. Phys.: Condens. Matter* 14 (2002) 13345-13350
6. “Photorefectance study of GaN/AlGa_N structures”, A. Wojcik, T. Piwonski, T.J. Ochalski, E. Kowalczyk, M. Bugajski, A. Grzegorzcyk, L. Macht and P.K. Larsen, *phys. stat. sol. (c)* 0 (2002) 491-494
7. “Photorefectance study of GaN/AlGa_N structures”, A. Wojcik, T. Piwonski, T.J. Ochalski, E. Kowalczyk, M. Bugajski, A. Grzegorzcyk, L. Macht and P.K. Larsen, *OPTICA APPLICATA* 32 (2002) 431
8. “Complementary study of defects in GaN by photo-etching and TEM”, J.L. Weyher, L. Macht, F.D. Tichelaar, H.W. Zandbergen, P.R. Hageman and P.K. Larsen, *Mater. Sci. Eng. B* 91-92 (2002) 280-284

9. "Influence of selective GaN islands on optical properties of GaN films grown on sapphire substrates", S. Haffouz, P.R. Hageman, V. Kirilyuk, L. Macht, J.L. Weyher and P.K. Larsen, *Mater. Sci. Eng. B* **97** (2003) 9-12
10. "Defects in wide band-gap semiconductors: selective etching and calibration by complementary methods", J.L. Weyher, L. Macht, *Eur. Phys. J. Appl. Phys.* **27**, 37 (2004)
11. "Nanopipes in GaN: photo-etching and TEM study", S. Lazar, J.L. Weyher, L. Macht, F.D. Tichelaar, H.W. Zandbergen, *Eur. Phys. J. Appl. Phys.* **27**, 275 (2004)
12. "An electrochemical study of photoetching of heteroepitaxial GaN: kinetics and morphology", L. Macht, J.J. Kelly, J.L. Weyher, A. Grzegorzczuk, P.K. Larsen, *J. Crystal Growth*, **273**, 347 (2005)
13. "Influence of the substrate misorientation of 4H-SiC substrates on the morphology and crack formation in hetero epitaxial grown GaN epilayers by MOCVD", M. Rudziski, P. R. Hageman, A. P. Grzegorzczuk, L. Macht, J. Pernot, T. C. Rödle, H. F. F. Jos, and P. K. Larsen, *physica status solidi (c)* – accepted for publication
14. "Influence of the nucleation layer morphology and epi layer structure on the resistivity of GaN films grown on c-plane sapphire by metalorganic chemical vapor phase epitaxy", A.P. Grzegorzczuk, L. Macht, P.R. Hageman, J.L. Weyher and P.K. Larsen, *J. Cryst. Growth*, **273**, 424 (2005)
15. "Statistical photoluminescence of dislocations and associated defects in MOCVD-grown heteroepitaxial GaN" L. Macht, A.P. Grzegorzczuk, J. Weyher, P.K. Larsen, *Phys Rev B* **71** (2005)
16. "Resistivity control of unintentionally doped GaN films", A.P. Grzegorzczuk, L. Macht, P.R. Hageman, M. Rudzinski and P.K. Larsen, *physica status solidi (c)* – submitted
17. "Micro photoluminescence mapping of laterally overgrown MOCVD GaN layers on patterned Si (111) substrates" L. Macht, P.R. Hageman, S. Haffouz, P.K. Larsen, submitted to *Appl. Phys. Lett.*
18. "Formation of cubic inclusions in a wurtzite GaN matrix during MOCVD growth on misoriented 4H-SiC substrates", M. Rudziski, E. Jezierska, J. Pernot, E. Bustarret, L. Macht, J. Borysiuk, P.R. Hageman, T. Rödle, H.F.F. Jos, P.K. Larsen, *journal of applied physics* – submitted

Curriculum Vitae

Lukasz Jerzy Macht was born on the 7th of June, 1975 in Warsaw, Poland. He graduated from secondary school in 1994 with firm intention of starting Computer Science studies at Warsaw University of Technology. Having failed the entry exam in physics he has decided to rectify his mistake and continue with physics, specialising in optoelectronics in the department of Technical Physics and Applied Mathematics. He obtained his master's degree from Warsaw University of Technology in 2000 as one of the first students to finish the newly renamed department of Applied Physics. The experimental work titled: "Optical characterisation of semiconductor microcavities with Bragg reflectors" was done at Institute of Electron Technology under supervision of Prof. M. Bugajski. In August 2000 he has begun his doctoral research at Katholieke Universiteit Nijmegen specialising in defect selective etching and optical characterisation of gallium nitride and other III-nitride materials. Prof. P. K. Larsen and Dr. J.L Weyher supervised his work there with the result of successful completion of this thesis. To his chagrin he has found out that he will be defending his work as one of the first PhD students from the newly renamed Radboud Universiteit Nijmegen. In March 2005 he has started working as Development Engineer in ASML, Veldhoven, hoping that at least ASML will not change it's name...¹

¹During his studies he has worked as night typist for Coopers & Lybrand, which has merged with another company and changed it's name to PricewaterhouseCoopers.